POLITECNICO DI MILANO

Facoltá di Ingegneria Industriale

Corso di Laurea in Ingegneria Spaziale

Static and dynamic analysis of anisotropic plates using variable-kinematic Ritz models

Relatore: Prof. Lorenzo Dozio

Tesi di Laurea di:
Matteo SPINELLI
Matr. 771296

Anno Accademico 2013 - 2014

Abstract

Plates are often used in many engineering applications as primary structures, and with the growing use of laminated composite and sandwich plates, accurate assessment of their response is becoming more and more crucial. Contrary to single-layer metallic structures made of isotropic materials, multilayered constructions are typically characterized by high shear deformation, displacements in the thickness direction may exhibit discontinuous derivatives in correspondence to each layer interface and, in addition for equilibrium reasons, transverse shear and normal stresses shall satisfy appropriate interlaminar continuity conditions. Several plate theories have been developed to calculate the flexural response of plates and to provide results that will match the solution of the elasticity equations. Since classical plate theories do not give acceptable results except in some particular cases, several advanced plate theories have been derived to correctly model the behaviour of thick and laminate plates.

This thesis is focused in the advanced modelling of thick laminate or sandwich plates, equipped with masses or patches and loaded with various types of static or time dependant forces. The bending, free and forced vibration problems are solved with different 2D theories adopting a variable kinematic approach based onto the Carrera unified formulation. The solution of the response problems is then sought adopting the Ritz method, capable of providing upper-bound vibration solutions for plates with arbitrary laminate layups and arbitrary boundary conditions.

The numerical results obtained with the present method is presented in order to show that, the more the plate is thin, also by a dynamical point of view, the more the mechanical displacements and stresses distributions along the thickness of the plate tend to be linear. In this case, classical plate theories give acceptable results and ESL theories, give very good results. Otherwise, as the plate begins to be thicker, classical plate theories are strongly not recommended and ESL theories do not correctly model the discontinuities of displacement and stresses at layers interfaces and layerwise theories are needed to correctly represent them, whereas ESL are still capable to give a rough approximation of the macroscopic dynamical response

of whole plate. This last statement falls down when thicker and very orthotropic plates, such as sandwiches, are considered. Then the adoption of LW theories becomes mandatory for all kind of analysis.

Estratto del lavoro svolto

Le piastre sono largamente usate come componenti strutturali primari in parecchi campi ingegneristici e, con il crescente uso di laminati in materiali compositi e piastre sandwich, la loro corretta modellazione é diventata un aspetto sempre piú cruciale. Contrariamente alle piastre isotrope e sottili, anche da un punto di vista dinamico, i laminati sono caratterizzati da rapporti spessore lato mediamente elevati, soprattutto nel caso di piastre sandwich dove le peculiari proprietá di queste ultime derivano proprio dal loro intrinseco spessore. Soprattutto, le diverse proprietá meccaniche tra i diversi strati del laminato fanno si che gli spostamenti

e gli sforzi possano esibire derivate discontinue in presenza delle interfacce tra gli strati. Inoltre, a tali interfacce gli sforzi normali e i tagli trasversali devono soddisfare appropriate condizioni di continuitá per ragioni di equilibro. Per questi motivi la modellazione attraverso le teorie classiche delle piastre non é piú realistica e numerose teorie avanzate sono state sviluppate per tener conto dei suddetti effetti senza dover per forza ricorrere a modellazioni completamente 3D.

Questa tesi é focalizzata sulla modellazione avanzata di laminati e piastre sandwich, equipaggiate con una varietá di masse e patches, soggette a diverse condizioni di carico statico e dinamico. I problemi flessionali e le vibrazioni libere e forzate sono modellati adottando differenti teorie 2D avanzate grazie ad un approccio a cinematica variabile basato sulla formulazione unificata di Carrera. La soluzione di tali problemi é poi ottenuta attraverso una classica espansione alla Ritz, tale da porre un limite superiore per le frequenze proprie di una piastra con arbitrari schemi di laminazione e arbitrarie combinazioni di condizioni al contorno.

I risultati numerici ottenuti con il metodo adottato sono presentati nel proseguo per mostrare come nel caso di piastre sottili, anche dal punto di vista dinamico, gli andamenti degli spostamenti e degli sforzi siano effettivamente lineari nello spessore della piastra, mentre nel caso di piastre con elevato grado di ortotropia e spessore comparabile con le altre dimensioni, ció non sia piú vero e le discontinuitá presenti alle interfacce non riescano ad essere correttamente valutate a meno di impiegare teorie con una cinematica

dedicata ad ogni strato del laminato. Verrá ora presentato un estratto riassuntivo dei risultati piú significativi trovati, utili per apprezzare le differenze caratteristiche dei risultati ottenibili attraverso due diverse famiglie di teorie avanzate: le ESL, nelle quali la cinematica é la stessa per descrivere ogni strato della piastra e le LW, nelle quali ogni strato ha una sua cinematica dedicata con opportune condizioni di continuitá interlaminare.

In figura 1 sono rappresentati gli andamenti nello spessore della piastra della componente xx degli sforzi, sia per una piastra sottile sia per una spessa, entrambe fatte dello stesso materiale ortotropo e con lo stesso schema di laminazione.

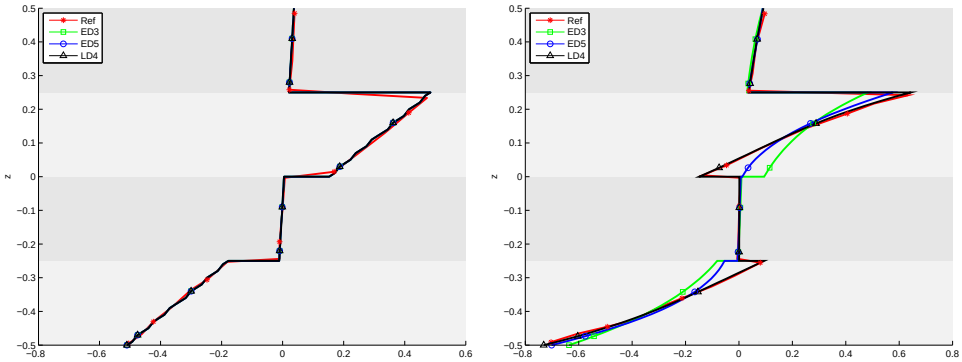

Figure 1: σ_{xx} adimensionale valutato a $(\frac{a}{2}, \frac{b}{2})$, per una piastra sottile, $\frac{h}{a} = 0.01$, (sinistra) ed una piastra spessa, $\frac{h}{a} = 0.25$, (destra). Laminato in materiale ortotropico, $\frac{E_1}{E_2} = 40$, schema di laminazione (0/90/0/90)

Come si puó notare, per il caso di piastra sottile gli andamenti per le varie teorie sono concordanti e lineari strato per strato, mentre nel caso di piastra spessa questo non é piú vero e si vengono inoltre a creare degli andamenti a $Zig\ Zag$, caratterizzati da derivate discontinue nelle interfacce tra gli strati. Per carpire questi andamenti l'adozione di teorie LW é richiesta, mentre le teorie ESL garantiscono solo una migliore approssimazione globale rispetto a ció che sarebbe possibile adottando teorie classiche. Questa approssimazione é migliorabile aumentando l'ordine della teoria adottata.

In tabella 1 sono riportate le prime sei frequenze proprie di una piastra sandwich quadrata con un riempimento estremamente soffice, sia nel caso di piastra sottile sia in quello di piastra moderatamente spessa.

Spessore	Teoria	Frequenze proprie adimensionali					
		$\bar{\omega_1}$	$\bar{\omega_2}$	$\bar{\omega_3}$	$\bar{\omega_4}$	$\bar{\omega_5}$	$\bar{\omega_6}$
$\frac{h}{a} = 0.01$	ED3	15.5455	39.2599	39.2599	55.1396	73.4883	73.4883
	ED5	12.8426	26.3405	26.3405	35.1669	41.6706	41.6706
	LD2	11.9457	23.4140	23.4140	30.9599	36.1634	36.1634
	LD3	11.9457	23.4140	23.4140	30.9599	36.1634	36.1634
$\frac{h}{a} = 0.1$	ED3	4.9618	8.1928	8.1928	10.5185	11.9857	11.9857
	ED5	2.1587	3.6851	3.6851	4.8601	5.8204	5.8204
	LD2	1.8492	3.2217	3.2217	4.2925	5.2270	5.2270
	LD3	1.8492	3.2217	3.2217	4.2925	5.2267	5.2267

Table 1: Prime sei frequenze proprie di una piastra sandwich con riempimento soffice e differenti spessori

Come si puó notare, le teorie ESL sovrastimano le frequenze sia nel caso sottile che in quello spesso, in quest'ultimo in maniera drammatica. Tale sovrastima nasce dalla descrizione del campo di spostamento di tutta la piastra tramite variabili globali, non capaci di approssimare efficacemente le grandi diversitá delle proprietá meccaniche tra le facce e il riempitivo del sandwich. Tale cattiva stima porta a sovrastimare la rigidezza della piastra stessa, portando non solo a delle frequenze proprie piú elevate ma anche ad una risposta dinamica completamente diversa, come si puó notare in figura 2.

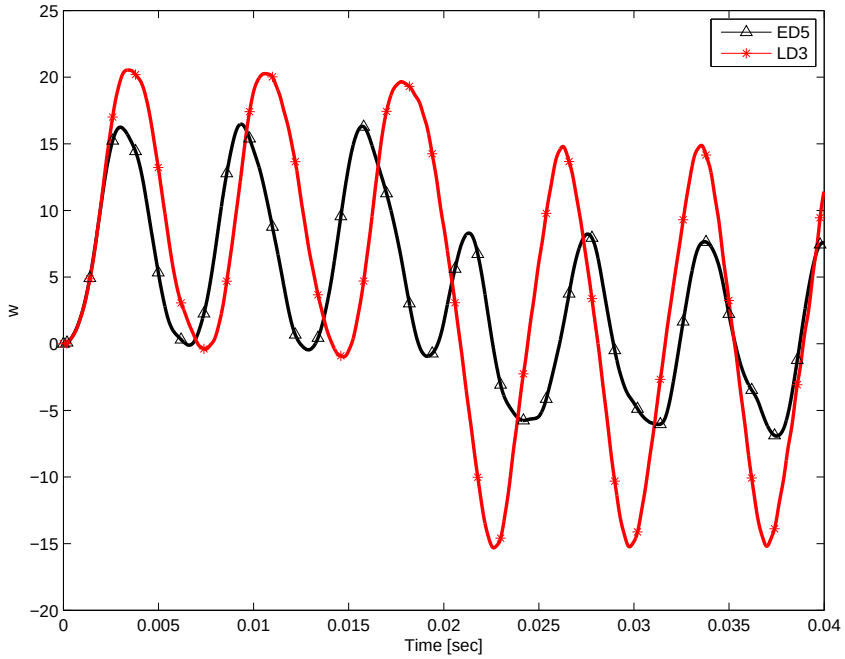

Figure 2: Spostamento trasversale adimensionale $\bar{w}(t)$. Risposta al transitorio valutata alle coordinate $(\frac{a}{2}, \frac{b}{2}, 0)$, per una piastra sandwich quadrata

Da questa figura é facile notare come la sovrastima della rigidezza della piastra porti ad una risposta dinamica totalmente diversa tra il modello ESL e quello LW, infatti la risposta ESL non solo é piú veloce ma con un ampiezza minore, entrambi classici indicatori di una rigidezza piú alta rispetto a quella del modello LW. Da notare come queste differenze siano evidenti anche se la teoria ESL considerata é del quinto ordine, cioé molto raffinata. ció porta a sconsigliare vivamente la modellazione di sandwich con teorie classiche o di basso ordine in quanto darebbero risultati assolutamente non veritieri. Queste differenze portano a dire che la modellazione di piastre sandwich puó essere fatta con modelli ESL solo nel caso interessi una rozza approssimazione di una risposta statica, mentre, per un'approssimazione piú realistica o se una risposta dinamica é cercata, l'adozione di teorie LW diventa obbligatoria.

Il lavoro é poi proseguito ipotizzando la presenza di equipaggiamento sulle superfici delle piastre, modellato come masse perfettamente incollate o sospese elasticamente e patches, cioé strati di dimensione ridotta dotati di una propria rigidezza. Le analisi sono state rivolte alla valutazione di come la presenza di equipaggiamento puó variare il comportamento dinamico caratteristico della piastra, creando possibili accoppiamenti indesiderati.

Table of Contents

List of Figures

List of Tables

List of Acronyms

CPT Classical Plate Theory

CUF Carrera Unified Formulation

ESL Equivalent Single Layer

FEM Finite Element Method

FRF Frequency Response Function

FSDT First-order Shear Deformation Theory

HSDT Higher-order Shear Deformation Theory

LW Layer Wise

DOF Number of Degrees Of Freedom

PVW Principle of Virtual Works

TSDT Third-order Shear Deformation Theory

ZZ Zigzag

Chapter 1

Introduction

In the past decades composite materials have been increasingly used in many engineering fields, such as civil, marine, aerospace and automotive, to create lightweight components with precise characteristics in terms of mechanical, electrical and chemical properties. With the growth of the knowledge of these materials, composite components which at the beginning were adopted to save weight in secondary part of structures, has became the backbone of almost all high performance structures to create efficient and lightweight primary structural components. Nowadays it is common that the chassis of racing car or the framework of a plane, and recently also its wings, are made by composite materials.

Space engineering has always been a field focused into the pursuit of extreme efficiency in all aspects of the whole design of spacecraft and rockets to save mass, since every minimal increase of weight led to other increases in terms of fuel or structural masses. Composite materials are commonly applied to spacecraft parts due to their high strength, feasible stiffness-to-weight ratios, and low thermal expansion coefficient. Despite the fact that the traditional aluminium honeycomb sandwich panel is the most commonly used panel type in satellite structures, the use of lightweight composite materials is increasing in the manufacturing of spacecraft structures thanks to the advantages that they have, not only for their light weight, but also for their durability and structural stability upon temperature variations when used in conjunction with metals.

As their operating characteristics, satellites experience several types of mechanical, thermal, and electromagnetic disturbances during their development, launch and operating life in space. Among them, vibration must be carefully considered in the design of structural components to sustain correctly the launch loads and do not create coupling between equipments attached to them. In fact, while the launch phase is carried out with con-

fidence, coupling between spacecraft equipments and structural components are subject of studies: the improvements of scientific instruments and the pursuit of new, challenging scientific goals, have arose new criticality in the structural design of a satellite: Spacecraft microvibrations are defined as very low amplitude disturbances which can occur at any frequency between 1 and 1000 Hz and are due to the normal functioning of spacecraft components, like reaction wheels or thrusters. Despite the low amplitude of these disturbances they can significantly degrade the performance of sensitive instruments [8].

The correct understandings of this phenomena, needed to design correctly the structure of the new generation of scientific spacecraft, and, to develop passive and also active vibration control and vibration suppression systems, is subordinate to a precise modelling of the components involved, to get realistic results from the structural analysis performed onto them. In a more general speaking, refined structural models are required every time a precise design of a component is sought, although it will be mounted in a spacecraft or in any kind of structure.

The spreading of composite materials, in conjunction with the need of precise components models, have led the way to 3D modelling techniques, better suited to handle the peculiar mechanical characteristics of composite materials which are anisotropic or, at least orthotropic. 3D models however are very large and requires powerful calculators to perform very demanding analysis in terms of computing power and time, which are not so suited when huge optimization studies have to be carried out in the preliminary stages of the design process. For this reason, when the shape of the structural component does not need a 3D modelling, its preferable to relay on lighter, and thus less computationally demanding, 2D modelling. This is the classical case of plates or shells with not accentuated curvatures, with which a 3D modelling is used principally to create fine benchmark models.

Plates are often used in many engineering applications as primary structures, and with the growing use of laminated composite and sandwich plates, accurate assessment of their response is becoming more and more crucial. Most of the satellites developed in the last years in the world have frame-panel composite structures, however new satellite structure design concept suggested to eliminate the need for a frame and joining composite sandwich panels together [9].

Contrary to single-layer metallic structures made of isotropic materials, multilayered constructions are typically characterized by high shear deformation, displacements in the thickness direction may exhibit discontinuous derivatives in correspondence to each layer interface and, in addition for equilibrium reasons, transverse shear and normal stresses shall satisfy appropriate interlaminar continuity conditions.

1.1 State of the art: Plate models

Several plate theories have been developed to calculate the flexural response of plates and to provide results that will match the solution of the elasticity equations. Effort has been done to identify which aspects of the plates behaviour shall be properly modelled, with the aim of obtaining a reliable but simple models without unnecessary complexity.

1.1.1 Classical plate theories

Among plate theories, the classical plate theory, CPT, is most widely known and adopted. It is based on the Kirchoff-Love hypothesis [7] which extend to plates the Bernoulli-Euler theory of beams, which assumes a linear variation of bending strain across thickness, neglecting the effects of transverse shear.

Another theory widely used is the first order shear deformation theory, $FSDT$, based on the Reissner-Mindlin plate model. Transverse shear strains are assumed to be uniform through the thickness of the plate as CPT, and as CPT, it fails to predict the changes in shear strains caused by the variation of material properties of each layer while multilayered plates are considered. Another drawback of this theory is the nonzero shear strain at top and bottom free surfaces of the plate that violates the physical boundary conditions. Normally, a shear correction factor is introduced to get nonzero shear strain at free lateral surfaces.

Both these theories gives acceptable results only for thin plates, vibrating at relatively low frequencies, where transverse shear effects are negligible. In fact, a plate to be considered *thin*, by a dynamical point of view, shall has not only one dimension very smaller with respect of the other two, but that dimension shall be also smaller of the dimension of the half waves associated at the highest vibration mode shape of interest.

Under those rigid hypothesis CPT and $FSDT$ gives a reasonable approximation of the plate dynamical behaviour with a simple model that could be handled by hand or by the calculation capabilities available at the time they were derived.

A refinement of $FSDT$ is the third order shear deformation theory $TSDT$, developed by [10]. $TSDT$ has only five degrees of freedom just as $FSDT$, but it accommodates a cubic variation of the transverse shear strains so that no shear correction factor is required.

1.1.2 Advanced plate theories

Classical plate theories are not capable to correctly model the mechanical behaviour in case of multilayered composite plates made of different materials with arbitrary stacking sequences and to overcome this problem, advanced plate theories have been developed. These more refined theories include an enriched set of kinematic variables while preserving the 2D nature of the models. Then, more complicate problems, including static and dynamic response of laminated and sandwich plates with moderate thickness to length ratios or high degree of orthotropy, can be solved with better accuracy, without the need of computational demanding 3D analysis.

The subsequent step to get a more refined plate model is the adoption of one of the displacement-based higher-order equivalent single layer ESL theories, where the conventional single-layer displacement form of $FSDT$ is enriched with various high-order terms as power series expansion of the thickness coordinate. The idea at the base of family of ESL theories is simple: augmenting the order of the theory, and so, adding terms of high order to the kinematic of the model, the precision of the modelling will be improved. As shown in the following of this work, this idea is not true at all, since after a certain point augmenting the order of the theory the approximation will not improve so much or not at all, especially if the property of the composite are highly orthotropic, the plate is thick or there is a great difference between the layers of the laminate.

To overcome this last problem and, to accurately model the through-the-thickness distribution of displacements and stresses due to the variations of material stiffness from layer to layer, layerwise LW theories have been developed [11]. LW theories models each layer of the laminate with independent degrees of freedom, hypothesizing that the layers are perfectly bonded. Using this family of theories, increasing the order of distribution of the unknowns parameters along the thickness of the plate, the results tend to completely converge to the exact 3D values also for multilayered or sandwich thick plates.

The implementation of these theories can be very difficult and cumbersome, especially for problems with which both ESL or LW theories can be adopted without a prior definite choose between them. A powerful approach, referred as Carrera unified formulation CUF [5], resolve this problem and permit to handle in an unified manner both families of ESL and LW axiomatic plate theories with variable kinematic properties [18]. The attribute variable kinematic stands for the property of the formulation of being invariant with respect to the specific plate theory. In other words, the kinematics of the plate model, from the very simple to the very complex, can be conveniently changed without the need of a new mathematical development each time.

1.2 Aim of the thesis

This thesis is focused in the advanced modelling of thick laminate or sandwich plates, equipped with masses or patches and loaded with various types of static or time dependant forces. The bending, free and forced vibration problems are solved with different 2D theories adopting a variable kinematic approach based onto the Carrera unified formulation.

Starting from the constitutive equations of plates expressed for a k-th layer, the first step of this work has the goal to find the fundamental CUF nuclei formulation of laminate plates, and then plates equipped with punctual and distributed loads, punctual and distributed attached masses, suspended masses and then patches.

The solution of the problem is then sought adopting the Ritz method, capable of providing upper-bound vibration solutions for plates with arbitrary laminate layups and arbitrary boundary conditions. Hence, once the nuclei are derived for the discretization chosen, the assembly procedure from nuclei to plate matrices is presented. Moreover, an overview of the solution methods adopted to calculate the dynamic responses in terms of time and frequencies is also presented.

Finally, a brief description and the numerical results of plate problems analyzed are presented. The results clearly show that, the more the plate is thin, the more the distribution of displacements along the thickness of the plate tends to be linear and so, classic plate theories are adequate in providing accurate results. On the other hand, as the plate thickness increases, advanced layerwise theories are necessary to correctly model the dynamic behaviour of the plate, especially in modelling softcore sandwich plates.

Chapter 2

Constitutive equations

2.1 Generalized Hooke's law

Constitutive equations are the mathematical laws describing how strain and stress are related each other for every materials and characterize theirs response to applied loads. In addition to the assumption of small displacements and displacement gradients, here we shall consider only elastic materials with linear behaviour. An elastic material will return to its initial configuration upon unloading and the configuration adopted by a stressed elastic material does not depend upon the history of loading.

The following dissertation is not intended to be comprehensive, for further details the interested reader might be relay on [12], [14].

Generalized Hooke's law is considered for mechanical case by employing a linear constitutive model for infinitesimal deformations. These equations are obtained in material coordinates and then modified in a general reference system.

In general, for an anisotropic material, the generalized Hooke's law is given in contracted notation as:

$$\sigma_{ij} = C_{ijkl}\epsilon_{kl} \tag{2.1}$$

Where σ_{ij} and ϵ_{kl} are respectively the stress and the strain tensors, and C_{ijkl} is the stiffness tensor, all referred to an orthogonal cartesian coordinate system (x_1, x_2, x_3). Both stress ad strain tensors are symmetric,

$$\sigma_{ij} = \sigma_{ji} \qquad\qquad \epsilon_{kl} = \epsilon_{lk} \tag{2.2}$$

Hence, only six independent components of stress are related to six independent components of strain. As a result, there are at most 36 distinct elastic

coefficients in the stiffness tensor since:

$$C_{ijkl} = C_{jikl} \tag{2.3}$$

Furthermore the elastic coefficients also possess the following symmetry:

$$C_{ijkl} = C_{klij} \tag{2.4}$$

Which reduces the the number of independent components of the stiffness tensor C to 21. Moreover, the following matrix notation can be adopted

$$\boldsymbol{\sigma} = \boldsymbol{C}\boldsymbol{\epsilon} \tag{2.5}$$

or, more explicitly, in the material coordinate system (x_1, x_2, x_3):

$$\begin{Bmatrix} \sigma_{11} \\ \sigma_{22} \\ \sigma_{33} \\ \sigma_{23} \\ \sigma_{31} \\ \sigma_{12} \end{Bmatrix} = \begin{bmatrix} C_{11} & C_{12} & C_{13} & C_{14} & C_{15} & C_{16} \\ & C_{22} & C_{23} & C_{24} & C_{25} & C_{26} \\ & & C_{33} & C_{34} & C_{35} & C_{36} \\ & & & C_{44} & C_{45} & C_{46} \\ & sym & & & C_{55} & C_{56} \\ & & & & & C_{66} \end{bmatrix} \begin{Bmatrix} \epsilon_{11} \\ \epsilon_{22} \\ \epsilon_{33} \\ \epsilon_{23} \\ \epsilon_{31} \\ \epsilon_{12} \end{Bmatrix} \tag{2.6}$$

It is also assumed that the above relation is invertible. Thus, the components of strain are related to the components of stress by

$$\boldsymbol{\epsilon} = \boldsymbol{C}^{-1}\boldsymbol{\sigma} = \boldsymbol{S}\boldsymbol{\sigma} \tag{2.7}$$

where S is the material compliance matrix.

What presented above refers to the general case of a solid body made of anisotropic material. Further reduction in the number of independent stiffness and compliance parameters comes from the material symmetry. When the material possesses one or more planes of symmetry, the number of independent elastic coefficients is reduced. For materials with three mutually orthogonal planes of symmetry, called *orthotropic materials*, the number of material parameters reduces to 9, while, materials which has identical mechanical properties in every direction are called *isotropic materials* and the number of material parameters have a further reduction to 3 parameters. In this thesis only isotropic and orthotropic materials are considered.

2.1.1 Isotropic material

For isotropic materials, the Hooke's law in the material coordinate system takes the following form:

$$\begin{Bmatrix} \sigma_{11} \\ \sigma_{22} \\ \sigma_{33} \\ \tau_{23} \\ \tau_{31} \\ \tau_{12} \end{Bmatrix} = \begin{bmatrix} C_{11} & C_{12} & C_{12} & 0 & 0 & 0 \\ C_{12} & C_{11} & C_{12} & 0 & 0 & 0 \\ C_{12} & C_{12} & C_{11} & 0 & 0 & 0 \\ 0 & 0 & 0 & C_{44} & 0 & 0 \\ 0 & 0 & 0 & 0 & C_{44} & 0 \\ 0 & 0 & 0 & 0 & 0 & C_{44} \end{bmatrix} \begin{Bmatrix} \epsilon_{11} \\ \epsilon_{22} \\ \epsilon_{33} \\ \gamma_{23} \\ \gamma_{31} \\ \gamma_{12} \end{Bmatrix} \tag{2.8}$$

Where the engineering stress and strain vectors have been used,

$$\tau_{23} = \sigma_{23} \tag{2.9}$$
$$\tau_{31} = \sigma_{31} \tag{2.10}$$
$$\tau_{12} = \sigma_{12} \tag{2.11}$$
$$\gamma_{23} = 2\epsilon_{23} \tag{2.12}$$
$$\gamma_{31} = 2\epsilon_{31} \tag{2.13}$$
$$\gamma_{12} = 2\epsilon_{12} \tag{2.14}$$

Due to their symmetry, isotropic materials involve only three elastic constants: C_{11}, C_{12} and C_{44}. Such components can be related to mechanical properties of the isotropic material:

$$C_{11} = \frac{E(1-\nu)}{(1+\nu)(1-2\nu)} \tag{2.15}$$
$$C_{12} = \frac{E\nu}{(1+\nu)(1-2\nu)} \tag{2.16}$$
$$C_{44} = G \tag{2.17}$$

where E is the Young modulus, ν is the Poisson ratio and $G = \frac{E}{2(1+\nu)}$ is the shear modulus of the material.

2.1.2 Orthotropic material

Orthotropic materials have three mutually orthogonal planes of elastic symmetry. In the material coordinate system, the Hooke's law takes the form:

$$\begin{Bmatrix} \sigma_{11} \\ \sigma_{22} \\ \sigma_{33} \\ \tau_{23} \\ \tau_{31} \\ \tau_{12} \end{Bmatrix} = \begin{bmatrix} C_{11} & C_{12} & C_{13} & 0 & 0 & 0 \\ C_{12} & C_{22} & C_{23} & 0 & 0 & 0 \\ C_{13} & C_{23} & C_{33} & 0 & 0 & 0 \\ 0 & 0 & 0 & C_{44} & 0 & 0 \\ 0 & 0 & 0 & 0 & C_{55} & 0 \\ 0 & 0 & 0 & 0 & 0 & C_{66} \end{bmatrix} \begin{Bmatrix} \epsilon_{11} \\ \epsilon_{22} \\ \epsilon_{33} \\ \gamma_{23} \\ \gamma_{31} \\ \gamma_{12} \end{Bmatrix} \tag{2.18}$$

The Hooke's law for orthotropic materials can be also rearranged in an alternative form, grouping the in-plane stress and strain components and the out-of-plane stress and stress components as well, taking the following form:

$$\begin{Bmatrix} \sigma_{11} \\ \sigma_{22} \\ \tau_{12} \\ \tau_{13} \\ \tau_{23} \\ \sigma_{33} \end{Bmatrix} = \begin{bmatrix} C_{11} & C_{12} & 0 & 0 & 0 & C_{13} \\ C_{12} & C_{22} & 0 & 0 & 0 & C_{23} \\ 0 & 0 & C_{66} & 0 & 0 & 0 \\ 0 & 0 & 0 & C_{55} & 0 & 0 \\ 0 & 0 & 0 & 0 & C_{44} & 0 \\ C_{13} & C_{23} & 0 & 0 & 0 & C_{33} \end{bmatrix} \begin{Bmatrix} \epsilon_{11} \\ \epsilon_{22} \\ \gamma_{12} \\ \gamma_{13} \\ \gamma_{23} \\ \epsilon_{33} \end{Bmatrix} \tag{2.19}$$

This formulation becomes very useful in developing the dynamics of laminated composite plates, as will be shown in the following chapters. Putting 2.19 in compact notation led to:

$$\boldsymbol{\sigma}_l = \boldsymbol{C}\boldsymbol{\epsilon}_l \tag{2.20}$$

Where the subscript l indicates this constitutive relation is written in the layer (or material) reference frame. Thus, for othotropic elastic bodies, there are 9 elastic constants. As done for the isotropic case, all of the components of the elastic matrix introduced above can be related to the mechanical properties of the material:

$$C_{11} = \frac{E_1(1 - \nu_{23}\nu_{32})}{\Delta} \tag{2.21}$$

$$C_{12} = \frac{E_1(\nu_{21} + \nu_{31}\nu_{23})}{\Delta} \tag{2.22}$$

$$C_{13} = \frac{E_1(\nu_{31} + \nu_{21}\nu_{32})}{\Delta} \tag{2.23}$$

$$C_{22} = \frac{E_2(1 + \nu_{31}\nu_{13})}{\Delta} \tag{2.24}$$

$$C_{23} = \frac{E_2(\nu_{32} + \nu_{31}\nu_{12})}{\Delta} \tag{2.25}$$

$$C_{33} = \frac{E_3(1 + \nu_{12}\nu_{21})}{\Delta} \tag{2.26}$$

$$C_{44} = G_{23} \tag{2.27}$$

$$C_{55} = G_{31} \tag{2.28}$$

$$C_{66} = G_{12} \tag{2.29}$$

where

$$\Delta = 1 - \nu_{12}\nu_{21} - \nu_{23}\nu_{32} - \nu_{31}\nu_{13} - 2\nu_{12}\nu_{32}\nu_{13} \tag{2.30}$$

and

$$\frac{\nu_{ij}}{E_i} = \frac{\nu_{ji}}{E_j} \qquad (i,j = 1,2,3) \tag{2.31}$$

where E_i are the Young moduli in the i material direction, ν_{ij} are the Poisson ratios and G_{ij} are the shear moduli in (i,j) planes respectively.

2.2 Reference frame rotation in multilayered plates

Composite plates are typically multilayered laminated plates, so it is convenient to write the Hooke's law both in the layer reference frame (x_1, x_2, x_3) and in the plate reference frame (x, y, z). In fact, composite laminates have several layers, each with different orientation of their material coordinates with respect to the plate coordinates. As presented by [11], consider the two different coordinate systems previously introduced such that x_3 axis is parallel to z axis and the x_1 axis is oriented at the angle ϑ counterclockwise from the $x$axis.

The coordinates of a material point in the two coordinate systems are related as follows:

$$\begin{Bmatrix} x \\ y \\ z \end{Bmatrix} = \begin{bmatrix} cos(\vartheta) & -sin(\vartheta) & 0 \\ sin(\vartheta) & cos(\vartheta) & 0 \\ 0 & 0 & 1 \end{bmatrix} \begin{Bmatrix} x_1 \\ x_2 \\ x_3 \end{Bmatrix} = \boldsymbol{L} \begin{Bmatrix} x_1 \\ x_2 \\ x_3 \end{Bmatrix} \tag{2.32}$$

Since the stress and strain tensors are second-order tensors, it is possible to transform them according to the formulas:

$$\boldsymbol{\sigma}_l = \boldsymbol{L}^T \boldsymbol{\sigma} \boldsymbol{L} \qquad \boldsymbol{\sigma} = \boldsymbol{L} \boldsymbol{\sigma}_l \boldsymbol{L}^T \tag{2.33}$$

$$\boldsymbol{\epsilon}_l = \boldsymbol{L}^T \boldsymbol{\epsilon} \boldsymbol{L} \qquad \boldsymbol{\epsilon} = \boldsymbol{L} \boldsymbol{\epsilon}_l \boldsymbol{L}^T \tag{2.34}$$

Where the subscript l indicates the value referred to the layer reference frame. Carrying out the matrix multiplications in Eqs. (2.33) and (2.34), with $\boldsymbol{L}$ defined by Eq. (2.32), ad rearranging the equations, yields:

$$\boldsymbol{\sigma} = \boldsymbol{T} \boldsymbol{\sigma}_l \qquad \boldsymbol{\epsilon}_l = \boldsymbol{T}^{-1} \boldsymbol{\epsilon} \tag{2.35}$$

$$\tag{2.36}$$

where,

$$\boldsymbol{T} = \begin{bmatrix} \cos^2(\vartheta) & \sin^2(\vartheta) & -2\cos(\vartheta)\sin(\vartheta) & 0 & 0 & 0 \\ \sin^2(\vartheta) & \cos^2(\vartheta) & 2\cos(\vartheta)\sin(\vartheta) & 0 & 0 & 0 \\ \cos(\vartheta)\sin(\vartheta) & -\cos(\vartheta)\sin(\vartheta) & \cos^2(\vartheta) - \sin^2(\vartheta) & 0 & 0 & 0 \\ 0 & 0 & 0 & \cos(\vartheta) & -\sin(\vartheta) & 0 \\ 0 & 0 & 0 & \sin(\vartheta) & \cos(\vartheta) & 0 \\ 0 & 0 & 0 & 0 & 0 & 1 \end{bmatrix} \tag{2.37}$$

Moreover $\boldsymbol{T}^{-1} = \boldsymbol{T}^T$ and $\boldsymbol{L}^{-1} = \boldsymbol{L}^T$ since are rotation matrices. Then, Eq. 2.20 can be rewritten as:

$$\boldsymbol{\sigma} = \boldsymbol{T}\boldsymbol{C}\boldsymbol{T}^T\boldsymbol{\epsilon} \tag{2.38}$$

$$\tag{2.39}$$

Finally it is possible to write Es. (2.38) in the following compact form,

$$\boldsymbol{\sigma} = \tilde{\boldsymbol{C}}\boldsymbol{\epsilon} \tag{2.40}$$

with

$$\tilde{\boldsymbol{C}} = \boldsymbol{T}\boldsymbol{C}\boldsymbol{T}^T \tag{2.41}$$

$$\boldsymbol{\sigma} = \begin{bmatrix} \sigma_{xx} & \sigma_{yy} & \tau_{xy} & \tau_{xz} & \tau_{yz} & \sigma_{zz} \end{bmatrix}^T \tag{2.42}$$

$$\boldsymbol{\epsilon} = \begin{bmatrix} \epsilon_{xx} & \epsilon_{yy} & \gamma_{xy} & \gamma_{xz} & \gamma_{yz} & \epsilon_{zz} \end{bmatrix}^T \tag{2.43}$$

Laminated composite plates are made of N_l layers and each layer is considered here to be homogeneous, operating in the elastic range. Since the material of each layer can be different from those of the others, the constitutive relation in Eq. (2.40) must be written for the k-th layer. Introducing the superscript k to denote the k-th layer, we can write:

$$\boldsymbol{\sigma}^k = \tilde{\boldsymbol{C}}^k\boldsymbol{\epsilon}^k \tag{2.44}$$

Now, is useful to divide the constitutive equations in the in-plane and out-of-plane components [21]. Stress and strain are partitioned as,

$$\boldsymbol{\sigma}_p^k = \begin{Bmatrix} \sigma_{xx}^k \\ \sigma_{yy}^k \\ \tau_{xy}^k \end{Bmatrix} \quad \boldsymbol{\sigma}_n^k = \begin{Bmatrix} \tau_{xz}^k \\ \tau_{yz}^k \\ \sigma_{zz}^k \end{Bmatrix} \quad \boldsymbol{\epsilon}_p^k = \begin{Bmatrix} \epsilon_{xx}^k \\ \epsilon_{yy}^k \\ \gamma_{xy}^k \end{Bmatrix} \quad \boldsymbol{\epsilon}_n^k = \begin{Bmatrix} \gamma_{xz}^k \\ \gamma_{yz}^k \\ \epsilon_{zz}^k \end{Bmatrix} \tag{2.45}$$

The matrix of stiffness coefficients, $\tilde{\boldsymbol{C}}^k$, follows a similar partition:

$$\tilde{\boldsymbol{C}}^k_{pp} = \begin{bmatrix} \tilde{C}^k_{11} & \tilde{C}^k_{12} & \tilde{C}^k_{16} \\ \tilde{C}^k_{12} & \tilde{C}^k_{22} & \tilde{C}^k_{26} \\ \tilde{C}^k_{16} & \tilde{C}^k_{26} & \tilde{C}^k_{66} \end{bmatrix} \qquad \tilde{\boldsymbol{C}}^k_{pn} = \begin{bmatrix} 0 & 0 & \tilde{C}^k_{13} \\ 0 & 0 & \tilde{C}^k_{23} \\ 0 & 0 & \tilde{C}^k_{36} \end{bmatrix} \tag{2.46}$$

$$\tilde{\boldsymbol{C}}^k_{np} = \begin{bmatrix} 0 & 0 & 0 \\ 0 & 0 & 0 \\ \tilde{C}^k_{13} & \tilde{C}^k_{23} & \tilde{C}^k_{36} \end{bmatrix} \qquad \tilde{\boldsymbol{C}}^k_{nn} = \begin{bmatrix} \tilde{C}^k_{55} & \tilde{C}^k_{45} & 0 \\ \tilde{C}^k_{45} & \tilde{C}^k_{44} & 0 \\ 0 & 0 & \tilde{C}^k_{33} \end{bmatrix} \tag{2.47}$$

Finally, it's possible to obtain the constitutive equations for the k-th layer in the plate reference system:

$$\boldsymbol{\sigma}^k_p = \tilde{\boldsymbol{C}}^k_{pp}\boldsymbol{\epsilon}^k_p + \tilde{\boldsymbol{C}}^k_{pn}\boldsymbol{\epsilon}^k_n \tag{2.48}$$

$$\boldsymbol{\sigma}^k_n = \tilde{\boldsymbol{C}}^k_{np}\boldsymbol{\epsilon}^k_p + \tilde{\boldsymbol{C}}^k_{nn}\boldsymbol{\epsilon}^k_n \tag{2.49}$$

Chapter 3

Advanced plate theories

The plate approximation makes possible to reduce a 3D problem to a 2D one. Plates are typically defined as 2D flat structures, where one dimension, generally the thickness h, is at least one order of magnitude lower than representative in-plane dimensions a and b which lies on the reference plate surface Ω.

A multilayered plate, which is the common case of plate made by composite materials, is a plate made by several layers bonded together under a lamination scheme that indicates the sequence and the relative direction of the layer reference frame (x_l, y_l, z) with respect to the plate reference frame (x, y, z), as stated in section 2.2 and sketched in figure: 3.1. The lamination scheme also indicates the layers thickness that can be different for each one. Ω is the middle reference surface of the multilayered plate while Ω_k is the reference surface for each k layer of thickness h_k. A local reference frame (x_k, y_k, z_k), directed as the plate reference frame, can be defined for each layer.

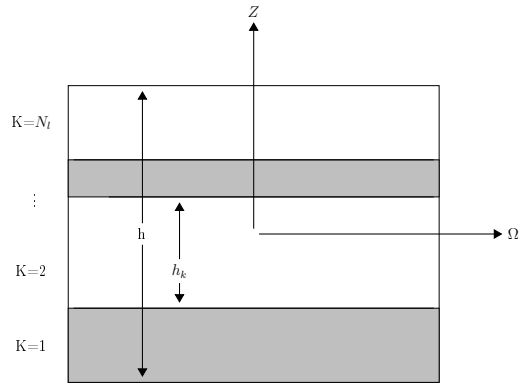

Figure 3.1: Geometrical notation for a multilayer plate

The 2D modeling of plates relies on the elimination of the thickness coordinate z, which is usually performed on integration of the equilibrium equations, compatibility equations, and physical constitutive relations.

While analyzing multilayered plates, new effects can arise with respect to isotropic plates. In fact in-plane anisotropies and transverse anisotrpies can occur. The former means that the structure has different mechanical properties in different in-plane directions, the latter means that the structures exhibit different mechanical properties in the thickness direction z. A consequence of in-plane anisotropy is coupling between shear and axial strains. Such a coupling leads to many complications in the solution procedure of an anisotropic structure. Discontinuous transverse mechanical properties cause a displacement field, $\boldsymbol{u}$, in the thickness direction which can exhibit a rapid change in its slopes corresponding to each layer interface. This effect is known as the *Zig Zag* form of the displacement field in the thickness direction z, and it is clearly visible in the sandwich structure. In-plane anisotrpy is taken into account making use of ESL family of theories while, in order to consider the *Zig Zag* form of displacements in deformed multilayered structures, a Layerwise approach may be necessary.

3.1 Carrera unified formulation

As stated by [5], the *Carrera unified formulation*, *CUF*, is a technique that permits to handle and implement easily a large variety of plate models in a unified manner. According to *CUF*, the obtained theories can have any order of expansion and can be chose between LW and ESL families select-

ing different thickness functions. ESL theories can be enriched to cope with those stated by Murakami to be capable of recognize the *Zig Zag* effects [19], however this kind of theories can not be adopted in this study.

With CUF, governing equations are written in terms of a fundamental nuclei which do not formally depend nor on the order of expansion N used in the z direction nor on the family of theories used.

CUF is based on the following general assumption:

$$\boldsymbol{u}(x,y,z,t) = F_\tau(z)\boldsymbol{u}_\tau(x,y,t) \qquad \tau = t,b,r \qquad r = 2,3,...,N \tag{3.1}$$

where $F_\tau(z)$ are given thickness functions and $\boldsymbol{u}_\tau(x,y,t)$ are unknown variables,

$$\boldsymbol{u}_\tau(x,y,t) = \begin{Bmatrix} u_\tau(x,y,t) \\ v_\tau(x,y,t) \\ w_\tau(x,y,t) \end{Bmatrix} \tag{3.2}$$

Note that the Einstein's convention of summation of indexes has been adopted in Eq (3.1). In this way, CUF reduces the 3D problem to a 2D one, obtaining the following displacements field,

$$\boldsymbol{u} = F_\tau \boldsymbol{u}_\tau = F_t\boldsymbol{u}_t + F_b\boldsymbol{u}_b + F_r\boldsymbol{u}_r = \begin{Bmatrix} F_t u_t + F_b u_b + F_r u_r \\ F_t v_t + F_b v_b + F_r v_r \\ F_t w_t + F_b w_b + F_r w_r \end{Bmatrix} \quad r = 2,3,...,N \tag{3.3}$$

Subscripts t and b indicate top and bottom and, as shown later, are useful in the assembling procedure of multilayered plates. N denotes the order of expansion used. Several theories can be implemented with this formulation, employing the appropriate thickness functions, which will assume a different formulation for each family of theories, as shown in the followings paragraphs.

3.2 Equivalent single layer theories

In ESL family of theories, the constant and linear terms have been denoted by subscript t and b, respectively. Higher order terms are denoted by the corresponding order in Taylor expansion as follows,

$$F_t(z) = 1 \tag{3.4}$$

$$F_b(z) = z \tag{3.5}$$

$$F_r(z) = z^r \qquad r = 2,3,...,N \tag{3.6}$$

These related theories will be indicated as EDN, where the first letter denotes that the kinematics is preserved for the whole layers of the plate, the second letter denotes that only displacements unknowns are used and the last number denotes the order of expansion in z. Shall be noted that z in the physical thickness coordinate, referred to the middle reference surface of the multilayered plate Ω.

3.2.1 ED4 theory

For example, $ED4$ theory, under CUF assumptions, will be formulated as:

$$\boldsymbol{u} = F_\tau \boldsymbol{u}_\tau \qquad\qquad \tau = t, b, 2, 3, 4 \tag{3.7}$$

where

$$F_t = 1 \qquad\qquad F_b = z \tag{3.8}$$

$$F_2 = z^2 \qquad\qquad F_3 = z^3 \qquad\qquad F_4 = z^4 \tag{3.9}$$

In explicit form

$$\boldsymbol{u} = \left\{ \begin{array}{c} u_0 + z u_1 + z^2 u_2 + z^3 u_3 + z^4 u_4 \\ v_0 + z v_1 + z^2 v_2 + z^3 v_3 + z^4 v_4 \\ w_0 + z w_1 + z^2 w_2 + z^3 w_3 + z^4 w_4 \end{array} \right\} \tag{3.10}$$

3.3 Layerwise theories

The family of LW theories involve kinematics which are independent for each layer. Hence, it is possible to write Eq. (3.3) as follows

$$\boldsymbol{u}^k = F_\tau \boldsymbol{u}_\tau^k = F_t \boldsymbol{u}_t^k + F_b \boldsymbol{u}_b^k + F_r \boldsymbol{u}_r^k = \left\{ \begin{array}{c} F_t u_t^k + F_b u_b^k + F_r u_r^k \\ F_t v_t^k + F_b v_b^k + F_r v_r^k \\ F_t w_t^k + F_b w_b^k + F_r w_r^k \end{array} \right\} \quad r = 2, 3, ..., N \tag{3.11}$$

The Taylor thickness expansion used for ESL theories is now substituted by a more convenient description to impose easily the interlaminar continuity for displacements. Moreover, in the case of LW models, the thickness functions are function of the local layer thickness coordinate $\zeta_k = \frac{2}{h_k} z - \frac{z_{k+1}+z_k}{h_k}$, defined in the domain $-1 \leq \zeta_k \leq +1$. This leds to thickness functions defined by

$$F_t(\zeta_k) = \frac{P_0 + P_1}{2} \tag{3.12}$$

$$F_b(\zeta_k) = \frac{P_0 - P_1}{2} \tag{3.13}$$

$$F_r(\zeta_k) = P_r - P_{r-2} \qquad\qquad r = 2, 3, ..., N \tag{3.14}$$

where $P_i(\zeta_k)$ is the Legendre polynomial of i-th order.
The chosen functions have the following useful properties:

$$\zeta_k = \begin{cases} 1 & \rightarrow \quad F_t = 1, \quad F_b = 0, \quad F_r = 0 \\ -1 & \rightarrow \quad F_t = 0, \quad F_b = 1, \quad F_r = 0 \end{cases} \tag{3.15}$$

Thus, the displacement variables $\boldsymbol{u}_b$ and $\boldsymbol{u}_t$ are respectively the displacements at the bottom and top surfaces of the layer and the inter-laminar continuity can be easily imposed as follows:

$$\boldsymbol{u}_t^k = \boldsymbol{u}_b^{k+1} \qquad\qquad k = 1, 2, ..., Nl - 1 \tag{3.16}$$

where N_l denotes the number of layers of the plate.

Such related theories will be indicated as LDN, where the first letter denotes that the kinematics is assumed independent for each layer of the plate, the second letter denotes that only displacement unknowns are used and the last number denotes the order of expansion in ζ_k direction.

3.3.1 LD4 theory

For example, $LD4$ theory, under CUF assumptions, the displacement field for the k-th layer will be formulated as:

$$\boldsymbol{u}^k(x, y, \zeta_k) = \left\{ \begin{array}{c} F_t(\zeta_k)u_t^k + F_b(\zeta_k)u_b^k + F_2(\zeta_k)u_3^k + F_3(\zeta_k)u_3^k + F_4(\zeta_k)u_4^k \\ F_t(\zeta_k)v_t^k + F_b(\zeta_k)v_b^k + F_2(\zeta_k)v_3^k + F_3(\zeta_k)v_3^k + F_4(\zeta_k)v_4^k \\ F_t(\zeta_k)w_t^k + F_b(\zeta_k)w_b^k + F_2(\zeta_k)w_3^k + F_3(\zeta_k)w_3^k + F_4(\zeta_k)w_4^k \end{array} \right\} \tag{3.17}$$

where the thickness function are formulate as in Eqs: (3.12 - 3.14), with the first five Legendre polynomials defined as:

$$P_0 = 1 \tag{3.18}$$

$$P_1 = \zeta_k \tag{3.19}$$

$$P_2 = \frac{3\zeta_k^2 - 1}{2} \tag{3.20}$$

$$P_3 = \frac{5\zeta_k^3 - 3\zeta_k}{2} \tag{3.21}$$

$$P_4 = \frac{35\zeta_k^4 - 30\zeta_k^2 + 3}{8} \tag{3.22}$$

$$\tag{3.23}$$

Chapter 4

Derivation of the equations of motion

The Principle of virtual works PVW has been used to retrieve the equation of motion of the plate firstly, and then for retrieve the terms related to the plates equipments. To exploit the whole potential of the CUF technique, and moreover to develop a formulation valid to analyze plates with every combination of homogeneous boundary conditions and arbitrary lamination scheme a Ritz-Galerkin approach is adopted for discretizing the continuous plate domain in its plane Ω.

The Ritz method is capable of providing a global approximation and an upper bound vibration solutions, has an high spectral accuracy and converge faster than local methods such as finite elements. Since the Ritz approximation will be derived relaying to CUF technique, the formulation can be defined as a *variable kinematic Ritz* formulation [22]. The formulation will be derived for both ESL and LW families of theories for rectangular and skew laminated plates with homogeneous boundary conditions and homogeneous layers. In this work, boundary conditions are considered to be homogeneous through the height of the same edge section, so, identical boundary conditions are imposed in each layer of the plate edge.

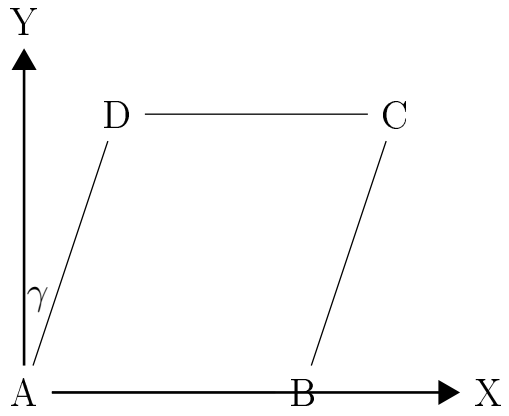

Figure 4.1: Geometrical notation for a skew plate

A skew flat laminated plate of total thickness h is considered. The plate has side lengths a,b, and skew angle γ with respect to y axis as shown in figure 4.1. The plate consists of N_l layers, which are assumed to be made of orthotropic material. The k-th layer has thickness h_k and is located between interfaces $z = z_k$ and $z = z_{k+1}$ in the thickness direction. In this work, the layer numbering begins at the bottom surface of the laminate. A four letter compact symbolic notation is used for describing simply supported (S), clamped (C) and free (F) boundary conditions, numbered in a counterclockwise direction beginning from edge DA.

4.1 Plate equation of motion

For the sake of convenience, the plate coordinate system is expressed in nondimensional form with the following change of variables:

$$\begin{cases} \xi = \frac{2}{a}(x - y\tan\gamma) - 1 \\ \eta = \frac{2}{b}(y\sec\gamma) - 1 \\ \zeta_k = \frac{2}{h_k}z - \frac{z_{k+1}+z_k}{h_k} \end{cases} \qquad \begin{Bmatrix} \frac{\partial}{\partial x} \\ \frac{\partial}{\partial y} \\ \frac{\partial}{\partial z} \end{Bmatrix} = \begin{bmatrix} \frac{2}{a} & 0 & 0 \\ -\frac{2}{a}\tan\gamma & \frac{2}{b}\sec\gamma & 0 \\ 0 & 0 & \frac{2}{h_k} \end{bmatrix} \begin{Bmatrix} \frac{\partial}{\partial \xi} \\ \frac{\partial}{\partial \eta} \\ \frac{\partial}{\partial \zeta_k} \end{Bmatrix} \tag{4.1}$$

The constitutive equation of a generic layer k, written in the plate reference coordinate system, are those derived in precedence and expressed in Eqs: (2.48-2.49).

According to the CUF formulation the displacement vector for each k-th lamina u^k is expressed as reported in Eq: (3.1), which, adopting the

adimensionalization of the reference system proposed above becomes:

$$\boldsymbol{u}(\xi,\eta,\zeta_k,t) = F_\tau(\zeta_k)\hat{\boldsymbol{u}}_\tau(\xi,\eta)e^{j\omega t} \qquad \tau = t,b,r \qquad r = 2,3,...,N \tag{4.2}$$

where the thickness functions $F_\tau(\zeta_k)$ are those defined in the previous chapter.

According to the outlined framework, the in-plane and out of plane strain components can be written in the following form:

$$\boldsymbol{\epsilon}_p^k(\xi,\eta,\zeta_k,t) = \boldsymbol{D}_p F_\tau(\zeta_k)\hat{\boldsymbol{u}}_\tau^k(\xi,\eta)e^{j\omega t} \tag{4.3}$$

$$\boldsymbol{\epsilon}_n^k(\xi,\eta,\zeta_k,t) = \boldsymbol{D}_n F_\tau(\zeta_k)\hat{\boldsymbol{u}}_\tau^k(\xi,\eta)e^{j\omega t} + \frac{2}{h_k}F_{\tau_{/\zeta_k}}(\zeta_k)\hat{\boldsymbol{u}}_\tau^k(\xi,\eta)e^{j\omega t} \tag{4.4}$$

$$\tag{4.5}$$

with

$$\boldsymbol{D}_p = \begin{bmatrix} \frac{2}{a}\frac{\partial}{\partial\xi} & 0 & 0 \\ 0 & \frac{2}{b}\sec\gamma\frac{\partial}{\partial\eta} - \frac{2}{a}\tan\gamma\frac{\partial}{\partial\xi} & 0 \\ \frac{2}{b}\sec\gamma\frac{\partial}{\partial\eta} - \frac{2}{a}\tan\gamma\frac{\partial}{\partial\xi} & \frac{2}{a}\frac{\partial}{\partial\xi} & 0 \end{bmatrix} \tag{4.6}$$

$$\boldsymbol{D}_n = \begin{bmatrix} 0 & 0 & \frac{2}{a}\frac{\partial}{\partial\xi} \\ 0 & 0 & \frac{2}{b}\sec\gamma\frac{\partial}{\partial\eta} - \frac{2}{a}\tan\gamma\frac{\partial}{\partial\xi} \\ 0 & 0 & 0 \end{bmatrix} \tag{4.7}$$

Under those assumption the PVW for a multilayered plate can be managed as follows, starting by its definition for the 3D continuum:

$$\int_V (\delta\epsilon_{ij}\sigma_{ij})dV = -\int_V \delta u_i \rho \ddot{u}_i dV \tag{4.8}$$

Then splitting the volume domain V in the plate surface Ω_k and ζ_k direction for the k-th lamina, the PVW can be expressed as:

$$\sum_k \int_{\Omega_k}\int_{\zeta_k} \left[\delta\boldsymbol{\epsilon}_p^{k^T}\boldsymbol{\sigma}_p^k + \delta\boldsymbol{\epsilon}_n^{k^T}\boldsymbol{\sigma}_n^k\right] d\zeta_k d\Omega_k = -\sum_k \int_{\Omega_k}\int_{\zeta_k} \delta\boldsymbol{u}^{k^T}\rho^k\ddot{\boldsymbol{u}}^k d\zeta_k d\Omega_k \tag{4.9}$$

Now, substituting the constitutive equations of Eqs: (2.48-2.49) derived in the previous chapter and then the definition of strains under CUF derived above in Eqs: (4.3-4.4), the PVW becomes:

$$\sum_k \int_{-1}^{+1}\int \Bigg[\delta\Big(\boldsymbol{D}_p\hat{\boldsymbol{u}}_\tau^k\Big)^T\Big(\tilde{\boldsymbol{C}}_{pp}^k\boldsymbol{D}_pE_{\tau s}^k\hat{\boldsymbol{u}}_s^k+\tilde{\boldsymbol{C}}_{pn}^k\boldsymbol{D}_nE_{\tau s}^k\hat{\boldsymbol{u}}_s^k+\tilde{\boldsymbol{C}}_{pn}^kE_{\tau s_{/\zeta_k}}^k\hat{\boldsymbol{u}}_s^k\Big)+$$
$$+\delta\Big(\boldsymbol{D}_n\hat{\boldsymbol{u}}_\tau^k\Big)^T\Big(\tilde{\boldsymbol{C}}_{np}^k\boldsymbol{D}_pE_{\tau s}^k\hat{\boldsymbol{u}}_s^k+\tilde{\boldsymbol{C}}_{nn}^k\boldsymbol{D}_nE_{\tau s}^k\hat{\boldsymbol{u}}_s^k+\tilde{\boldsymbol{C}}_{nn}^kE_{\tau s_{/\zeta_k}}^k\hat{\boldsymbol{u}}_s^k\Big)+$$
$$+\delta\Big(\hat{\boldsymbol{u}}_\tau^k\Big)^T\Big(\tilde{\boldsymbol{C}}_{np}^k\boldsymbol{D}_pE_{\tau/\zeta_k s}^k\hat{\boldsymbol{u}}_s^k+\tilde{\boldsymbol{C}}_{nn}^k\boldsymbol{D}_nE_{\tau/\zeta_k s}^k\hat{\boldsymbol{u}}_s^k+$$
$$\tilde{\boldsymbol{C}}_{nn}^kE_{\tau/\zeta_k s/\zeta_k}^k\hat{\boldsymbol{u}}_s^k\Big)\Bigg]\frac{ab}{4}\cos\gamma d\xi d\eta e^{j\omega t}=$$
$$=\boldsymbol{\omega}^2\sum_k\int_{-1}^{+1}\int\delta\hat{\boldsymbol{u}}_\tau^kE_{\tau s}^k\boldsymbol{\rho}^k\hat{\boldsymbol{u}}_s^k\frac{ab}{4}\cos\gamma d\xi d\eta e^{j\omega t} \tag{4.10}$$

where the plate domain Ω_k is been referred to the adimensional reference frame (ξ,η) proposed above and the followings thickness integrals has been introduced:

4.1.1 Thickness integrals in ESL theories

The thickness integrals of ESL models are defined over all the plate thickness. The thickness integrals for each layer k take the form:

$$E_{\tau s}^k=\int_{z_k}^{z_{k+1}}F_\tau(z)F_s(z)dz \tag{4.11}$$
$$E_{\tau_{/z}s}^k=\int_{z_k}^{z_{k+1}}F_{\tau_{/z}}(z)F_s(z)dz \tag{4.12}$$
$$E_{\tau s_{/z}}^k=\int_{z_k}^{z_{k+1}}F_\tau(z)F_{s_{/z}}(z)dz \tag{4.13}$$
$$E_{\tau_{/z}s_{/z}}^k=\int_{z_k}^{z_{k+1}}F_{\tau_{/z}}(z)F_{s_{/z}}(z)dz \tag{4.14}$$

where $\tau,s=t,r,b$ and $k=1,...,N_l$.

4.1.2 Thickness integrals in LW theories

The thickness functions of LW models are defined over all the plate thickness. The thickness integrals for each layer k take the form:

$$E^k_{\tau s} = \frac{h_k}{2}\int_{-1}^{+1} F_\tau(\zeta_k)F_s(\zeta_k)d\zeta_k \tag{4.15}$$

$$E^k_{\tau_{/\zeta_k} s} = \int_{-1}^{+1} F_{\tau_{/\zeta_k}}(\zeta_k)F_s(\zeta_k)d\zeta_k \tag{4.16}$$

$$E^k_{\tau s_{/\zeta_k}} = \int_{-1}^{+1} F_\tau(\zeta_k)F_{s_{/\zeta_k}}(\zeta_k)d\zeta_k \tag{4.17}$$

$$E^k_{\tau_{/\zeta_k} s_{/\zeta_k}} = \frac{2}{h_k}\int_{-1}^{+1} F_{\tau_{/\zeta_k}}(\zeta_k)F_{s_{/\zeta_k}}(\zeta_k)d\zeta_k \tag{4.18}$$

where $\tau, s = t, r, b$, $k = 1, ..., N_l$ and h_k is the thickness of the k-th layer

Adopting the thickness integrals the triple integrals in the PVW become double integrals on the plain domain (ξ, η), hence it is possible to introduce the Ritz approximation.

4.1.3 Ritz approximation

A standard Ritz solution is sought by expressing the components of each displacement unknown as sets of bidimensional finite series based appropriate admissible shape functions $N_{\delta\tau i}$ $(\delta = u, v, w)$:

$$\begin{Bmatrix} \hat{u}^k_\tau \\ \hat{v}^k_\tau \\ \hat{w}^k_\tau \end{Bmatrix} = \begin{bmatrix} N_{u\tau i}(\xi,\eta) & 0 & 0 \\ 0 & N_{v\tau i}(\xi,\eta) & 0 \\ 0 & 0 & N_{w\tau i}(\xi,\eta) \end{bmatrix} \begin{Bmatrix} c^k_{u\tau i} \\ c^k_{v\tau i} \\ c^k_{w\tau i} \end{Bmatrix} \tag{4.19}$$

The bidimensional shape functions employed in this thesis are defined as:

$$N_{\delta\tau i} = \Phi_{\delta\tau m}(\xi)\Psi_{\delta\tau n}(\eta) \qquad\qquad m, n = 1, ..., P \tag{4.20}$$

where

$$\Phi_{\delta\tau m}(\xi) = f_{\delta\tau}(\xi)p_m(\xi) \tag{4.21}$$

$$\Psi_{\delta\tau n}(\eta) = g_{\delta\tau}(\eta)p_n(\eta) \tag{4.22}$$

P is the order of expansion in each direction ξ and η, and

$$p_l(\chi) = \cos[(l-1)\arccos(\chi)] \qquad l = m, n \qquad \chi = \xi, \eta \tag{4.23}$$

is the one-dimensional Chebyshev polynomial along χ direction. The Chebyshev polynomial set is a complete and orthogonal series in the interval $[-1, +1]$. This ensures that better convergence and numerical stability can be accomplished compared with other polynomial set [4]. $f_{\delta\tau}$ and $g_{\delta\tau}$ are boundary

compliant functions corresponding to the type of boundary conditions along ξ and η respectively, and, are defined as:

$$f_{\delta\tau}(\xi) = (1-\xi)^{e_1}(1+\xi)^{e_2} \tag{4.24}$$
$$g_{\delta\tau}(\eta) = (1-\eta)^{e_1}(1+\eta)^{e_2} \tag{4.25}$$

where e_1 and e_2 assumes values 0 or 1 with respect to the boundary conditions and the direction considered.
The hypothesis of homogeneous boundary condition makes that the above Ritz functions are considered to be layer independent and they can be written in compact form as:

$$\hat{\boldsymbol{u}}^k_\tau = \boldsymbol{N}_{\tau i}(\xi,\eta)\boldsymbol{c}^k_{\tau i} \tag{4.26}$$

Putting the Eq: (4.26) in the PVW expression previously derived yields:

$$\begin{aligned}
\sum_k \int_{-1}^{+1}\int \Bigg\{ \delta \boldsymbol{c}^{k^T}_{\tau i} \Bigg[\Big(\boldsymbol{D}_p \boldsymbol{N}_{\tau i}\Big)^T \Big(E^k_{\tau s}\tilde{\boldsymbol{C}}^k_{pp}\boldsymbol{D}_p\boldsymbol{N}_{sj} + E^k_{\tau s}\tilde{\boldsymbol{C}}^k_{pn}\boldsymbol{D}_n\boldsymbol{N}_{sj} + E^k_{\tau s_{/\zeta_k}}\tilde{\boldsymbol{C}}^k_{pn}\boldsymbol{N}_{sj}\Big) + \\
+ \Big(\boldsymbol{D}_n \boldsymbol{N}_{\tau i}\Big)^T \Big(E^k_{\tau s}\tilde{\boldsymbol{C}}^k_{np}\boldsymbol{D}_p\boldsymbol{N}_{sj} + E^k_{\tau s}\tilde{\boldsymbol{C}}^k_{nn}\boldsymbol{D}_n\boldsymbol{N}_{sj} + E^k_{\tau s_{/\zeta_k}}\tilde{\boldsymbol{C}}^k_{nn}\boldsymbol{N}_{sj}\Big) + \\
+ \boldsymbol{N}^T_{\tau i}\Big(E^k_{\tau_{/\zeta_k} s}\tilde{\boldsymbol{C}}^k_{np}\boldsymbol{D}_p\boldsymbol{N}_{sj} + E^k_{\tau_{/\zeta_k} s}\tilde{\boldsymbol{C}}^k_{nn}\boldsymbol{D}_n\boldsymbol{N}_{sj} + \\
+ E^k_{\tau_{/\zeta_k} s_{/\zeta_k}}\tilde{\boldsymbol{C}}^k_{nn}\boldsymbol{N}_{sj}\Big) \Bigg] \boldsymbol{c}^k_{sj} \Bigg\} \frac{ab}{4}\cos\gamma d\xi d\eta = \\
= \boldsymbol{\omega}^2 \sum_k \delta \boldsymbol{c}^{k^T}_{\tau i} \int_{-1}^{+1}\int \boldsymbol{N}^T_{\tau i} E^k_{\tau s}\boldsymbol{\rho}^k \boldsymbol{N}_{sj}\frac{ab}{4}\cos\gamma d\xi d\eta \boldsymbol{c}^k_{sj}
\end{aligned} \tag{4.27}$$

Now, as stated for the PVW, the the virtual works had to vanish and considering the arbitrariness of the virtual variation, the resultant plate equation of motion is:

$$\sum_k \boldsymbol{K}^k_{\tau sij}\boldsymbol{c}^k_{sj} = \boldsymbol{\omega}^2 \sum_k \boldsymbol{M}^k_{\tau sij}\boldsymbol{c}^k_{sj} \tag{4.28}$$

where the 3x3 matrices $\boldsymbol{K}^k_{\tau sij}$ and $\boldsymbol{M}^k_{\tau sij}$ are the Ritz fundamental nuclei of the Carrera unified formulation. Hence, introducing the following notation,

as stated in [22]:

$$I^{ef}_{\alpha m\beta\bar{m}} = \int_{-1}^{+1} \frac{d^e}{d\xi^e}[\phi_{\alpha\tau m}(\xi)]\frac{d^f}{d\xi^f}[\phi_{\beta s\bar{m}}(\xi)]d\xi \qquad m,\bar{m} = 1,2,\cdots,P \tag{4.29}$$

$$J^{ef}_{\alpha n\beta\bar{n}} = \int_{-1}^{+1} \frac{d^e}{d\eta^e}[\psi_{\alpha\tau n}(\eta)]\frac{d^f}{d\eta^f}[\psi_{\beta s\bar{n}}(\eta)]d\eta \qquad n,\bar{n} = 1,2,\cdots,P \tag{4.30}$$

which are the surface integrals of the Ritz shape functions. These integrals have been calculated numerically adopting the Gauss-Legendre method. Now for the k-th layer the terms of the Ritz stiffness nuclei can be explicitly written as:

$$\begin{aligned} K^k_{\tau sij}(1,1) = &\left(E^k_{\tau s}\tilde{C}^k_{11}\frac{b}{a}\cos\gamma - 2E^k_{\tau s}\tilde{C}^k_{16}\frac{b}{a}\sin\gamma + E^k_{\tau s}\tilde{C}^k_{66}\frac{b}{a}\tan\gamma\sin\gamma\right) I^{11}_{umu\bar{m}}J^{00}_{unu\bar{n}} \\ &+ \left(E^k_{\tau s}\tilde{C}^k_{16} - E^k_{\tau s}\tilde{C}^k_{66}\tan\gamma\right)\left(I^{10}_{umu\bar{m}}J^{01}_{unu\bar{n}} + I^{01}_{umu\bar{m}}J^{10}_{unu\bar{n}}\right) \\ &+ E^k_{\tau s}\tilde{C}^k_{66}\frac{a}{b}\sec\gamma I^{00}_{umu\bar{m}}J^{11}_{unu\bar{n}} + E^k_{\tau_{/\zeta_k}s_{/\zeta_k}}C^k_{55}\frac{ab}{4}\cos\gamma I^{00}_{umu\bar{m}}J^{00}_{unu\bar{n}} \end{aligned} \tag{4.31}$$

$$\begin{aligned} K^k_{\tau sij}(1,2) = &\left(E^k_{\tau s}\tilde{C}^k_{16}\frac{b}{a}\cos\gamma - E^k_{\tau s}\tilde{C}^k_{12}\frac{b}{a}\sin\gamma - E^k_{\tau s}\tilde{C}^k_{66}\frac{b}{a}\sin\gamma\right. \\ &\left. + E^k_{\tau s}\tilde{C}^k_{26}\frac{b}{a}\tan\gamma\sin\gamma\right) I^{11}_{umv\bar{m}}J^{00}_{unv\bar{n}} \\ &+ \left(E^k_{\tau s}\tilde{C}^k_{12} - E^k_{\tau s}\tilde{C}^k_{26}\tan\gamma\right) I^{10}_{umv\bar{m}}J^{01}_{unv\bar{n}} \\ &+ \left(E^k_{\tau s}\tilde{C}^k_{66} - E^k_{\tau s}\tilde{C}^k_{26}\tan\gamma\right) I^{01}_{umv\bar{m}}J^{10}_{unv\bar{n}} \\ &+ E^k_{\tau s}\tilde{C}^k_{26}\frac{a}{b}\sec\gamma I^{00}_{umv\bar{m}}J^{11}_{unv\bar{n}} + E^k_{\tau_{/\zeta_k}s_{/\zeta_k}}C^k_{45}\frac{ab}{4}\cos\gamma I^{00}_{umv\bar{m}}J^{00}_{unv\bar{n}} \end{aligned} \tag{4.32}$$

$$\begin{aligned} K^k_{\tau sij}(1,3) = &\left(E^k_{\tau s_{/\zeta_k}}\tilde{C}^k_{13}\frac{b}{2}\cos\gamma - E^k_{\tau s_{/\zeta_k}}\tilde{C}^k_{36}\frac{b}{2}\sin\gamma\right) I^{10}_{umw\bar{m}}J^{00}_{unw\bar{n}} \\ &+ E^k_{\tau s_{/\zeta_k}}\tilde{C}^k_{36}\frac{a}{2}I^{00}_{umw\bar{m}}J^{10}_{unw\bar{n}} \\ &+ \left(E^k_{\tau_{/\zeta_k}s}\tilde{C}^k_{55}\frac{b}{2}\cos\gamma - E^k_{\tau_{/\zeta_k}s}\tilde{C}^k_{45}\frac{b}{2}\sin\gamma\right) I^{01}_{umwv\bar{m}}J^{00}_{unw\bar{n}} \\ &+ E^k_{\tau_{/\zeta_k}s}C^k_{45}\frac{a}{2}I^{00}_{umw\bar{m}}J^{01}_{unw\bar{n}} \end{aligned} \tag{4.33}$$

$$
\begin{aligned}
K^k_{\tau sij}(2,1) = &\left(E^k_{\tau s}\tilde{C}^k_{16}\frac{b}{a}\cos\gamma - E^k_{\tau s}\tilde{C}^k_{12}\frac{b}{a}\sin\gamma - E^k_{\tau s}\tilde{C}^k_{66}\frac{b}{a}\sin\gamma \right.\\
&\left. + E^k_{\tau s}\tilde{C}^k_{26}\frac{b}{a}\tan\gamma\sin\gamma \right) I^{11}_{vmu\bar{m}}J^{00}_{vnu\bar{n}}\\
&+ \left(E^k_{\tau s}\tilde{C}^k_{12} - E^k_{\tau s}\tilde{C}^k_{26}\tan\gamma \right) I^{01}_{vmu\bar{m}}J^{10}_{vnu\bar{n}}\\
&+ \left(E^k_{\tau s}\tilde{C}^k_{66} - E^k_{\tau s}\tilde{C}^k_{26}\tan\gamma \right) I^{10}_{vmu\bar{m}}J^{01}_{vnu\bar{n}}\\
&+ E^k_{\tau s}\tilde{C}^k_{26}\frac{a}{b}\sec\gamma I^{00}_{vmu\bar{m}}J^{11}_{vnu\bar{n}} + E^k_{\tau_{/\zeta_k}s_{/\zeta_k}}C^k_{45}\frac{ab}{4}\cos\gamma I^{00}_{vmu\bar{m}}J^{00}_{vnu\bar{n}}
\end{aligned}
\tag{4.34}
$$

$$
\begin{aligned}
K^k_{\tau sij}(2,2) = &\left(E^k_{\tau s}\tilde{C}^k_{66}\frac{b}{a}\cos\gamma - 2E^k_{\tau s}\tilde{C}^k_{26}\frac{b}{a}\sin\gamma + E^k_{\tau s}\tilde{C}^k_{22}\frac{b}{a}\tan\gamma\sin\gamma \right) I^{11}_{vmv\bar{m}}J^{00}_{vnv\bar{n}}\\
&+ \left(E^k_{\tau s}\tilde{C}^k_{26} - E^k_{\tau s}\tilde{C}^k_{22}\tan\gamma \right) \left(I^{10}_{vmv\bar{m}}J^{01}_{vnv\bar{n}} + I^{01}_{vmv\bar{m}}J^{10}_{vnv\bar{n}} \right)\\
&+ E^k_{\tau s}\tilde{C}^k_{22}\frac{a}{b}\sec\gamma I^{00}_{vmv\bar{m}}J^{11}_{vnv\bar{n}} + E^k_{\tau_{/\zeta_k}s_{/\zeta_k}}C^k_{44}\frac{ab}{4}\cos\gamma I^{00}_{vmv\bar{m}}J^{00}_{vnv\bar{n}}
\end{aligned}
\tag{4.35}
$$

$$
\begin{aligned}
K^k_{\tau sij}(2,3) = &\left(E^k_{\tau s_{/\zeta_k}}\tilde{C}^k_{36}\frac{b}{2}\cos\gamma - E^k_{\tau s_{/\zeta_k}}\tilde{C}^k_{23}\frac{b}{2}\sin\gamma \right) I^{10}_{vmw\bar{m}}J^{00}_{vnw\bar{n}}\\
&+ E^k_{\tau s_{/\zeta_k}}\tilde{C}^k_{23}\frac{a}{2}I^{00}_{vmw\bar{m}}J^{10}_{vnw\bar{n}}\\
&+ \left(E^k_{\tau_{/\zeta_k}s}\tilde{C}^k_{45}\frac{b}{2}\cos\gamma - E^k_{\tau_{/\zeta_k}s}\tilde{C}^k_{44}\frac{b}{2}\sin\gamma \right) I^{01}_{vmw\bar{m}}J^{00}_{vnw\bar{n}}\\
&+ E^k_{\tau_{/\zeta_k}s}C^k_{44}\frac{a}{2}I^{00}_{vmw\bar{m}}J^{01}_{vnw\bar{n}}
\end{aligned}
\tag{4.36}
$$

$$
\begin{aligned}
K^k_{\tau sij}(3,1) = &\left(E^k_{\tau s_{/\zeta_k}}\tilde{C}^k_{55}\frac{b}{2}\cos\gamma - E^k_{\tau s_{/\zeta_k}}\tilde{C}^k_{45}\frac{b}{2}\sin\gamma \right) I^{10}_{wmu\bar{m}}J^{00}_{wnu\bar{n}}\\
&+ E^k_{\tau s_{/\zeta_k}}\tilde{C}^k_{45}\frac{a}{2}I^{00}_{wmu\bar{m}}J^{10}_{wnu\bar{n}}\\
&+ \left(E^k_{\tau_{/\zeta_k}s}\tilde{C}^k_{13}\frac{b}{2}\cos\gamma - E^k_{\tau_{/\zeta_k}s}\tilde{C}^k_{36}\frac{b}{2}\sin\gamma \right) I^{01}_{wmu\bar{m}}J^{00}_{wnu\bar{n}} +\\
&+ E^k_{\tau_{/\zeta_k}s}C^k_{36}\frac{a}{2}I^{00}_{wmu\bar{m}}J^{01}_{wnu\bar{n}}
\end{aligned}
\tag{4.37}
$$

$$
\begin{aligned}
K^k_{\tau sij}(3,2) = &\left(E^k_{\tau s_{/\zeta_k}} \tilde{C}^k_{45} \frac{b}{2} \cos\gamma - E^k_{\tau s_{/\zeta_k}} \tilde{C}^k_{44} \frac{b}{2} \sin\gamma \right) I^{10}_{wmv\bar{m}} J^{00}_{wnv\bar{n}} \\
&+ E^k_{\tau s_{/\zeta_k}} \tilde{C}^k_{44} \frac{a}{2} I^{00}_{wmv\bar{m}} J^{10}_{wnv\bar{n}} \\
&+ \left(E^k_{\tau_{/\zeta_k} s} \tilde{C}^k_{36} \frac{b}{2} \cos\gamma - E^k_{\tau_{/\zeta_k} s} \tilde{C}^k_{23} \frac{b}{2} \sin\gamma \right) I^{01}_{wmv\bar{m}} J^{00}_{wnv\bar{n}} \\
&+ E^k_{\tau_{/\zeta_k} s} C^k_{23} \frac{a}{2} I^{00}_{wmv\bar{m}} J^{01}_{wnv\bar{n}}
\end{aligned}
\tag{4.38}
$$

$$
\begin{aligned}
K^k_{\tau sij}(3,3) = &\left(E^k_{\tau s} \tilde{C}^k_{55} \frac{b}{a} \cos\gamma - 2E^k_{\tau s} \tilde{C}^k_{45} \frac{b}{a} \sin\gamma + E^k_{\tau s} \tilde{C}^k_{44} \frac{b}{a} \tan\gamma \sin\gamma \right) I^{11}_{wmw\bar{m}} J^{00}_{wnw\bar{n}} \\
&+ \left(E^k_{\tau s} \tilde{C}^k_{45} - E^k_{\tau s} \tilde{C}^k_{44} \tan\gamma \right) \left(I^{10}_{wmw\bar{m}} J^{01}_{wnw\bar{n}} + I^{01}_{wmw\bar{m}} J^{10}_{wnw\bar{n}} \right) \\
&+ E^k_{\tau s} \tilde{C}^k_{44} \frac{a}{b} \sec\gamma I^{00}_{wmw\bar{m}} J^{11}_{wnw\bar{n}} + E^k_{\tau_{/\zeta_k} s_{/\zeta_k}} C^k_{33} \frac{ab}{4} \cos\gamma I^{00}_{wmw\bar{m}} J^{00}_{wnw\bar{n}}
\end{aligned}
\tag{4.39}
$$

while explicit non-null terms of the mass Ritz nucleus are:

$$
M^k_{\tau sij}(1,1) = E^k_{\tau s} \rho^k \frac{ab}{4} \cos\gamma I^{00}_{umu\bar{m}} J^{00}_{unu\bar{n}} \tag{4.40}
$$

$$
M^k_{\tau sij}(2,2) = E^k_{\tau s} \rho^k \frac{ab}{4} \cos\gamma I^{00}_{vmv\bar{m}} J^{00}_{vnv\bar{n}} \tag{4.41}
$$

$$
M^k_{\tau sij}(3,3) = E^k_{\tau s} \rho^k \frac{ab}{4} \cos\gamma I^{00}_{wmw\bar{m}} J^{00}_{wnw\bar{n}} \tag{4.42}
$$

4.1.4 Assembly procedure of fundamental nuclei

The Ritz nuclei necessitate an expansion procedure to find the mass and stiffness plate matrices and this assembly procedure is done in three expansion steps. The first one is a layer-level expansion, in which the nuclei are expanded over τ and s indices according to the general assumption of the unified formulation. The second expansion is a multilayer-level expansion over layer index k, according to lamination sequence of the modelled plate. The third step is the expansion of the multilayer-level matrices over indices i and j, according to the square value of Ritz approximation order, $M = P^2$. In the following is presented the assembly process of the stiffness matrix only, the mass matrix is assembled in the same way.

First of all, the fundamental nuclei are expanded at a layer level through variation of the theory-related indices τ and s over the previously defined ranges:

$$\boldsymbol{K}_{ij}^{k} = \begin{bmatrix} \boldsymbol{K}_{ttij}^{k} & \boldsymbol{K}_{trij}^{k} & \boldsymbol{K}_{tbij}^{k} \\ \boldsymbol{K}_{rtij}^{k} & \boldsymbol{K}_{rrij}^{k} & \boldsymbol{K}_{rbij}^{k} \\ \boldsymbol{K}_{btij}^{k} & \boldsymbol{K}_{brij}^{k} & \boldsymbol{K}_{bbij}^{k} \end{bmatrix} \tag{4.43}$$

The fundamental nuclei are grouped into 3×3 matrices, while after the first expansion the layer level matrices has dimensions of $3(N+1) \times 3(N+1)$. Multilayer-level expansion is the second step and is carried out over index k from ($k = N_l$ to $k = 1$), where k is the layer index and N_l is the number of layers of the plate. The multilayer-level expansions is different for LW and ESL families of theories and in the two cases is carried out as followings.

The ESL multilayer-level expansions, since displacement variables and their variations are the same for each layer, is a simply summation:

$$\boldsymbol{K}_{ij}^{ESL} = \sum_{k=1}^{N_l} \boldsymbol{K}_{ij}^{k} \tag{4.44}$$

In LW multilayer-level expansion, since variables are defined independently for each layer, the layer matrix are expanded in a way which enforce the continuity at the interfaces as written in Eq. (3.16).

$$\boldsymbol{K}_{ij}^{LW} = \begin{bmatrix} \boldsymbol{K}_{ttij}^{N_l} & \boldsymbol{K}_{trij}^{N_l} & \boldsymbol{K}_{tbij}^{N_l} & & \\ \boldsymbol{K}_{rtij}^{N_l} & \boldsymbol{K}_{rrij}^{N_l} & \boldsymbol{K}_{rbij}^{N_l} & & \\ \boldsymbol{K}_{btij}^{N_l} & \boldsymbol{K}_{brij}^{N_l} & \boldsymbol{K}_{bbij}^{N_l} + \boldsymbol{K}_{ttij}^{N_l-1} & \boldsymbol{K}_{trij}^{N_l-1} & \boldsymbol{K}_{tbij}^{N_l-1} \\ & & \boldsymbol{K}_{rtij}^{N_l-1} & \boldsymbol{K}_{rrij}^{N_l-1} & \boldsymbol{K}_{rbij}^{N_l-1} \\ & & \boldsymbol{K}_{btij}^{N_l-1} & \boldsymbol{K}_{brij}^{N_l-1} & \boldsymbol{K}_{bbij}^{N_l-1} + \boldsymbol{K}_{ttij}^{N_l-2} \\ & & & & \ddots \end{bmatrix} \tag{4.45}$$

After the multilayer-level expansion the matrices has dimensions respectively of $3(N+1) \times 3(N+1)$ for ESL and of $3(N+1)N_l - 3(N_l-1) \times 3(N+1)N_l - 3(N_l-1)$ for LW problems. The third and last step is the plate expansion, carried out through variation of Ritz-related indices i and

j, following a similar to nuclei-to-layer expansion:

$$\boldsymbol{K} = \begin{bmatrix} \boldsymbol{K}_{11}^{th} & \boldsymbol{K}_{12}^{th} & \cdots & \boldsymbol{K}_{1M}^{th} \\ \boldsymbol{K}_{21}^{th} & \boldsymbol{K}_{22}^{th} & \cdots & \boldsymbol{K}_{2M}^{th} \\ \vdots & \vdots & & \vdots \\ \boldsymbol{K}_{M1}^{th} & \boldsymbol{K}_{M2}^{th} & \cdots & \boldsymbol{K}_{MM}^{th} \end{bmatrix} \tag{4.46}$$

where matrices $\boldsymbol{K}_{ij}^{th}$ are the multilayer-level matrices derived before and M is the square value of Ritz approximation order P. The matrices of the plate has dimensions respectively of $[3(N+1)]M \times [3(N+1)]M$ for ESL and of $[3(N+1)N_l - 3(N_l-1)]M \times [3(N+1)N_l - 3(N_l-1)]M$ for LW problems.

4.2 Derivation of loads fundamental nuclei

The PVW stated in Eq: (4.8) takes into account only the stiffness and the inertia of the plate and after its solution the eigenvalue analysis of the plate can be performed. To be able to calculate the forced response of a plate a new terms shall be added to the PVW:

$$\int_V (\delta\epsilon_{ij}\sigma_{ij})dV = -\int_V \delta u_i \rho \ddot{u}_i dV + \int_{\bar{\Omega}} \delta u_i p d\bar{\Omega} \tag{4.47}$$

where p is a generic force distributed onto the surface $\bar{\Omega}$, portion of the plate surface, located at thickness $\bar{z}$ with respect of the plate reference plane Ω.

$$\boldsymbol{p}(x, y, \bar{z}) = \begin{Bmatrix} p_x \\ p_y \\ p_z \end{Bmatrix} \tag{4.48}$$

Then, adopting the adimensionalization of the reference system proposed above becomes:

$$\boldsymbol{p}(\xi, \eta, \bar{\zeta_k}) = \begin{Bmatrix} p_\xi(\xi, \eta, \bar{\zeta_k}) \\ p_\eta(\xi, \eta, \bar{\zeta_k}) \\ p_{\zeta_k}(\xi, \eta, \bar{\zeta_k}) \end{Bmatrix} \tag{4.49}$$

where p_δ are the load amplitudes at coordinates $(\xi, \eta, \bar{\zeta_k})$ in direction δ. Now, managing the integral on the forced plate surface $\bar{\Omega}$, the force PVW term can be expressed as:

$$\sum_k \delta(k - \bar{k}) \int_{\Omega_k} \delta \boldsymbol{u}^{k^T}(\bar{\zeta_k}) \boldsymbol{H}(\bar{\xi}, \bar{\eta}) \boldsymbol{p}(\xi, \eta) d\Omega_k \tag{4.50}$$

in which a combination of unitary step functions $\boldsymbol{H}(\bar{\xi},\bar{\eta})$ has been used to expand the generic loaded surface $\bar{\Omega}$ to the plate domain Ω_k, while the dirak δ has been used to put the integral into a summation over the layers of the plate. In fact the term $\delta(k-\bar{k})$ has unitary value only when the $\bar{k}$-th layer, in which the load is applied, is taken into account in the summation.

Substituting the CUF formulation of the displacement vector for each k-th lamina u^k expressed in Eq: (4.2) and the Ritz approximation of Eq: (4.26) leds to:

$$\sum_k \delta(k-\bar{k}) \left(\delta \boldsymbol{c}_{\tau i}^{k^T} \int_{-1}^{+1}\int \boldsymbol{H}(\bar{\xi},\bar{\eta}) \boldsymbol{N}_{\tau i}^T F_\tau^k(\bar{\zeta_k}) \boldsymbol{p}(\xi,\eta) \frac{ab}{4} \cos\gamma d\xi d\eta \right) \tag{4.51}$$

in which, the effect of the combination of step functions is to vary the integrals extreme to integrate the Ritz shape functions only onto the loaded surface as followings:

$$\sum_k \delta(k-\bar{k}) \left(\delta \boldsymbol{c}_{\tau i}^{k^T} \int_{\bar{\xi}}\int_{\bar{\eta}} \boldsymbol{N}_{\tau i}^T F_\tau^k(\bar{\zeta_k}) \boldsymbol{p}(\xi,\eta) \frac{ab}{4} \cos\gamma d\xi d\eta \right) \tag{4.52}$$

Now, as stated for the PVW, the the virtual works had to vanish and considering the arbitrariness of the virtual variation, the resultant component of the equation of motion, which has to be added in the right side of Eq: (4.28), is:

$$\sum_k \delta(k-\bar{k}) \boldsymbol{F}_{\tau i} \tag{4.53}$$

where the 3×1 vector $\boldsymbol{F}_{\tau i}$ is the Ritz fundamental nuclei of loads. The load geometrical distribution can be taken into account into the following manner:

$$\boldsymbol{p}(\xi,\eta,\bar{\zeta_k}) = \begin{Bmatrix} p_\xi \\ p_\eta \\ p_{\zeta_k} \end{Bmatrix} \bar{p_\xi}(\xi)\bar{p_\eta}(\eta) \tag{4.54}$$

where $\bar{p_\xi}(\xi)\bar{p_\eta}(\eta)$ are the geometrical functions which defines the amplitude of the loads point by point with respect to the maximum amplitude in each direction. Hence, introducing the following notation:

$$L_{\alpha m}^{\Phi} = \frac{a}{2}\int_{\bar{\xi}} \phi_{\alpha\tau m}(\xi)\bar{p_\xi}(\xi)d\xi \qquad m=1,2,\cdots,P \tag{4.55}$$

$$L_{\alpha n}^{\Psi} = \frac{b}{2}\cos\gamma \int_{\bar{\eta}} \psi_{\alpha\tau n}(\eta)\bar{p_\eta}(\eta)d\eta \qquad n=1,2,\cdots,P \tag{4.56}$$

which are the load surface integrals of the Ritz shape functions. These integrals have been calculated numerically adopting the Gauss-Legendre method.

These integrals have been defined taking into account also the terms related to the change of variables caused by the adimensionalization of the reference frame since they shall be integrated into the domain defined by $(\bar{\xi}, \bar{\eta})$, which in general is a portion of the plate surface, but as can be the whole plate, it can be also a point in the case of a concentrate force. In this last case the *integrals* are no more integrals but the Ritz shape function evaluate at the force coordinate:

$$L^{\Phi}_{\alpha m} = \phi_{\alpha\tau m}(\bar{\xi}) \qquad m = 1, 2, \cdots, P \tag{4.57}$$

$$L^{\Psi}_{\alpha n} = \psi_{\alpha\tau n}(\bar{\eta}) \qquad n = 1, 2, \cdots, P \tag{4.58}$$

and the terms related to the change of variables are no more present, since also in te PVW there is no need of an integral. This leads to a formulation of the nuclei which is invariant of the spatial distribution of the loads. Now for the k-th layer the terms of the Ritz load nuclei can be explicitly written as:

$$F^{\bar{k}}_{\tau i}(1) = F^{k}_{\tau}(\bar{\zeta_k}) L^{\Phi}_{\alpha m} L^{\Psi}_{\alpha n} p_{\xi} \tag{4.59}$$

$$F^{\bar{k}}_{\tau i}(2) = F^{k}_{\tau}(\bar{\zeta_k}) L^{\Phi}_{\alpha m} L^{\Psi}_{\alpha n} p_{\eta} \tag{4.60}$$

$$F^{\bar{k}}_{\tau i}(3) = F^{k}_{\tau}(\bar{\zeta_k}) L^{\Phi}_{\alpha m} L^{\Psi}_{\alpha n} p_{\zeta_k} \tag{4.61}$$

Load nuclei can now be assembled in a similar way of plate matrices, with the only difference that a vector is involved instead of a matrix. Shall be remarked that the presence of the term $\delta(k - \bar{k})$ has the effect of give a non zero nuclei only for the $\bar{k}$-th layer on which the load is applied. For other layers the load nuclei are automatically zeroes. In this thesis only load applied on the top or bottom surfaces have been considered. At layer level load vector become:

$$\boldsymbol{F}^{k}_{i} = \begin{Bmatrix} \boldsymbol{F}^{k}_{ti} \\ \boldsymbol{F}^{k}_{ri} \\ \boldsymbol{F}^{k}_{bi} \end{Bmatrix} \tag{4.62}$$

Then, multilayer level load vectors, for ESL and LW theories are assembled as follows:

$$\boldsymbol{F}^{ESL}_{i} = \sum_{k=1}^{N_l} \boldsymbol{F}^{k}_{i} \tag{4.63}$$

$$\boldsymbol{F}_{ij}^{LW} = \begin{Bmatrix} \boldsymbol{F}_{ti}^{N_l} \\ \boldsymbol{F}_{ri}^{N_l} \\ \boldsymbol{F}_{bi}^{N_l} + \boldsymbol{F}_{ti}^{N_l-1} \\ \boldsymbol{F}_{ri}^{N_l-1} \\ \boldsymbol{F}_{bi}^{N_l-1} \\ \vdots \end{Bmatrix} \tag{4.64}$$

Thus, the Ritz expansion:

$$\boldsymbol{F} = \begin{Bmatrix} \boldsymbol{F}_{1}^{th} \\ \boldsymbol{F}_{2}^{th} \\ \vdots \\ \boldsymbol{F}_{M}^{th} \end{Bmatrix} \tag{4.65}$$

After the assembly procedures, when the plate load vector $\boldsymbol{F}$ have been built, the time dependence can be taken into account as:

$$\boldsymbol{F}(t) = \boldsymbol{F} P_{temp}(t) \tag{4.66}$$

where $P_{temp}(t)$ is a load temporal function which describes the time behaviour of loads with respect their maximum amplitude with respect to time.

4.3 Derivation of attached masses fundamental nuclei

The PVW can be enriched to take into account the presence of N_m attached masses, defined as distributed masses which does not prevent the deformation of the plate and are attached at its surface. This hypothesis permits to describe the mass with the coordinates of the plate which describe the motion of the surface at which the mass is attached. Thus, at the PVW of Eq: (4.8) a new term will be added:

$$\int_V (\delta\epsilon_{ij}\sigma_{ij})dV = -\int_V \delta u_i \rho \ddot{u}_i dV - \sum_{m=1}^{N_m} \int_{\bar{\Omega}_m} \delta u_i \bar{m}_m \ddot{u}_i d\bar{\Omega}_m \tag{4.67}$$

where $\bar{m}_m$ is the density for unit surface of the m-th attached mass and $\bar{\Omega}_m$ is the area occupied by the mass on the plate surface. Now, managing the $\bar{\Omega}_m$ integral, the new PVW term for the m-th attached mass can be expressed as:

$$-\sum_k \delta(k-\bar{k}) \int_{\Omega_k} \delta \boldsymbol{u}^{k^T}(\bar{\zeta_k}) \boldsymbol{H}(\bar{\xi},\bar{\eta}) \bar{m}_m \ddot{\boldsymbol{u}}^k(\bar{\zeta_k}) d\Omega_k \tag{4.68}$$

As for load nuclei derivation, also in this case a dirak function and a combination of step functions have been used. Substituting the CUF formulation of the displacement vector for each k-th lamina u^k expressed in Eq: (4.2) and the Ritz approximation of Eq: (4.26) leds to:

$$-\boldsymbol{\omega}^2 \sum_k \delta(k-\bar{k}) \left(\delta \boldsymbol{c}^{k^T}_{\tau i} \int_{\bar{\xi}} \int_{\bar{\eta}} \boldsymbol{N}^T_{\tau i} F^{k^T}_{\tau}(\bar{\zeta_k}) \bar{m}_m F^k_s(\bar{\zeta_k}) \boldsymbol{N}_{sj} \frac{ab}{4} \cos\gamma d\xi d\eta \right) \boldsymbol{c}^k_{sj} \tag{4.69}$$

Now, as stated for the PVW, the the virtual works had to vanish and considering the arbitrariness of the virtual variation, the resultant component of the equation of motion for the m-th attached mass, which has to be added in the right side of Eq: (4.28), is:

$$-\boldsymbol{\omega}^2 \sum_k \delta(k-\bar{k}) \boldsymbol{M}^m_{\tau sij} \tag{4.70}$$

where the 3×3 $\boldsymbol{M}^m_{\tau sij}$ is the nuclei mass matrix for the m-th attached mass. The surface integrals are defined as:

$$I^{Amass}_{\alpha m \beta \bar{m}} = \frac{a}{2} \int_{\bar{\xi}} \phi_{\alpha \tau m}(\xi) \phi_{\beta s \bar{m}}(\xi) d\xi \qquad m, \bar{m} = 1, 2, \cdots, P \tag{4.71}$$

$$J^{Amass}_{\alpha n \beta \bar{n}} = \frac{b}{2} \cos\gamma \int_{\bar{\eta}} \psi_{\alpha \tau n}(\eta) \psi_{\beta s \bar{n}}(\eta) d\eta \qquad n, \bar{n} = 1, 2, \cdots, P \tag{4.72}$$

As done before, the surface integrals have been defined taking into account also the terms related to the change of variables caused by the adimensionalization of the reference frame to be changed in case of punctual attached masses positioned at coordinates (ξ_m, η_m):

$$I^{Amass}_{\alpha m \beta \bar{m}} = \phi_{\alpha \tau m}(\xi_m) \phi_{\beta s \bar{m}}(\xi_m) \qquad m, \bar{m} = 1, 2, \cdots, P \tag{4.73}$$

$$J^{Amass}_{\alpha n \beta \bar{n}} = \psi_{\alpha \tau n}(\eta_m) \psi_{\beta s \bar{n}}(\eta_m) \qquad n, \bar{n} = 1, 2, \cdots, P \tag{4.74}$$

This leads to a formulation of the nuclei which is invariant of the spatial distribution of the attached mass. Now for the k-th layer the terms of the Ritz attached mass nuclei can be explicitly written as:

$$M^m_{\tau sij}(1,1) = F^k_{\tau}(\bar{\zeta_k}) F^k_s(\bar{\zeta_k}) \bar{m}_m I^{Amass}_{umu\bar{m}} J^{Amass}_{unu\bar{n}} \tag{4.75}$$

$$M^m_{\tau sij}(2,2) = F^k_{\tau}(\bar{\zeta_k}) F^k_s(\bar{\zeta_k}) \bar{m}_m I^{Amass}_{vmv\bar{m}} J^{Amass}_{vnv\bar{n}} \tag{4.76}$$

$$M^m_{\tau sij}(3,3) = F^k_{\tau}(\bar{\zeta_k}) F^k_s(\bar{\zeta_k}) \bar{m}_m I^{Amass}_{wmw\bar{m}} J^{Amass}_{wnw\bar{n}} \tag{4.77}$$

Where the thickness functions shall be evaluate at:

ESL:	$\bar{z} = \frac{h}{2}$	$\bar{k} = N_l$	if attached mass is located on top surface
	$\bar{z} = -\frac{h}{2}$	$\bar{k} = 1$	if attached mass is located under bottom surface
LW:	$\bar{\zeta_k} = +1$	$\bar{k} = N_l$	if attached mass is located on top surface
	$\bar{\zeta_k} = -1$	$\bar{k} = 1$	if attached mass is located under bottom surface

Table 4.1: Thickness function for attached masses

Now, the nuclei mass matrix can be assembled in the same way of the mass matrix of the plate, taking into account the presence of the dirak function, which implies that the only non null nuclei are those referred to the $\bar{k}$ layer on which the mass is attached. This process can be done for each attached mass present on the plate and then the mass matrices of the attached masses can be summed with the plate mass matrix to compute the system mass matrix, which will be then used in the dynamical analysis.

4.4 Derivation of suspended masses fundamental nuclei

The suspended masses considered in this work as been modelled as point masses mounted onto massless linear springs, which can extend only in the direction of the device and have infinite stiffness out of that direction. This type of device can be mounted only on the top surface or under the bottom surface of the plate, hence, the thickness function shall be evaluated as reported in tab: 4.1, and only for the related layer. The PVW can be enriched to take into account the presence of N_s suspended masses, defined as a point mass $\bar{m}$ suspended onto a spring of stiffness k_0, applied at coordinates(ξ_s, η_s) and directed in z direction. Thus, at the PVW of Eq: (4.8) new terms will

be added:

$$\begin{aligned}\int_V (\delta\epsilon_{ij}\sigma_{ij})dV = &-\int_V \delta u_i \rho \ddot{u}_i dV - \sum_{N_s} \delta z_s \bar{m}_s \ddot{z}_s \\ &- \sum_{s=1}^{N_s} \delta[z_s - u_z(\xi_s,\eta_s,\bar{\zeta_{k_s}})] k_{0_s}[z_s - u_z(\xi_s,\eta_s,\bar{\zeta_{k_s}})] \\ &- \sum_{s=1}^{N_s} \delta u_x(\xi_s,\eta_s,\bar{\zeta_{k_s}}) \bar{m}_s \ddot{u}_x(\xi_s,\eta_s,\bar{\zeta_{k_s}}) \\ &- \sum_{s=1}^{N_s} \delta u_y(\xi_s,\eta_s,\bar{\zeta_{k_s}}) \bar{m}_s \ddot{u}_y(\xi_s,\eta_s,\bar{\zeta_{k_s}})\end{aligned} \tag{4.78}$$

The first added term is related to the inertia of the suspended mass in the direction of the device, z in this case, which shall be described employing a further degrees of freedom for each s-th suspended mass. The second term is the virtual work done by the spring stiffness, which works for its elongation, so, for the difference between the displacement of the mass and the displacement of the plate in z direction. The third and fourth terms are related to the inertia of the suspended mass in the other two directions, as the mass is attached to the plate, since the spring has infinite stiffness in those directions.
Now the effects of the added terms can be described with the CUF displacement field expressed in Eq: (4.2) and the Ritz approximation of Eq: (4.26). Each term will be described separately. Taking into account the third and fourth terms added at Eq: (4.78), they can be described as in the previous case of concentrated attached mass, neglecting the contribution in the devices direction, hence in this case the fundamental nuclei are directly defined as:

$$M^s_{\tau sij}(1,1) = F^k_\tau(\bar{\zeta_{k_s}}) F^k_s(\bar{\zeta_{k_s}}) \bar{m}_s I^{Amass}_{umu\bar{m}} J^{Amass}_{unu\bar{n}} \tag{4.79}$$

$$M^s_{\tau sij}(2,2) = F^k_\tau(\bar{\zeta_{k_s}}) F^k_s(\bar{\zeta_{k_s}}) \bar{m}_s I^{Amass}_{vmv\bar{m}} J^{Amass}_{vnv\bar{n}} \tag{4.80}$$

$$M^s_{\tau sij}(3,3) = 0 \tag{4.81}$$

with the surface integrals evaluate as described in Eqs: (4.73) and (4.74) at the devices coordinate. The nuclei can be assembled as described before for plate mass nuclei to create the matrix $\boldsymbol{M}^s$ with the same dimension of the plate matrices.

The second term added at Eq: (4.78), can be seen as:

$$
\begin{aligned}
-\sum_{s=1}^{N_s} \delta u_z(\xi_s, \eta_s, \bar{\zeta_{k_s}}) k_{0_s} u_z(\xi_s, \eta_s, \bar{\zeta_{k_s}}) + \sum_{s=1}^{N_s} \delta u_z(\xi_s, \eta_s, \bar{\zeta_{k_s}}) k_{0_s} z_s \\
+ \sum_{s=1}^{N_s} \delta z_s k_{0_s} u_z(\xi_s, \eta_s, \bar{\zeta_{k_s}}) - \sum_{s=1}^{N_s} z_s k_{0_s} z_s
\end{aligned}
\tag{4.82}
$$

The first term of Eq: (4.82), under the CUF assumption and the Ritz approximation of Eq: (4.26), has a very similar description of concentrated mass since it its related to a concentrate stiffness, so, the fundamental nuclei can be retrieved in a very similar way, considering only the contribution in the devices direction, leading to:

$$K^s_{\tau sij}(1,1) = 0 \tag{4.83}$$
$$K^s_{\tau sij}(2,2) = 0 \tag{4.84}$$
$$K^s_{\tau sij}(3,3) = F^k_\tau(\bar{\zeta_{k_s}}) F^k_s(\bar{\zeta_{k_s}}) k_{0_s} I^{Amass}_{vmv\bar{m}} J^{Amass}_{vnv\bar{n}} \tag{4.85}$$

with the surface integrals evaluate as described in Eqs: (4.73) and (4.74) at the devices coordinate. The nuclei can be assembled as described before for plate stiffness nuclei to create the matrix $\boldsymbol{K}^s$ with the same dimension of the plate matrices.

The second term of Eq: (4.82) becomes:

$$\sum_{s=1}^{N_s} \left[\sum_k \delta(k - \bar{k}_s) \left(\delta \boldsymbol{c}^{k^T}_{\tau i} \boldsymbol{N}^T_{\tau i}(\xi_s, \eta_s) F^k_\tau(\bar{\zeta_{k_s}}) \boldsymbol{k}_{0_s} z_s \right) \right] \tag{4.86}$$

where,

$$\boldsymbol{k}_{0_s}(1) = 0 \tag{4.87}$$
$$\boldsymbol{k}_{0_s}(2) = 0 \tag{4.88}$$
$$\boldsymbol{k}_{0_s}(3) = k_{0_s} \tag{4.89}$$

This term is now very similar with that encountered in derivation of load fundamental nuclei, then the derivation of the nuclei on the mixed stiffness matrices can be directly written as:

$$K^{uz}_{\tau i}(1) = 0 \tag{4.90}$$
$$K^{uz}_{\tau i}(2) = 0 \tag{4.91}$$
$$K^{uz}_{\tau i}(3) = -F^k_\tau(\bar{\zeta_{k_s}}) L^\Phi_{\alpha m} L^\Psi_{\alpha n} k_{0_s} \tag{4.92}$$

with shape functions integrals evaluated as stated in Eqs: (4.57) and (4.58) at the device coordinate. The minus sign has been putted into the nuclei to consider that the contribution will be moved in the left side of the PVW statement, as done for the other suspended mass nuclei before. The nuclei can be assembled as described before for load nuclei to create the matrix $\boldsymbol{K}^{uz}$ with the same number of rows of the plate matrices and columns equal at the number of the suspended masses. The third term of Eq: (4.82) has the same description of the just view second term leading to:

$$\boldsymbol{K}^{zu} = \boldsymbol{K}^{uz^T} \tag{4.93}$$

The fourth term of Eq: (4.82) and the first therm of Eq: (4.78) have the effect of putting the mass and stiffness values of the s-th device into diagonal matrices of dimension $N_s \times N_s$:

$$\boldsymbol{M}^{zz} = diag\{\bar{m}_s\} \tag{4.94}$$
$$\boldsymbol{K}^{zz} = diag\{k_{0_s}\} \tag{4.95}$$

Now collecting all z_s degrees of freedom into the vector $\boldsymbol{z}$ the augmented system equation of motion, resulting from PVW of Eq: (4.78) considering also the presence of a forcing term, can be written as follows:

$$\begin{bmatrix} \boldsymbol{M}^{plate} + \boldsymbol{M}^{s} & 0 \\ 0 & \boldsymbol{M}^{zz} \end{bmatrix} \begin{Bmatrix} \ddot{\boldsymbol{u}} \\ \ddot{\boldsymbol{z}} \end{Bmatrix} + \begin{bmatrix} \boldsymbol{K}^{plate} + \boldsymbol{K}^{s} & \boldsymbol{K}^{uz} \\ \boldsymbol{K}^{zu} & \boldsymbol{K}^{zz} \end{bmatrix} \begin{Bmatrix} \boldsymbol{u} \\ \boldsymbol{z} \end{Bmatrix} = \begin{Bmatrix} \boldsymbol{F} \\ 0 \end{Bmatrix} \tag{4.96}$$

which can be seen in the following compact notation:

$$\boldsymbol{M}_{augm}\ddot{\boldsymbol{u}}_{augm} + \boldsymbol{K}_{augm}\boldsymbol{u}_{augm} = \boldsymbol{F}_{augm} \tag{4.97}$$

and treated as usual.

4.5 Derivation of patches fundamental nuclei

To consider the stiffness effect of attached distributed masses theirs thickness shall be considered. To do that, under CUF assumptions, it is no more possible to use the displacements of the surface of the layer at which they are attached and an independent formulation of the displacement of patches shall be used.

For this reason, patches have been treated as layers of reduced dimension, adding in the PVW statement a layer dependant combination of step functions $\boldsymbol{H}^k(\bar{\xi}, \bar{\eta})$, similarly at what done before for zonal loads and distributed

masses, to vary the domain of integration of the k-th layer from the surface of the plate Ω_k to the surface of the patch $\bar{\Omega}_k$, when in the layer summation the *layer* which contains the patch is take into account. Refers as *layer* of patches is not very accurate, but take meaning considering that patches are considered as layer with a surface of reduced dimension. For this reason, when patched have to be accounted, the caption *layer* will be used.

$$\begin{aligned}&\sum_k \int_{\Omega_k}\int_{\zeta_k} \boldsymbol{H}^k(\bar{\xi},\bar{\eta})\left[\delta\boldsymbol{\epsilon}_p^{k^T}\boldsymbol{\sigma}_p^k + \delta\boldsymbol{\epsilon}_n^{k^T}\boldsymbol{\sigma}_n^k\right] d\zeta_k d\Omega_k \\ &= -\sum_k \int_{\Omega_k}\int_{\zeta_k} \delta\boldsymbol{u}^{k^T}\boldsymbol{H}^k(\bar{\xi},\bar{\eta})\rho^k\ddot{\boldsymbol{u}}^k d\zeta_k d\Omega_k\end{aligned} \tag{4.98}$$

From there, the derivation of fundamental nuclei is quite straight forward and led to the same mass and stiffness nuclei of the plate case, with the difference that the surface integrals of Eqs: (4.29) and (4.30), have to be calculate on the domain described by $\boldsymbol{H}^k(\bar{\xi},\bar{\eta})$ and not always in the interval $[-1,+1]$, which however do not coincides only when the *layer* of the patch is considered.

This formulation can be also extent to consider the presence of two or more patches in the same *layer*. In fact, using a summation over the o-th object present in the k-th layer and remembering that for classical layer the only object present is the layer itself, is possible to write:

$$\begin{aligned}&\sum_k \left\{\sum_o \int_{\Omega_k}\int_{\zeta_k} \boldsymbol{H}^k(\bar{\xi}_o,\bar{\eta}_o)\left[\delta\boldsymbol{\epsilon}_{p_o}^{k^T}\boldsymbol{\sigma}_{p_o}^k + \delta\boldsymbol{\epsilon}_{n_o}^{k^T}\boldsymbol{\sigma}_{n_o}^k\right] d\zeta_k d\Omega_k\right\} \\ &= -\sum_k \left\{\sum_o \int_{\Omega_k}\int_{\zeta_k} \delta\boldsymbol{u}^{k^T}\boldsymbol{H}^k(\bar{\xi}_o,\bar{\eta}_o)\rho^k\ddot{\boldsymbol{u}}^k d\zeta_k d\Omega_k\right\}\end{aligned} \tag{4.99}$$

From there, the derivation of fundamental nuclei is carried on as before and led to the same mass and stiffness nuclei of the plate case with same consideration made before on the surface integrals domain. Difference in this case arises in the calculation of the layer level matrices when *layers* of patches are considered. In that case if more than one patch is present, the layer level matrices for each patch shall be calculated and then summed, prior to be inserted in the multilayer level matrices.

The formulation presented so far for patches works only for ESL theories while convergence problems are arose with LW theories, probably because of the hypothesis of homogeneous boundary condition, after the adoption of the same Ritz functions of the plate, which does not take into account that the

patches edges are free and not subjected to the plate boundary conditions. Difference between the two families of theories in the capabilities of solute anyway the problems with the right convergence referring to the Ritz expansion order can be searched into the different CUF unknowns formulation: for ESL the degrees of freedom are the same for the whole problem, while for LW theories the degrees of freedom related to *layers* of patches are no more defined onto the whole domain.

Chapter 5

Methods for plate problems solving

Once the system mass and stiffness matrix and the load vector have been assembled, its static and dynamic responses can be evaluated. To do that, in some cases it is possible to proceed directly employing pre-implemented routines, while in other cases it have to be implemented taking into account known methods.

5.1 Static response

The static response of the system can be easily found solving the Eq. (5.2):

$$\boldsymbol{K}\boldsymbol{c} = \boldsymbol{F} \tag{5.1}$$

in the Ritz unknowns $\boldsymbol{c}$, which can be done directly using pre-implemented routines.

5.1.1 Displacements and stresses recovery

After the solution of the bending problem, displacements can be recovered from the vector $\boldsymbol{c}$, taking into account the Ritz expansion of Eq: (4.26) to recover the CUF displacements and then the real displacements using the CUF formulation of Eq: (3.1).

Stresses can be recovered in the same way adding another step, using the constitutive equation presented in Eqs: (2.48) and (2.49) with the real displacements. This way of stresses recovering gives good results with LW theories, while out of plane stress resultants of ESL theories present a discontinuous behaviour which degrades heavily the accuracy of the results. To

overcome this problem, for ESL theories, the out of plane stresses have been recovered solving the equilibrium equation:

$$\nabla \cdot \{\boldsymbol{\sigma}\} = \mathbf{0} \tag{5.2}$$

in the unknowns σ_{xz} and σ_{yz} starting from the well approximated σ_{xx}, σ_{yy} and σ_{xy}, leading to a remarkable improving of the accuracy of ESL theories in the stresses recovery.

5.2 Eigenvalue problem

The system natural frequencies can be found solving the Eq. (5.3):

$$\boldsymbol{K} - \boldsymbol{\omega}^2 \boldsymbol{M} = \mathbf{0} \tag{5.3}$$

in the unknowns $\boldsymbol{\omega}$, which can be done directly using pre-implemented routines.

5.3 Modal reduction

The modal reduction technique has been used to have the possibility of handle still accurate model of dramatically reduced order. This is done taking a subset of the system eigenvector matrix coming from the eigenvalue problem, with columns equal to the order of the desired reduction, then premultiplying and postmultiplying the matrices of mass and stiffness of the system with the transpose and the subset eigenvector matrix respectively. The load vector will be only premultiplied by the transpose of the subset eigenvector matrix.

This approach decouples the equations of motion and allows to solve a small number of equations instead of systems of thousands equations coupled together. After the solution of time and frequency response in the modal unknowns, premultiplying them by the matrix of eigenvector subset the Ritz unknowns can be retrieved.

5.4 Time response

The time response of the full system have been calculated adopting the Newmark integration method, described in [25], to integrate directly the equation of motion:

$$\boldsymbol{M}\ddot{\boldsymbol{c}}(t) + \boldsymbol{K}\boldsymbol{c}(t) = \boldsymbol{F}(t) \tag{5.4}$$

The modal model time response have been calculated solving the following equation for each DOF of the model, as stated by [26]

$$q_i(t) = \frac{1}{M\omega_0}\int_0^t \sin[\omega_0(t-\tau)]Q_i(\tau)d\tau + q_0\cos(\omega_o t) + \frac{\dot{q}_0}{\omega_0}\sin(\omega_o t) \tag{5.5}$$

5.5 Frequency response

The frequency response is sought imposing a sinusoidal response at each frequency ω:

$$\boldsymbol{F}(t) = \boldsymbol{F}e^{j\omega t} \tag{5.6}$$

$$\boldsymbol{u}(t) = \boldsymbol{u}e^{j\omega t} \tag{5.7}$$

Then, Eq: (5.4) can be seen as:

$$(-\boldsymbol{\omega}^2\boldsymbol{M} + \boldsymbol{K})\boldsymbol{c} = \boldsymbol{F} \tag{5.8}$$

which can be directly resolved for retrieve the unknowns $\boldsymbol{c}$ at each frequency of interest ω.

The Ritz unknowns $\boldsymbol{c}$ can be computed also using the modal model, resolving for each frequency of interest ω:

$$q_i = \frac{1}{m_i(\omega_i^2 - \omega^2}Q_i \tag{5.9}$$

then, premultiplying the modal unknowns by the matrix of eigenvector subset for each ω the same solution of the full model frequency response is obtained.

Once calculated the Ritz coordinates $\boldsymbol{c}$ for each frequency ω, the FRF of the model, $J(\omega)$, can be evaluated as [2]

$$u(\omega) = |J(\omega)|F(\omega) \tag{5.10}$$

where both the Ritz approximation of Eq: (4.26) and the CUF displacements field of Eq: (3.1) shall be inserted to retrieve the real displacements from the Ritz unknowns.

Chapter 6

Finite elements models

Three FEM models have been designed to model plates with attached distributed masses and patches since no reliable benchmarks have been found in the literature.

6.1 Isotropic-1 model

The Isotropic-1 FEM model is the model of a fully clamped isotropic squared plate with a square isotropic patch at its center. This loaded plate has been modelled in three version, the first represent the plate without any loadings, in the second a distribute attached mass without stiffness has been inserted, while in the third case its stiffness has been considered. In all cases the boundary conditions have been modelled using a rigid RBE3 element to constraint the edge nodes.

This model has been constructed adopting a full 3D technique, using 3D Hex meshing solid elements, as depicted in figure 6.1, and relying on 2D isotropic plate elements, as depicted in figure 6.2, founding that the results of both models are very accurate.

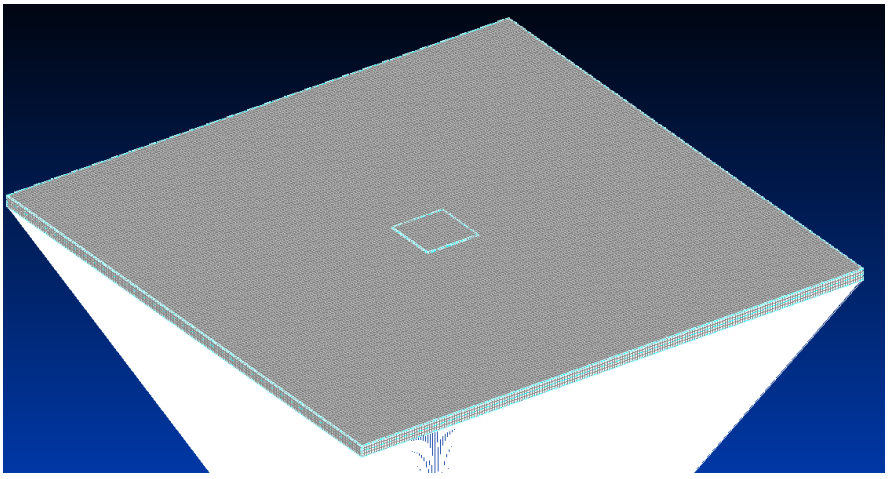

Figure 6.1: Full 3D Isotropic-1 finite element model

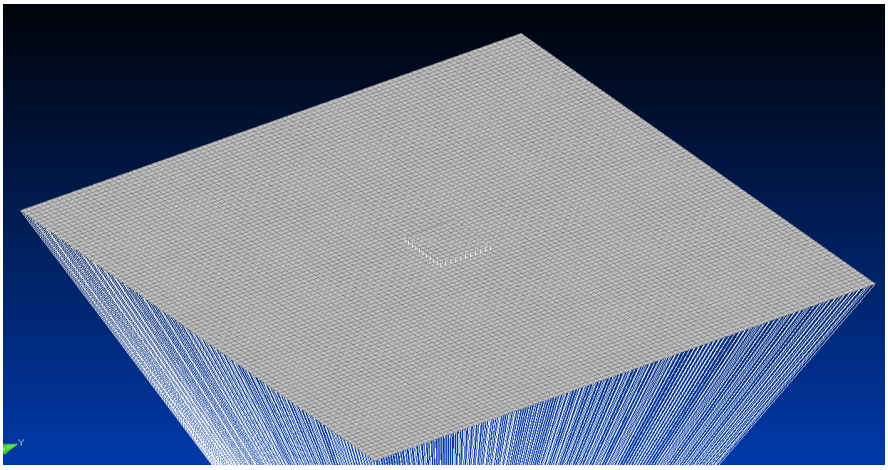

Figure 6.2: 2D Isotropic-1 finite element model

6.2 Laminate-5 model

The laminate-5 FEM model is the model of a FCCF squared laminate plate with different loading conditions, each one modelled with a specific FEM model. In the first case only the laminate plate is considered, it has been modelled relying onto 2D laminate elements, which have a LW formulation. The second case refers to the plate with an attached distributed mass at its center mounted onto the top surface, while in the third case a patch of the same dimension of the attached mass has been inserted in the same position instead of the mass, to consider the stiffening effects of the patch. In the

fourth case, two patches have been mounted on the plate, as depicted in figure 6.3. In all cases the boundary conditions have been modelled using a rigid RBE3 element to constraint the edge nodes.

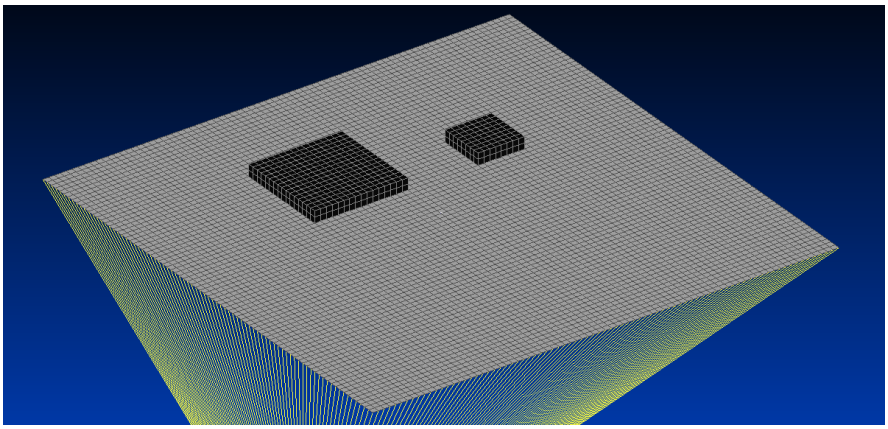

Figure 6.3: Laminate-5 finite element model

6.3 Sandwich-9 model

The Sandwich-9 FEM model is the model of a fully clamped sandwich plate, with a two layers crossply faces and a very soft core, which have been modelled using 2D laminate elements for the faces and 3D Hex meshing solid elements to model the core, similary to what done in [17]. This base model have been improved in other three versions, all with an attached mass at the center of the top surface, but with different boundary conditions: the first is a fully clamped (CCCC) sandwich plate depicted in figure 6.4, the second is a cantilever plate (CFFF) and the third is a partially clamped plate (FCCF). In all cases the boundary conditions have been modelled using a rigid RBE3 element to constraint the edge nodes.

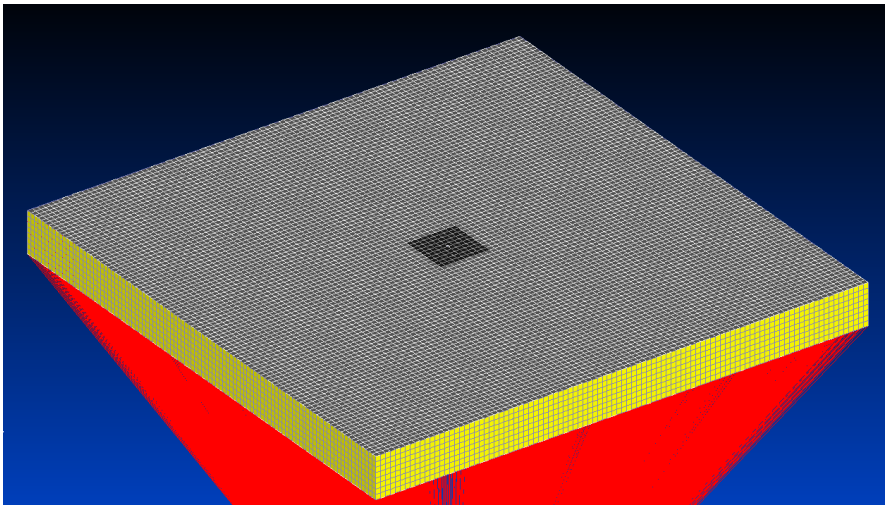

Figure 6.4: Laminate-5 finite element model

Chapter 7

Results

A large numerical investigation has been conducted to validate the code implemented with the theories described in the previous chapters. Several cases has been analyzed for each one of the aspects considered, like bending or direct time integration, comparing the results obtained with those reported onto research publications of various authors, or, adopting validated finite element models as benchmark when comparable results are not found in literature.

The campaign of validation has been conducted comparing displacements and stresses for static analysis and the natural frequencies for dynamic analysis. Time and frequency response have been validated also comparing the resulting plots of the analysis

The validated code has then been used to analyze new interesting cases, like equipped sandwich plates, and also to present new results of the cases studied which are not present in the documents used for the validation.

7.1 Material Properties

The plates considered in the analysis are made of isotropic and orthotropic materials, whose mechanical characteristics are presented in table 7.1 for materials with dimensional properties. Since adimensionalization are widely adopted in literature, adimensional property material have been modelled to create some characteristic case of orthotropic materials with definite stiffness ratios between their principal directions. The characteristics of adimensional materials are presented in 7.2.

Isotropic $[GPa]$	E_1	E_2	E_3	G_{12}	G_{23}	G_{13}	ν_{12}	ν_{23}	ν_{13}	$\rho\ [Kg]$
Al7075	73	73	73	28.077	28.077	28.077	0.3	0.3	0.3	2800
Al6061	69	69	69	25.939	25.939	25.939	0.33	0.33	0.33	2700
Al5086	71	71	71	26.400	26.400	26.400	0.33	0.33	0.33	2660
Al2024	72.4	72.4	72.4	27.015	27.015	27.015	0.34	0.34	0.34	2780
Steel	205.1	205.1	205.1	78.884	78.884	78.884	0.3	0.3	0.3	7850
Orthotropic										
CFRP7	181.0	10.3	10.3	7.17	2.87	7.17	0.28	0.33	0.28	1578
CFRP8	50	10	10	5	5	5	0.25	0.25	0.25	1600
Mat4	276	6.9	6.9	6.9	6.9	6.9	0.25	0.3	0.25	681.8
Mat5	0.577	0.577	0.577	0.107	0.222	0.107	0.0025	0.0025	0.0025	1000
BoEp	208	18.9	18.9	5.7	2.317	5.7	0.23	0.23	0.23	2000
ArEp	76	5.6	5.6	2.3	2.089	2.3	0.34	0.34	0.34	1460
RaoF	131	10.34	10.34	6.895	6.895	6.205	0.22	0.49	0.22	1627
Sandwich cores $[MPa]$	E_1	E_2	E_3	G_{12}	G_{23}	G_{13}	ν_{12}	ν_{23}	ν_{13}	$\rho\ [Kg]$
RaoC	6.89	6.89	6.89	3.45	3.45	3.45	0	0	0	97
OrthoCore	137.9	137.9	137.9	0	51.71	134.45	0	0	0	121.83
Nomex	0.01	0.01	75.85	0	22.5	22.5	0	0	0	32

Table 7.1: Mechanical properties of dimensional materials

Isotropic	E_1	E_2	E_3	G_{12}	G_{23}	G_{13}	ν_{12}	ν_{23}	ν_{13}	ρ
Isot	1	1	1	0.4	0.4	0.4	0.25	0.25	0.25	1
Isot2	1	1	1	0.385	0.385	0.385	0.3	0.3	0.3	1
Orthotropic										
CFRP1	40	1	1	0.6	0.5	0.6	0.25	0.25	0.25	1
CFRP2	25.1	4.8	0.75	1.36	0.47	1.2	0.036	0.171	0.25	1
CFRP3	40	1	1	0.6	0.5	0.5	0.25	0.25	0.25	1
CFRP4	25	1	1	0.5	0.2	0.5	0.25	0.25	0.25	1
CFRP5	10	1	1	0.6	0.5	0.6	0.25	0.25	0.25	1
CFRP6	30	1	1	0.5	0.35	0.5	0.3	0.49	0.3	1
CFRP9	10	1	1	0.5	0.2	0.5	0.25	0.25	0.25	1
Sandwich cores	E_1	E_2	E_3	G_{12}	G_{23}	G_{13}	ν_{12}	ν_{23}	ν_{13}	ρ
Core1	1	1	1	0.016	0.06	0.06	0.25	0.25	0.25	1
Mat1	2	1	1	1.1	0.3846	1.1	0.3	0.3	0.3	1

Table 7.2: Mechanical properties of adimensional materials

7.2 Static Analysis

Several stacking sequence, geometries and loading conditions have been considered to validate the capability of the code to get the correct response of plates statically loaded and present the differences which characterize the plates theories considered.

The static response analyses gives results in terms of displacements and stresses, which in this thesis, are calculated at the following coordinates:

$$\begin{array}{rlll} \text{Transverse displ.} & \text{w} & \text{computed at:} & (\frac{a}{2}, \frac{b}{2}, 0) \\ \text{Sigma}_x & \sigma_{xx} & \text{computed at:} & (\frac{a}{2}, \frac{b}{2}, \frac{h}{2}) \\ \text{Sigmay}_y & \sigma_{yy} & \text{computed at:} & (\frac{a}{2}, \frac{b}{2}, \frac{h}{2}) \\ \text{Sigma}_{xy} & \sigma_{xy} & \text{computed at:} & (0, 0, -\frac{h}{2}) \\ \text{Sigma}_{xz} & \sigma_{xz} & \text{computed at:} & (0, \frac{b}{2}, 0) \\ \text{Sigma}_{yz} & \sigma_{yz} & \text{computed at:} & (\frac{a}{2}, 0, 0) \end{array}$$

Then the values of displacements and stresses are adimensionalized with respect to the followings adimensionalizations:

$$\begin{aligned} \text{Transverse displ. } \bar{w} &= \frac{100h^3E_2}{P_z a^4} w \\ S_x &= \frac{h^2}{P_z a^2}\sigma_{xx} \\ S_y &= \frac{h^2}{P_z a^2}\sigma_{yy} \\ S_{xy} &= \frac{h^2}{P_z a^2}\sigma_{xy} \\ S_{xz} &= \frac{h}{P_z a}\sigma_{xz} \\ S_{yz} &= \frac{h}{P_z a}\sigma_{yz} \end{aligned}$$

The young modulus used in the adimensianalization is E_2, related to the mechanical properties of the top layer of the plate, while, P_z is the maximum amplitude of the load considered unless differently specified in problems description.

7.2.1 Convergence Analysis

The approximation obtained by the Ritz method can be made as accurate as desired by increasing the number of terms in the expansion, but it is truncated to a finite value due to computational time and computer capability. Therefore, the accuracy of the approximate solution is affected by the rate of convergence associated with the choice of the set of trial functions.

First of all a preliminary study has been done to assess the convergence of the solution with respect to the proposed Ritz expansion. The transverse displacements and stress S_x are obtained with various boundary conditions, load geometries and lamination schemes and are reported in the followings tables.

In tables 7.3 and 7.4 are shown the variation of displacements and stress S_x obtained with two different boundary conditions, for various ESL and LW theories, with respect of the order of the Ritz expansion. The plate considered is a square three layer laminate with an height to side ratio of $\frac{h}{a} = 0.1$. All layers have the same thickness and are made of CFRP1 and the lamination scheme is (0/90/0). The load applied is a pressure of constant distribution P_z which acts on the top surface of the plate.

BCS	Theory	Displacement $\bar{w}$						
		P	7	9	10	11	12	13
CFSF	ED2		0.4152	0.4151	0.4151	0.4151	0.4151	0.4151
	ED5		0.4621	0.4622	0.4622	0.4622	0.4622	0.4622
	LD2		0.4612	0.4613	0.4613	0.4613	0.4613	0.4613
	LD4		0.4628	0.4629	0.4629	0.4630	0.4630	0.4630
FCCF	ED2		1.3460	1.3466	1.3466	1.3466	1.3468	1.3468
	ED5		1.4408	1.4432	1.4429	1.4430	1.4432	1.4433
	LD2		1.4394	1.4415	1.4413	1.4414	1.4416	1.4417
	LD4		1.4469	1.4494	1.4491	1.4492	1.4495	1.4496

Table 7.3: Convergence of $\bar{w}$ for different theories. Different boundary conditions

BCS	Theory	Stress S_x						
		P	7	9	10	11	12	13
CFSF	ED2		0.4442	0.4434	0.4434	0.4438	0.4438	0.4437
	ED5		0.5278	0.5194	0.5194	0.5229	0.5229	0.5217
	LD2		0.5246	0.5205	0.5205	0.5219	0.5219	0.5215
	LD4		0.5291	0.5185	0.5186	0.5243	0.5243	0.5214
FCCF	ED2		-0.4248	-0.4258	-0.4251	-0.4251	-0.4256	-0.4256
	ED5		-0.3680	-0.3774	-0.3767	-0.3730	-0.3739	-0.3752
	LD2		-0.3709	-0.3757	-0.3748	-0.3736	-0.3744	-0.3748
	LD4		-0.3682	-0.3803	-0.3796	-0.3732	-0.3741	-0.3773

Table 7.4: Convergence of S_x stress for different theories. Different boundary conditions

In tables 7.5 and 7.6 are shown the variation of displacements and stress S_y obtained with two different distribution of pressure, for various ESL and LW theories, with respect of the order of the Ritz expansion P. The plate considered is a rectangular, fully clamped, four layer laminate with an

height to side ratio $\frac{h}{a} = 0.1$ and a form factor $\frac{b}{a} = 1.5$. All layers have the same thickness and are made of CFRP4 and the lamination scheme is (0/90/0/90). The load applied is a pressure with a bisinusoidal distribution $p_z = P_z \sin(\pi \frac{x}{a}) \sin(\pi \frac{y}{b})$, which acts on the top surface of the plate.

Pressure distribution	Theory	Displacement $\bar{w}$						
		P	7	9	10	11	12	13
Triangular (x direction)	ED3		0.3491	0.3481	0.3482	0.3485	0.3485	0.3484
	ED6		0.3803	0.3797	0.3798	0.3800	0.3800	0.3800
	LD3		0.3968	0.3959	0.3961	0.3965	0.3965	0.3964
Bisinusoidal	ED3		0.5014	0.5006	0.5006	0.5009	0.5009	0.5008
	ED6		0.5474	0.5469	0.5470	0.5472	0.5472	0.5472
	LD3		0.5712	0.5706	0.5707	0.5710	0.5710	0.5709

Table 7.5: Convergence of $\bar{w}$ for different theories. Different load distribution

Pressure distribution	Theory	Stress S_y						
		P	7	9	10	11	12	13
Triangular (x direction)	ED3		0.1181	0.1132	0.1155	0.1154	0.1143	0.1146
	ED6		0.1222	0.1173	0.1203	0.1197	0.1179	0.1186
	LD3		0.1244	0.1187	0.1221	0.1219	0.1196	0.1200
Bisinusoidal	ED3		0.2140	0.2106	0.2122	0.2120	0.2113	0.2116
	ED6		0.2236	0.2205	0.2224	0.2218	0.2208	0.2214
	LD3		0.2275	0.2239	0.2261	0.2257	0.2243	0.2247

Table 7.6: Convergence of S_y stress for different theories. Different load distribution

In tables 7.7 and 7.8 are shown the variation of displacements and stress S_x obtained with two different lamination sequences, for various ESL and LW theories, with respect of the order of the Ritz expansion P. The plate considered is a squared, simply supported, two layer laminate with an height to side ratio of $\frac{h}{a} = 0.1$. All layers have the same thickness and are made of CFRP3. The load applied is a pressure with a sinusoidal distribution $p_z = P_z \sin(\pi \frac{y}{b})$, which acts on the top surface of the plate.

Lamination scheme	Theory	Displacement $\bar{w}$						
		P	7	9	10	11	12	13
$(-45/45)$	ED1		0.5126	0.5126	0.5128	0.5128	0.5129	0.5129
	ED4		0.6246	0.6283	0.6289	0.6296	0.6298	0.6298
	LD1		0.5919	0.5956	0.5956	0.5961	0.5963	0.5963
$(-30/60)$	ED1		0.6792	0.6803	0.6810	0.6812	0.6815	0.6816
	ED4		0.7862	0.7916	0.7924	0.7933	0.7940	0.7944
	LD1		0.7615	0.7668	0.7674	0.7683	0.7690	0.7692

Table 7.7: Convergence of $\bar{w}$ for different theories. Different lamination scheme

Lamination scheme	Theory	Stress S_x						
		P	7	9	10	11	12	13
$(-45/45)$	ED1		0.2655	0.2638	0.2663	0.2640	0.2656	0.2640
	ED4		0.2855	0.2902	0.3000	0.2931	0.2982	0.2933
	LD1		0.2647	0.2777	0.2807	0.2760	0.2808	0.2811
$(-30/60)$	ED1		0.1885	0.1888	0.1917	0.1907	0.1919	0.1917
	ED4		0.1997	0.2086	0.2118	0.2078	0.2118	0.2104
	LD1		0.1907	0.1994	0.2027	0.1996	0.2027	0.2030

Table 7.8: Convergence of S_x stress for different theories. Different lamination scheme

These results indicates that a Ritz expansion of order 11 is sufficiently to get the convergence of the results for what concerns displacements. From now, if not specified differently, all the results presented are calculated using an eleventh order Ritz expansion.

7.2.2 Problem I - Crossply square plate loaded by a transverse pressure with constant distribution

A simply supported square plate loaded by a constant transverse distribution of pressure P_z has been considered in tables 7.9,7.10 and figures from 7.1 to 7.10. The plates are made of CFRP4, and follow a different lamination scheme: before a symmetrical laminate of three layers (0/90/0) is considered and then an anti-symmetrical laminate of four layers (0/90/0/90) is used for further investigation. All layers of the laminate are of the same thickness. For both lamination scheme thin and thick plates are considered: the height to side ratio is $h/a = 0.01$ for the thin and $h/a = 0.25$ for the thick plate. The

reference values are those calculated by [6] with a layerwise mixed formulation of the fourth order, so they can be considered highly accurate.

Results reported in table 7.9 are relative to the symmetric laminate in both thin and thick configuration.

$\frac{h}{a}$	Theory	$\bar{w}$	S_x	S_y	S_{xy}	S_{xz}	S_{yz}
0.01	ED3	0.6706	0.8081	0.0309	0.0429	0.7318	0.4045
	ED5	0.6709	0.8082	0.0309	0.0430	0.7314	0.4046
	LD1	0.6702	0.8087	0.0323	0.0428	0.7250	0.4044
	Ref	0.6713	0.8083		0.0428	0.7201	0.3852
0.25	ED3	2.8714	1.1031	0.1196	0.1001	0.4810	0.4657
	ED5	2.9169	1.0881	0.1164	0.0989	0.4793	0.5136
	LD1	2.9454	1.0049	0.1209	0.0886	0.4374	0.4014
	Ref	3.0444	1.1173		0.0973	0.4435	0.4956

Table 7.9: Transverse displacement and stresses for a square plate with three layers (0/90/0). Uniform transverse pressure

The performance obtained by different ESL and LW theories can be compared plotting the stresses distributions through the thickness of the laminate. Plots relative at theories used in table 7.9 are presented for both thin and thick plate, in figures from 7.1 to 7.5.

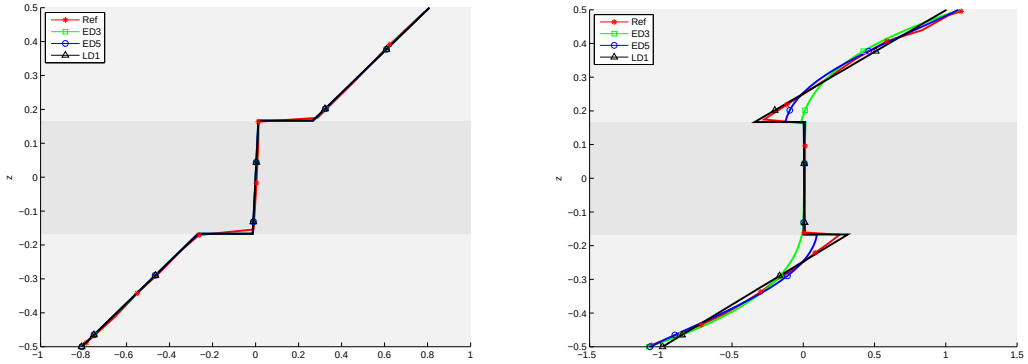

Figure 7.1: S_x $(\frac{a}{2}, \frac{b}{2})$, for a thin (left) and a thick (right) (0/90/0) laminate

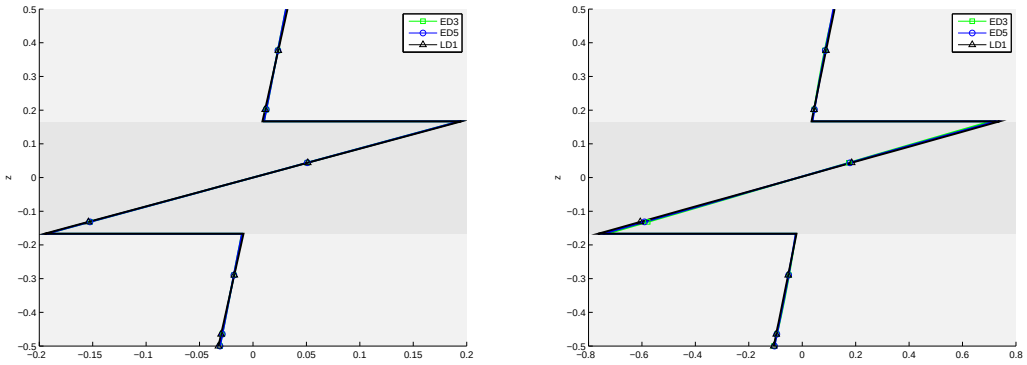

Figure 7.2: S_y $(\frac{a}{2}, \frac{b}{2})$, for a thin (left) and a thick (right) (0/90/0) laminate

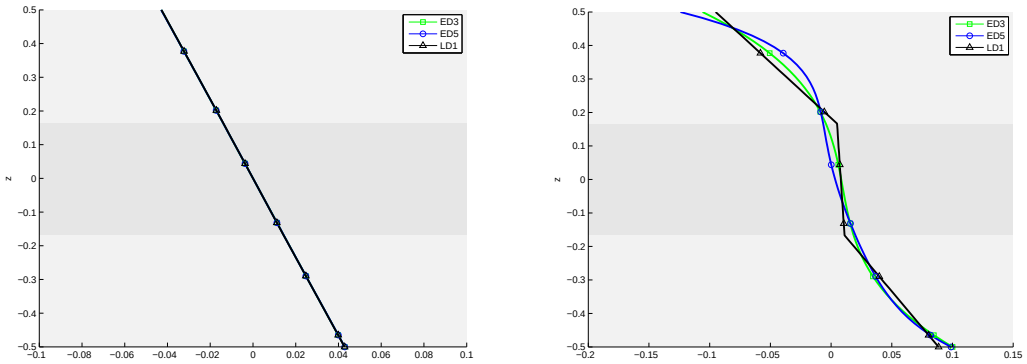

Figure 7.3: S_{xy} $(0, 0)$, for a thin (left) and a thick (right) (0/90/0) laminate

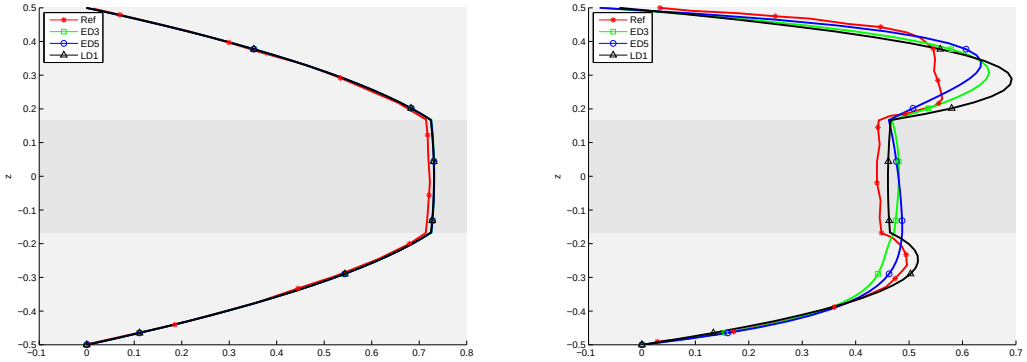

Figure 7.4: S_{xz} $(0, \frac{b}{2})$, for a thin (left) and a thick (right) (0/90/0) laminate

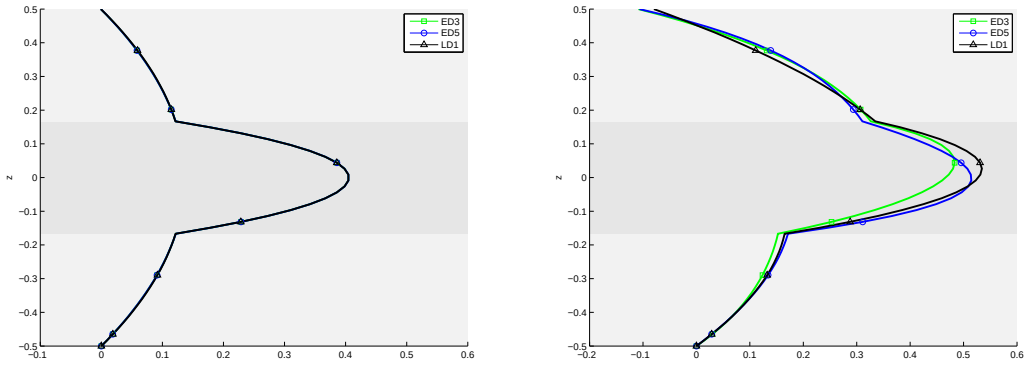

Figure 7.5: S_{yz} $(\frac{a}{2}, 0)$, for a thin (left) and a thick (right) (0/90/0) laminate

As expected, for the thin plate, both ESL and LW theories get very similar results and are both capable to compute the displacements of the loaded plate while, for the thick plate the results obtained suggest that the LW theories can get better results than the ESL theories, also with lower order theories since LW kinematic models use distinct degrees of freedom for each layer and so the in-layer distribution of stresses and displacements is not influenced by the others layer's one, except for the continuity hypothesis. It is clearly shown in figure 7.1 which shows that ESL models are not capable to get the sudden S_x stress variation around layers interfaces and, also in all layers thickness as shown in figure 7.4, in which the S_{xz} stress behaviour is correctly approximate in top and center layers by all models but only the LW model approximate also the bottom layer behaviour.

Now the anti-symmetric square crossply will be considered, both the thin and thick laminate are analyzed and the numeric results with the through the thickness stress distribution are presented in table 7.10 and figures from 7.6 to 7.10.

$\frac{h}{a}$	Theory	$\bar{w}$	S_x	S_y	S_{xy}	S_{xz}	S_{yz}
0.01	ED4	0.8117	0.0543	0.7371	0.0445	0.6217	0.6219
	LD2	0.8123	0.0542	0.7371	0.0446	0.6214	0.6216
	LD4	0.8123	0.0542	0.7371	0.0446	0.6214	0.6216
	Ref	0.8123	0.0542	0.7371	0.0445	0.6058	
0.25	ED4	2.7054	0.1057	0.9776	0.0796	0.4489	0.4882
	LD2	2.9619	0.1116	1.0158	0.0878	0.4295	0.4543
	LD4	2.9680	0.1111	1.0087	0.0891	0.4365	0.4617
	Ref	2.9679	0.1141	1.011	0.0891	0.4209	

Table 7.10: Transverse displacement and stresses for a square plate with four layers (0/90/0/90). Uniform transverse pressure

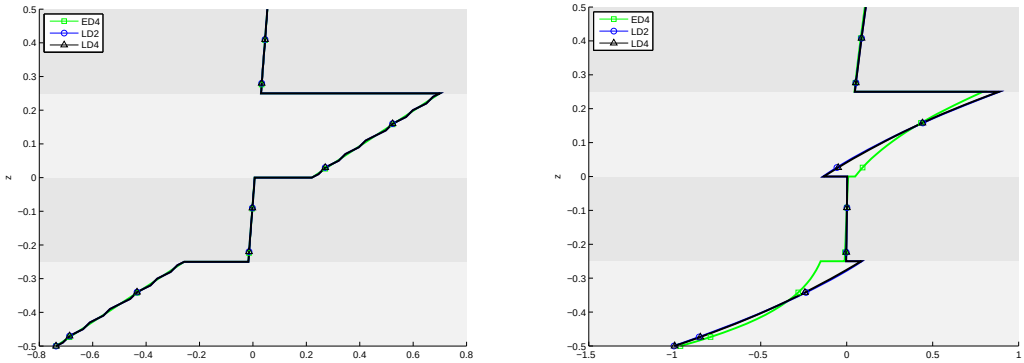

Figure 7.6: S_x $(\frac{a}{2}, \frac{b}{2})$, for a thin (left) and a thick (right) (0/90/0/90) laminate

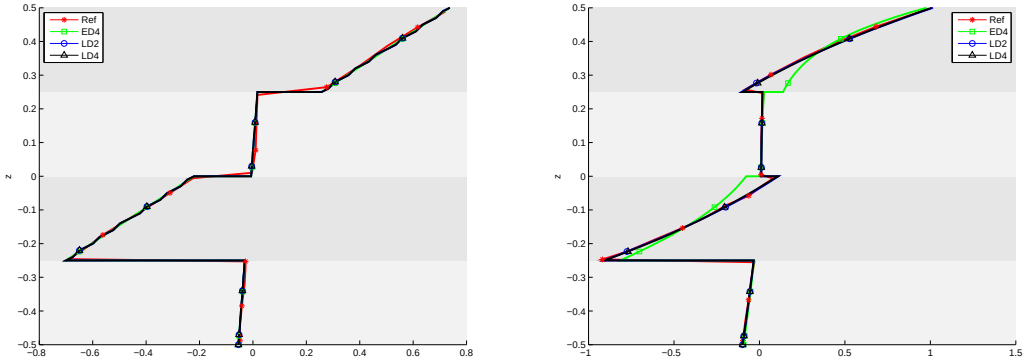

Figure 7.7: S_y $(\frac{a}{2}, \frac{b}{2})$, for a thin (left) and a thick (right) (0/90/0/90) laminate

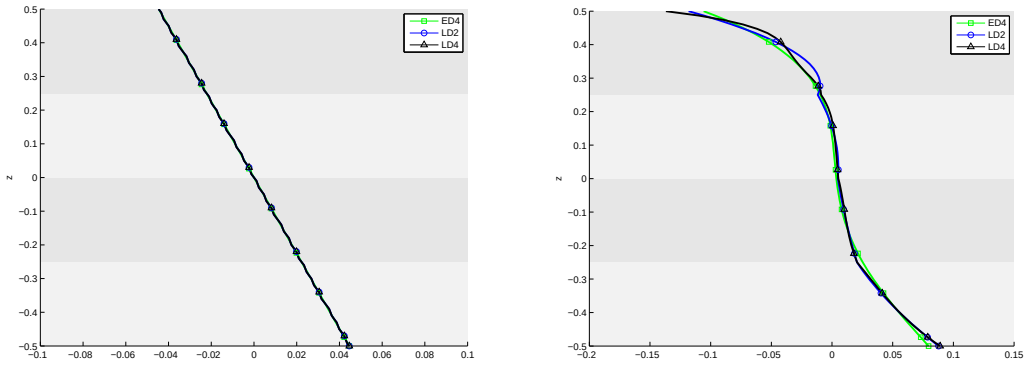

Figure 7.8: S_{xy} $(0, 0)$, for a thin (left) and a thick (right) (0/90/0/90) laminate

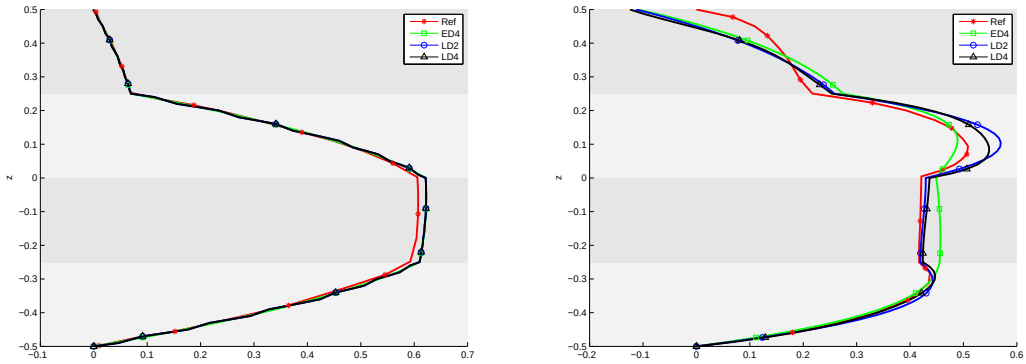

Figure 7.9: S_{xz} $(0, \frac{b}{2})$, for a thin (left) and a thick (right) (0/90/0/90) laminate

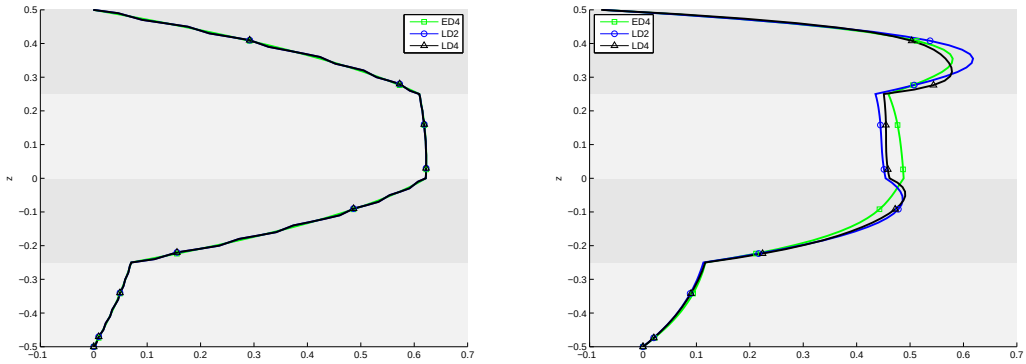

Figure 7.10: S_{yz} $(\frac{a}{2}, 0)$, for a thin (left) and a thick (right) (0/90/0/90) laminate

Consideration made for the three layer plate considered before are here empathized by the presence of a fourth layer which makes more difficult to describe the stresses behaviour of the thick plate only by global degrees of

freedom of ESL theories as shown also for S_y and S_{yz} in figures 7.7 and 7.10, also adopting an ESL theory of a relative high order. The use of $ED6$ might give a better approximation as reported later, but with a large model, which cam be also larger than the $LD2$ model used here, capable to get always the correct approximation of all stresses behaviour in plate thickness. This last model can be a wise choice to create a relatively small model with respect of an $LD4$ model, sacrificing something in terms of fine approximation, but maintaining the capability of predict the correct stress and displacements for the whole plate with a more effective model.

7.2.3 Problem II - Crossply square plate loaded by a transverse pressure with triangular distribution

A simply supported square plate loaded by a triangular transverse distribution of pressure $p_z = P_z \frac{x}{a}$, has been considered. The plate is made of CFRP4, and follow a symmetrical lamination scheme of three layers (0/90/0) of equal thickness. Both thin and thick plates are considered: the height to side ratio is $\frac{h}{a} = 0.01$ for the thin plate and $\frac{h}{a} = 0.25$ for the thick plate. Results related with this problem are presented in table 7.11 and figures from 7.11 to 7.15. The reference values are those calculated by [6] with a layerwise mixed formulation of the fourth order, so they can be considered highly accurate.

$\frac{h}{a}$	Theory	$\bar{w}$	S_x	S_y	S_{xy}	S_{xz}	S_{yz}
0.01	ED2	0.3345	0.4036	0.0154	0.0183	0.2494	0.2021
	ED4	0.3353	0.4040	0.0154	0.0184	0.2494	0.2022
	LD3	0.3356	0.4637	0.0638	0.0303	0.2495	0.2022
	Ref	0.3356	0.4042			0.2499	
0.25	ED2	1.1635	0.3377	0.0464	0.0250	0.2169	0.2750
	ED4	1.4343	0.5489	0.0580	0.0360	0.1838	0.2255
	LD3	1.5223	0.6539	0.1340	0.0751	0.1681	0.2517
	Ref	1.5222	0.5592			0.1656	

Table 7.11: Transverse displacement and stresses for a square plate with three layers (0/90/0). Transverse pressure with triangular distribution

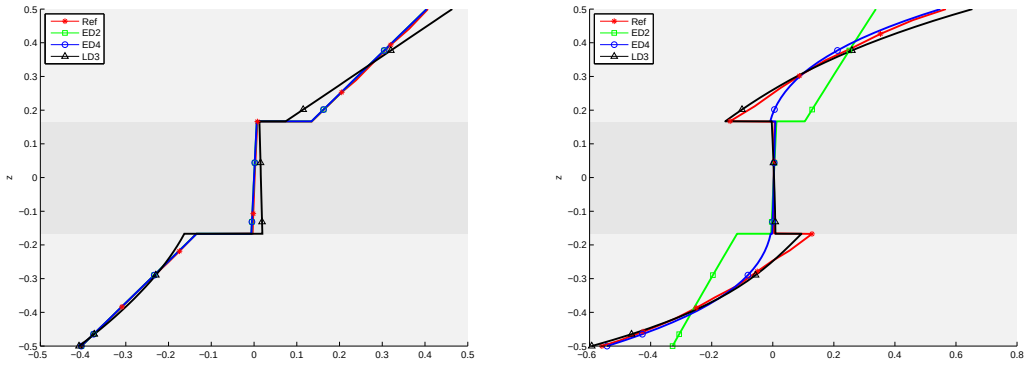

Figure 7.11: S_x $(\frac{a}{2}, \frac{b}{2})$, for a thin (left) and a thick (right) (0/90/0) laminate

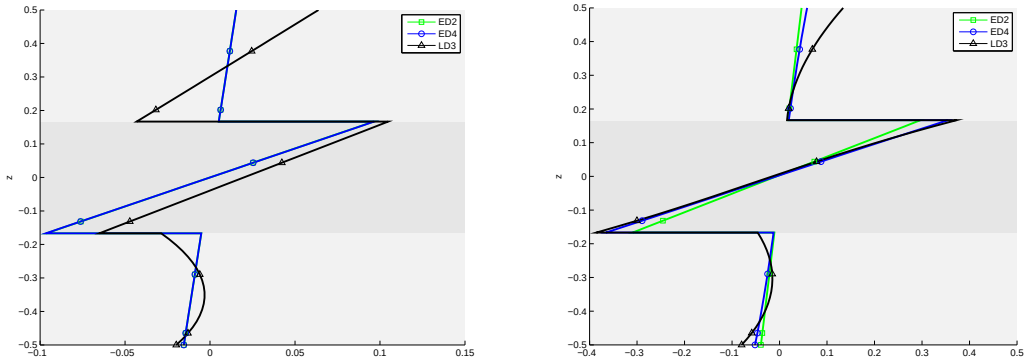

Figure 7.12: S_y $(\frac{a}{2}, \frac{b}{2})$, for a thin (left) and a thick (right) (0/90/0) laminate

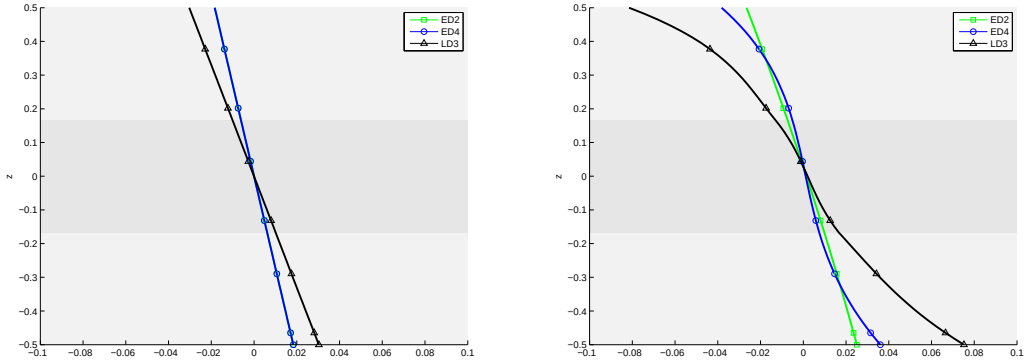

Figure 7.13: S_{xy} $(0, 0)$, for a thin (left) and a thick (right)(0/90/0) laminate

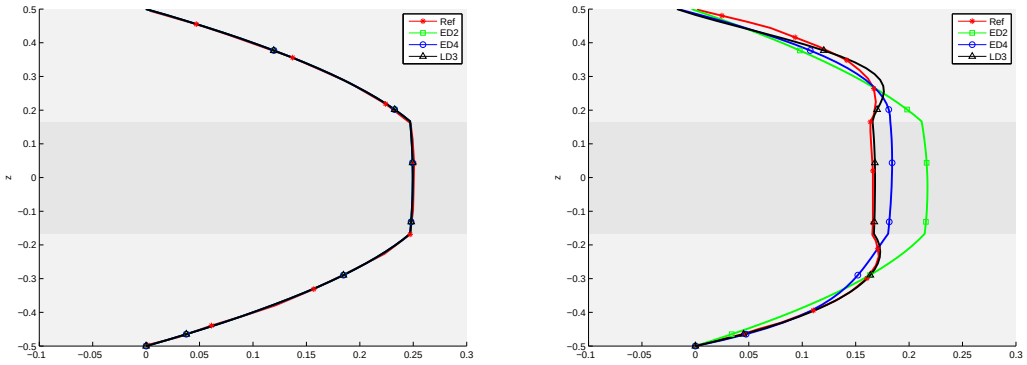

Figure 7.14: S_{xz} $(0, \frac{b}{2})$, for a thin (left) and a thick (right) (0/90/0) laminate

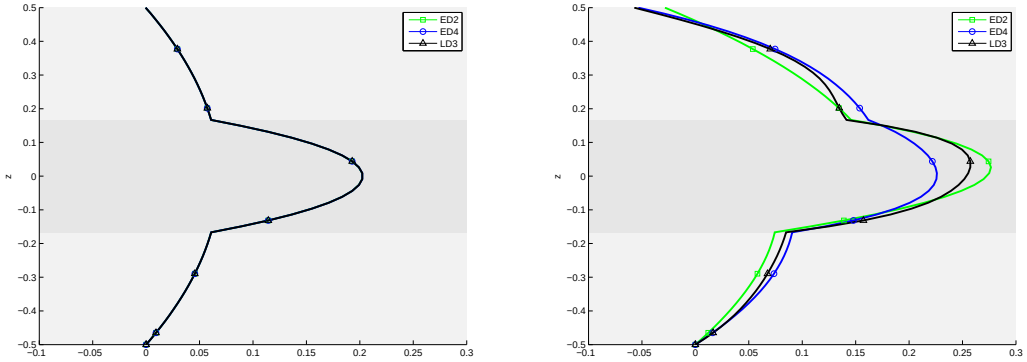

Figure 7.15: S_{yz} $(\frac{a}{2}, 0)$, for a thin (left) and a thick (right) (0/90/0) laminate

These plots indicates that for thick laminates layerwise kinematic theories shall be adopted if precise displacements and stresses values are required, moreover the choice of an high order LW theory become mandatory if the through the thickness stresses precise behaviour is sought. ESL theories however are good if the laminate is thin or if a rough approximation of the displacements and stresses is sufficient. In this latter case, anyway, an higher order theory shall be preferred.

7.2.4 Problem III - Crossply square plate loaded by a transverse pressure with bitriangular distribution

A simply supported square plate has been considered. The plate is loaded by a bitriangular transverse distribution of pressure,

$$\begin{aligned} p_z &= P_z \tfrac{2x}{a} && \text{if } 0 \leq x \leq \tfrac{a}{2} \\ p_z &= P_z(2 - \tfrac{2x}{a}) && \text{if } \tfrac{a}{2} \leq x \leq a \end{aligned}$$

The plate is made of CFRP4, and follow an anti-symmetrical lamination scheme of four layers (0/90/0/90) of equal thickness. Both thin and thick plates are considered: the height to side ratio is $\frac{h}{a} = 0.01$ for the thin plate and $\frac{h}{a} = 0.25$ for the thick plate. Results related with this problem are presented in table 7.12 and figures from 7.16 to 7.20. The reference values are those calculated by [6] with a layerwise mixed formulation of the fourth order, so they can be considered highly accurate.

$\frac{h}{a}$	Theory	$\bar{w}$	S_x	S_y	S_{xy}	S_{xz}	S_{yz}
0.01	ED3	0.5210	0.0371	0.4691	0.0263	0.2568	0.4392
	ED5	0.5213	0.0372	0.4693	0.0263	0.2568	0.4391
	LD4	0.5217	0.0371	0.4692	0.0263	0.2569	0.4389
	Ref	0.5225	0.0372			0.2701	0.4261
0.25	ED3	1.7030	0.0894	0.5979	0.0455	0.2396	0.3796
	ED5	1.8245	0.0890	0.6404	0.0479	0.2242	0.3472
	LD4	1.9765	0.0918	0.6658	0.0496	0.2235	0.3121
	Ref	1.9802	0.0955			0.2239	0.3132

Table 7.12: Transverse displacement and stresses for a square plate with four layers (0/90/0/90). Transverse pressure with bitriangular distribution

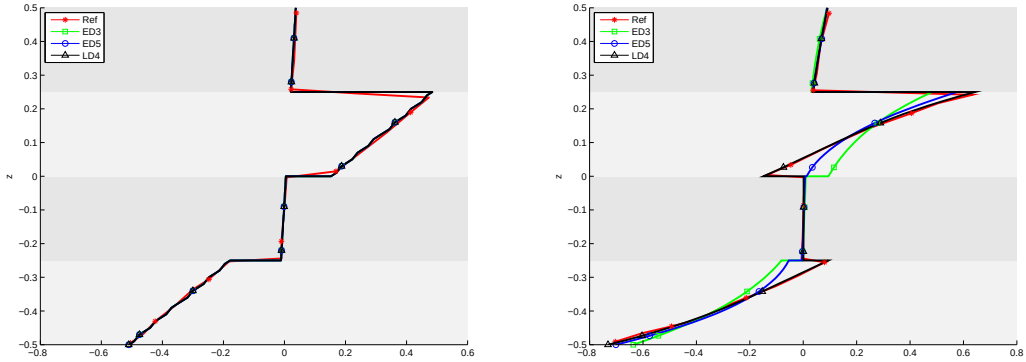

Figure 7.16: S_x $(\frac{a}{2}, \frac{b}{2})$, for a thin (left) and a thick (right) (0/90/0/90) laminate

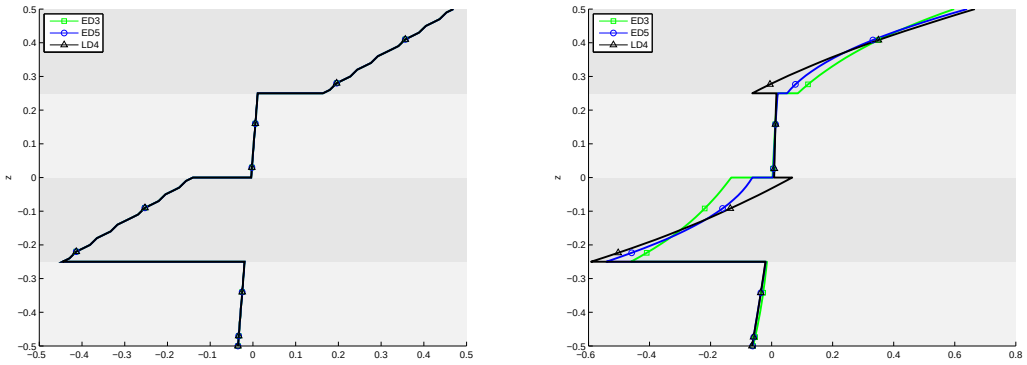

Figure 7.17: S_y $(\frac{a}{2}, \frac{b}{2})$, for a thin (left) and a thick (right) (0/90/0/90) laminate

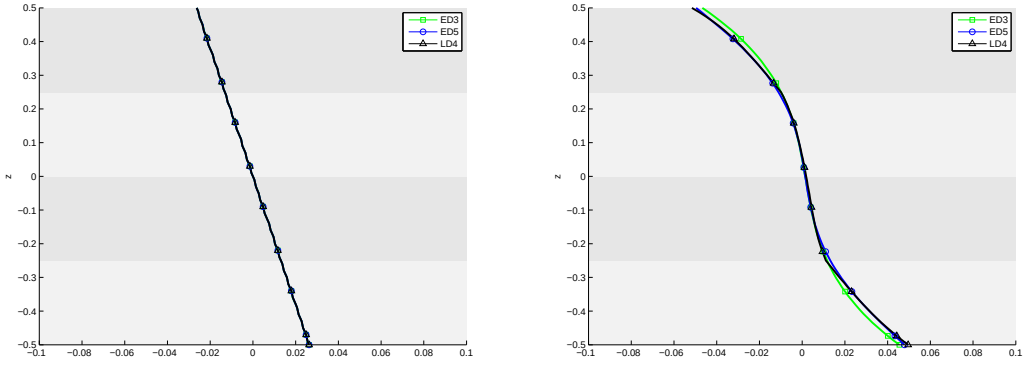

Figure 7.18: S_{xy} $(0, 0)$, for a thin (left) and a thick (right) (0/90/0/90) laminate

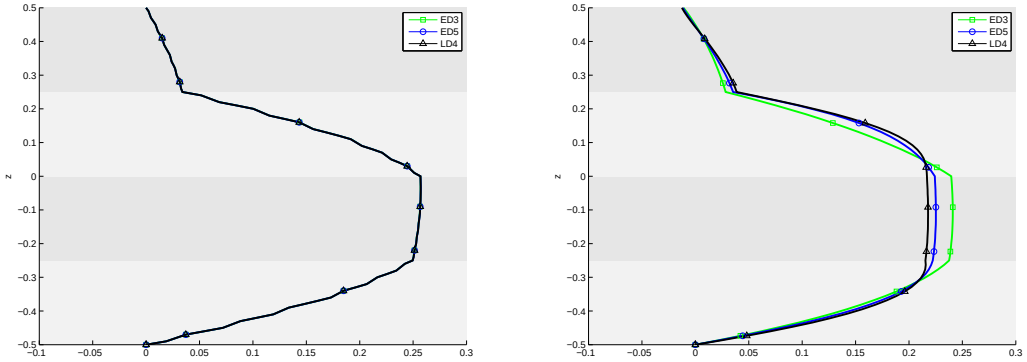

Figure 7.19: S_{xz} $(0, \frac{b}{2})$, for a thin (left) and a thick (right) (0/90/0/90) laminate

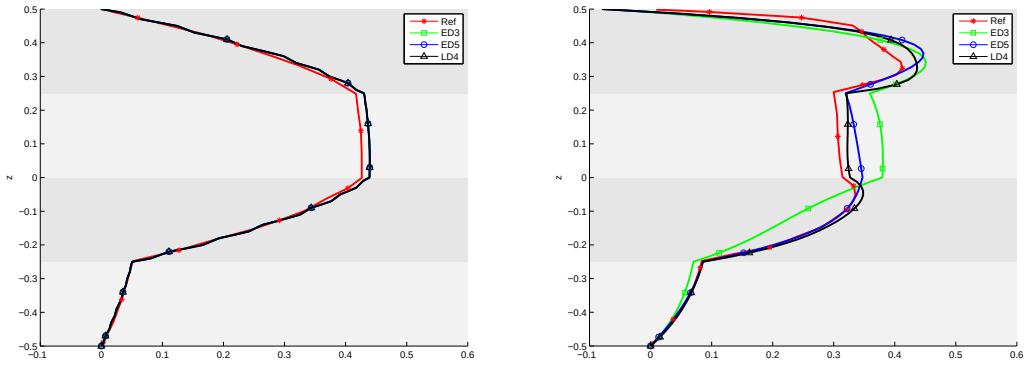

Figure 7.20: S_{yz} $(\frac{a}{2}, 0)$, for a thin (left) and a thick (right) (0/90/0/90) laminate

Results reported in table 7.12 and figures from 7.16 to 7.20 shows that consideration made for *Problem I* and *II* are still valid in this case, where also a refined ESL theory like $ED5$ fails in getting the correct stresses behaviour into the thickness of the thick laminate. However, both ESL theories adopted here are capable to give a quite good approximation of displacements and stresses values in the points considered.

7.2.5 Problem IV - Crossply square plate loaded by a transverse pressure with sinusoidal distribution

A simply supported square plate loaded by a sinusoidal transverse distribution of pressure $p_z = P_z \sin(\pi \frac{x}{a})$, has been considered. The plate is made of CFRP4, and follow a symmetrical lamination scheme of four layers (0/90/90/0) of equal thickness. Both thin and thick plates are considered: the height to side ratio is $\frac{h}{a} = 0.05$ for the thin plate and $\frac{h}{a} = 0.25$ for the thick plate. Results related with this problem are presented in table 7.13 and figures from 7.21 to 7.25. The reference values are those calculated by [15] with a mixed MLPG formulation of the fifth order.

$\frac{h}{a}$	Theory	$\bar{w}$	S_x	S_y	S_{xy}	S_{xz}	S_{yz}
0.05	ED2	0.4811	0.5287	0.0289	0.0220	0.3341	0.1485
	ED4	0.5073	0.5430	0.0305	0.0229	0.3292	0.1546
	LD3	0.5130	0.5428	0.0307	0.0231	0.3282	0.1556
	Ref	0.5063	0.5400	0.3050	0.0224	0.4735	0.1260
0.25	ED2	1.4899	0.4334	0.0628	0.0287	0.2738	0.2672
	ED4	1.8708	0.7219	0.0872	0.0447	0.2263	0.2952
	LD3	1.9367	0.7204	0.0890	0.0458	0.2192	0.2915
	Ref	1.8930	0.7125	0.6313	0.0459	0.3575	0.2675

Table 7.13: Transverse displacement and stresses for a square plate with four layers (0/90/90/0). Transverse pressure with sinusoidal distribution

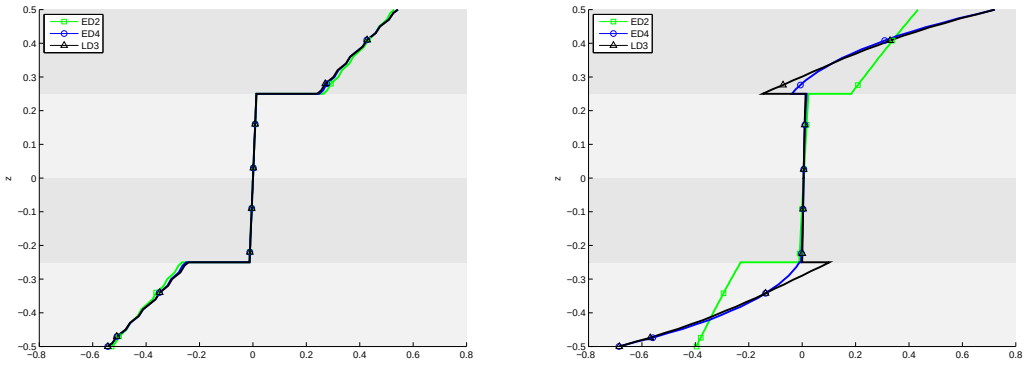

Figure 7.21: S_x $(\frac{a}{2}, \frac{b}{2})$, for a thin (left) and a thick (right) (0/90/90/0) laminate

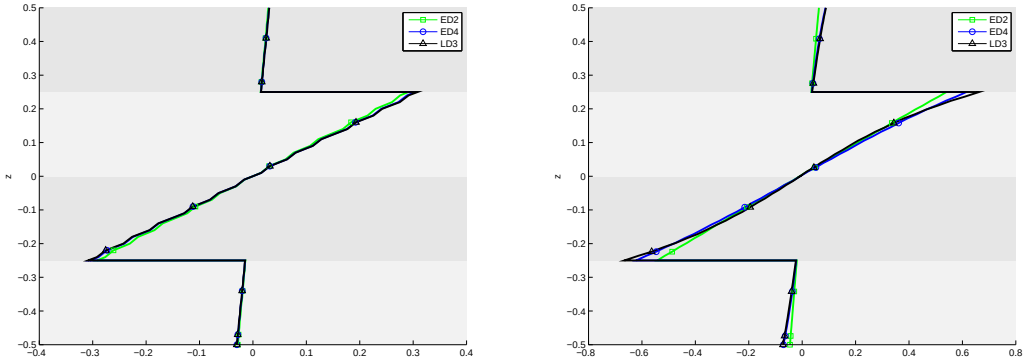

Figure 7.22: S_y $(\frac{a}{2}, \frac{b}{2})$, for a thin (left) and a thick (right) (0/90/90/0) laminate

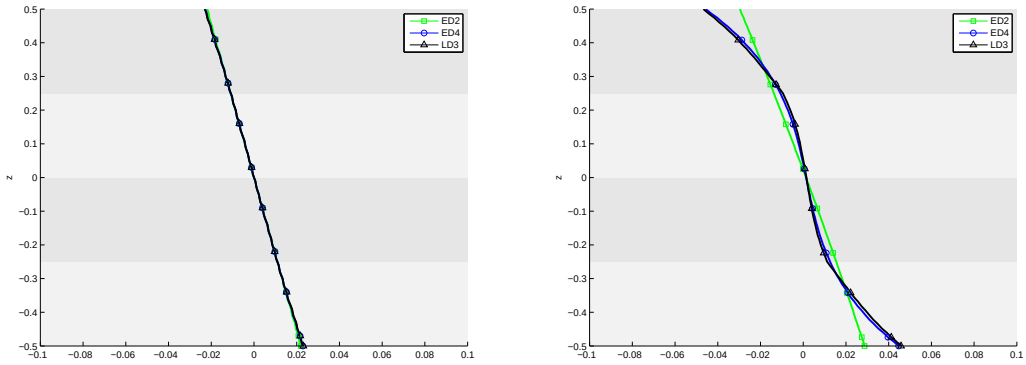

Figure 7.23: S_{xy} $(0, 0)$, for a thin (left) and a thick (right) (0/90/90/0) laminate

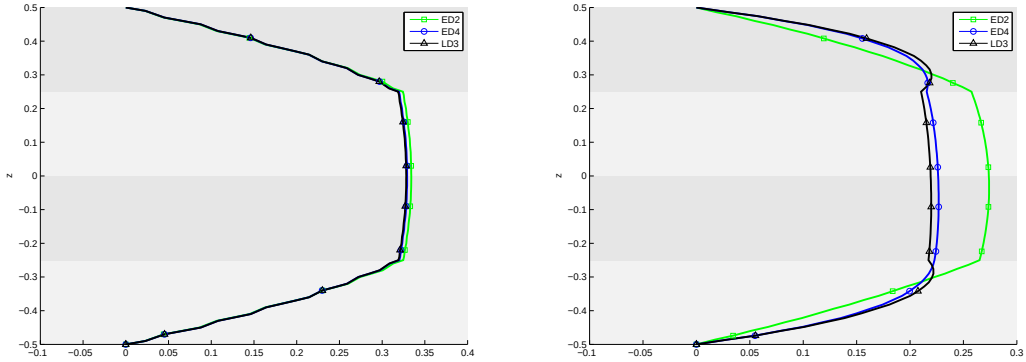

Figure 7.24: S_{xz} $(0, \frac{b}{2})$, for a thin (left) and a thick (right) (0/90/90/0) laminate

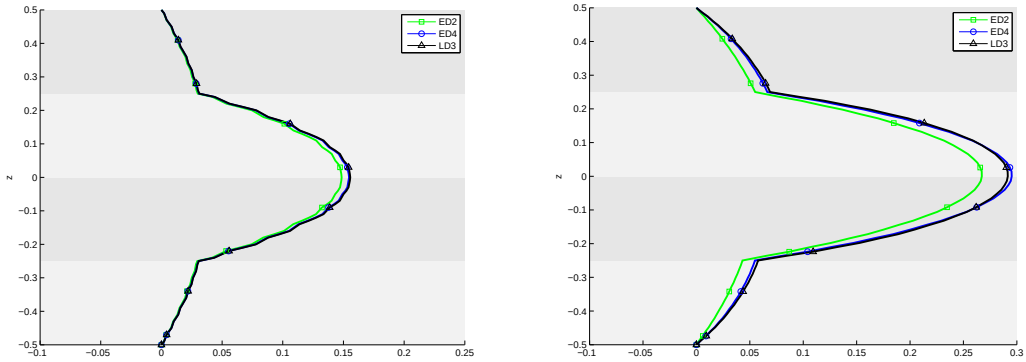

Figure 7.25: S_{yz} $(\frac{a}{2}, 0)$, for a thin (left) and a thick (right) (0/90/90/0) laminate

The symmetry of the laminate adopted helps ESL theories in getting a better approximation of stress behaviour like in first case of *Problem I*, in which the difference between a LW approach lie in the capability of this one

to get the sudden stresses variation around layers interfaces as depicted in figures 7.21 and 7.24.

A thing shall be noticed: the reference values of S_y stress are very high with respect of the values obtained. An explanation could be that the authors of [15] have reported the wrong thickness at which they had evaluate the S_y stress. The orientation of the layers suggest that the maximum value of S_y shall be reached in the thickness of the two central layers of 90° orientation, whereas in the other two layers with 0° orientation maintain a value in proximity of zero, as like as the S_x stress which has the opposite behaviour, reaching its maximum in the layers with 0° orientation. This is due to the orthotropicy of the material of which the plate is made that makes the in-plane stresses go higher in the fiber direction.

7.2.6 Problem V - Crossply square plate loaded by a transverse pressure with bisinusoidal distribution

A simply supported square plate loaded by a bisinusoidal transverse distribution of pressure $p_z = P_z \sin(\pi \frac{x}{a}) \sin(\pi \frac{y}{b})$, has been considered. The plate is made of CFRP4, and follow a symmetrical lamination scheme of four layers (0/90/90/0) of equal thickness. Both thin and thick plates are considered: the height to side ratio is $\frac{h}{a} = 0.05$ for the thin plate and $\frac{h}{a} = 0.25$ for the thick plate. Results related with this problem are presented in table 7.14 and figures from 7.26 to 7.30. The reference values are those calculated by [1] with a discrete shear gap finite elements formulation.

$\frac{h}{a}$	Theory	$\bar{w}$	S_x	S_y	S_{xy}	S_{xz}	S_{yz}
0.01	ED3	0.4344	0.5389	0.0268	0.0214	0.3388	0.1389
	ED6	0.4345	0.5388	0.0268	0.0214	0.3388	0.1389
	LD3	0.4346	0.5388	0.0268	0.0214	0.3388	0.1389
	Ref	0.4347	0.539	0.271	0.0214	0.339	0.139
0.25	ED3	1.8732	0.7248	0.0899	0.0446	0.2258	0.2949
	ED6	1.8960	0.7135	0.0881	0.0454	0.2214	0.2903
	LD3	1.9367	0.7204	0.0890	0.0458	0.2193	0.2915
	Ref	1.954	0.720	0.666	0.0467	0.270	

Table 7.14: Transverse displacement and stresses for a square plate with four layers (0/90/90/0). Transverse pressure with bisinusoidal distribution

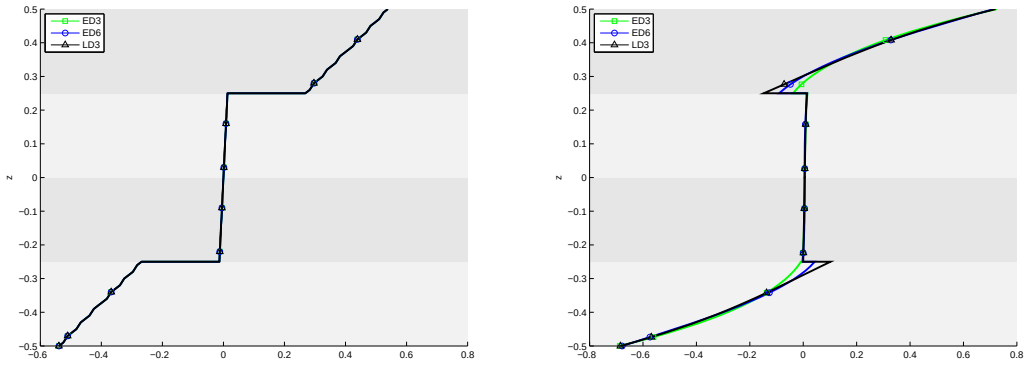

Figure 7.26: S_x $(\frac{a}{2}, \frac{b}{2})$, for a thin (left) and a thick (right) (0/90/90/0) laminate

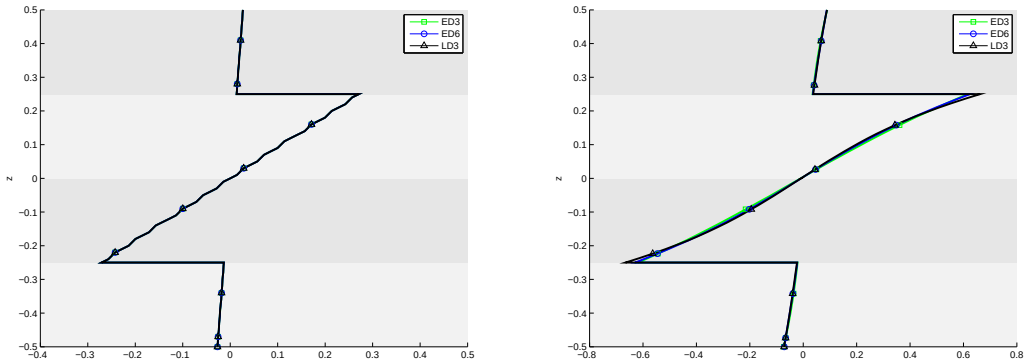

Figure 7.27: S_y $(\frac{a}{2}, \frac{b}{2})$, for a thin (left) and a thick (right) (0/90/90/0) laminate

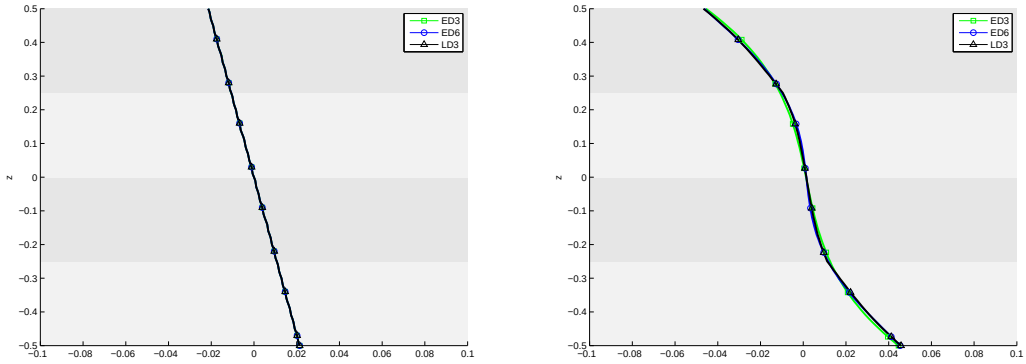

Figure 7.28: S_{xy} $(0, 0)$, for a thin (left) and a thick (right) (0/90/90/0) laminate

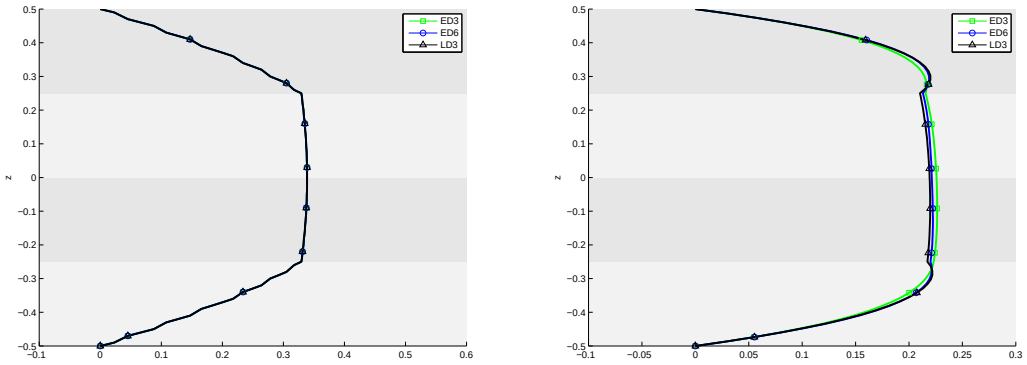

Figure 7.29: S_{xz} $(0, \frac{b}{2})$, for a thin (left) and a thick (right) (0/90/90/0) laminate

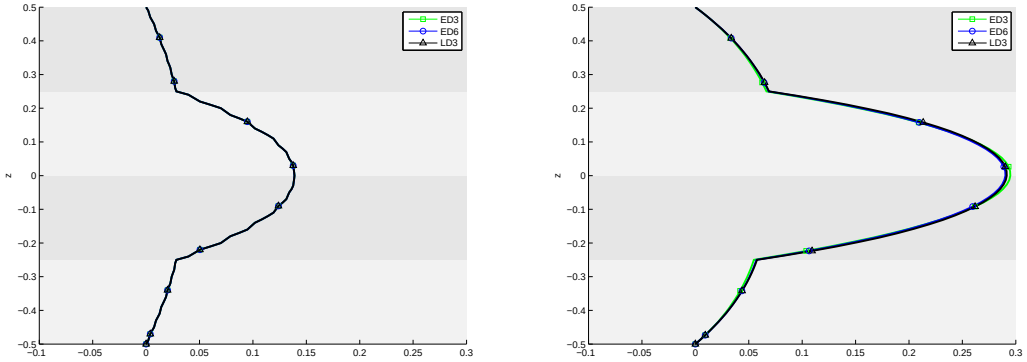

Figure 7.30: S_{yz} $(\frac{a}{2}, 0)$, for a thin (left) and a thick (right) (0/90/90/0) laminate

Comments made for *Problem IV* are confirmed, moreover can be appreciated how ESL $ED6$ can approximate in a better way the trough the thickness behaviour of S_x and S_{xz} stresses near the layers interfaces as shown in figures 7.26 and 7.29.

Also in this case the reference values of S_y stress are very high with respect of the values obtained. The reason can be sought in the same deduction depicted in *Problem IV* looking at figure 7.27.

7.2.7 Problem VI - Square sandwich plate loaded by a transverse pressure with constant distribution

Now a square plate is considered, it consists of a two skins with equal thickness $0.1h$ made by CFRP4 while the inner layer, the weak core, has a thickness $0.8h$ and it's made by Core1. Both a moderately thin and thick plates are considered: the height to side ratio is $\frac{h}{a} = 0.1$ for the moderately thin plate and $\frac{h}{a} = 0.25$ for the thick plate. Results related with this problem are

presented in table 7.15 and figures from 7.31 to 7.35. The reference values are those calculated by [6] with a layerwise mixed formulation of the fourth order, so they can be considered highly accurate.

$\frac{h}{a}$	Theory	$\bar{w}$	S_x	S_y	S_{xy}	S_{xz}	S_{yz}
0.1	ED4	2.9352	1.5166	0.1185	0.1323	0.5001	0.2274
	LD2	3.0804	1.5026	0.1247	0.1359	0.5133	0.2570
	LD4	3.0828	1.5053	0.1239	0.1372	0.5158	0.2385
	Ref	3.083	1.509			0.5276	
0.25	ED4	10.0373	1.9218	0.2575	0.2387	0.3764	0.2565
	LD2	10.6275	1.8697	0.2657	0.2506	0.4123	0.3375
	LD4	10.6813	1.8880	0.2693	0.2559	0.4288	0.3234
	Ref	10.682	1.902			0.4074	

Table 7.15: Transverse displacement and stresses for a square sandwich plate. Transverse pressure with constant distribution

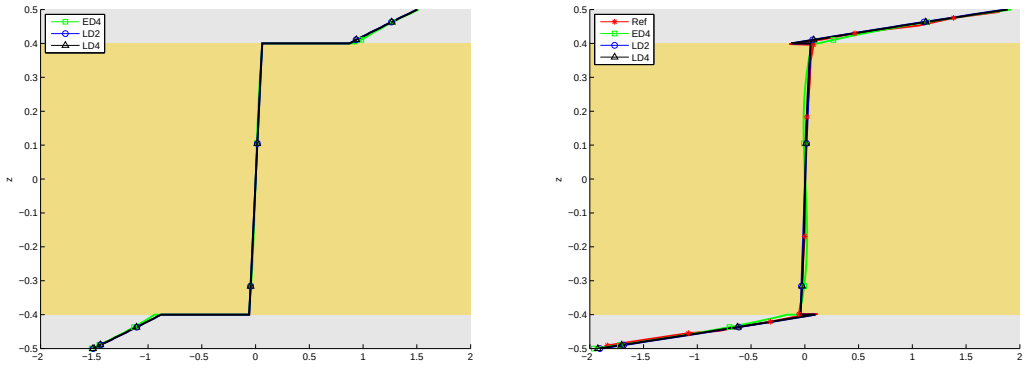

Figure 7.31: S_x $(\frac{a}{2}, \frac{b}{2})$, for a moderately thin (left) and a thick (right) sandwich plate

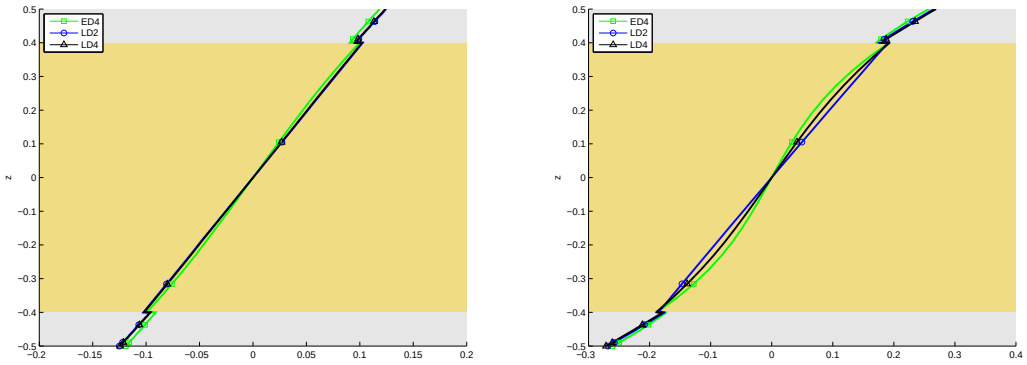

Figure 7.32: S_y $(\frac{a}{2}, \frac{b}{2})$, for a moderately thin (left) and a thick (right) sandwich plate

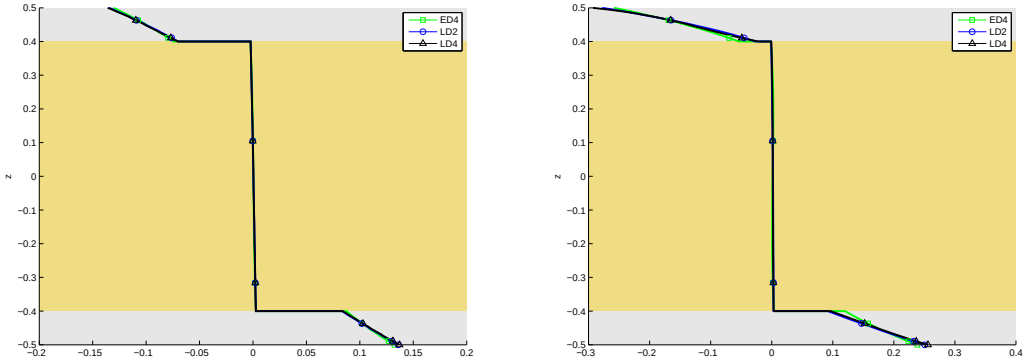

Figure 7.33: S_{xy} $(0, 0)$, for a moderately thin (left) and a thick (right) sandwich plate

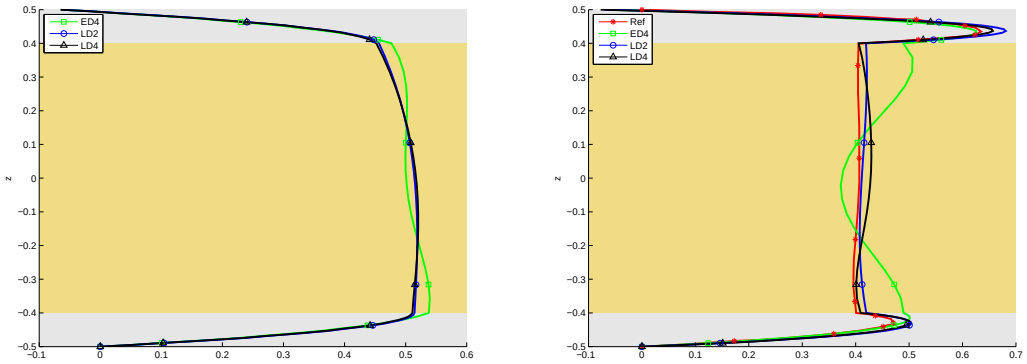

Figure 7.34: S_{xz} $(0, \frac{b}{2})$, for a moderately thin (left) and a thick (right) sandwich plate

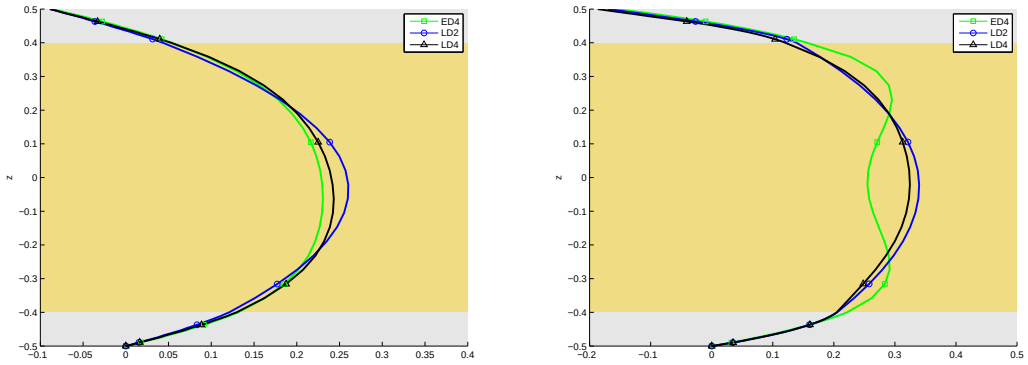

Figure 7.35: S_{yz} $(\frac{a}{2}, 0)$, for a moderately thin (left) and a thick (right) sandwich plate

The weak core makes predominant the effect related to transverse normal deformability and causes an increase of the differences among different theories in the thick plate case with respect distribution of out of plane stresses S_{xz} and S_{yz} as shown in figures 7.34 and 7.35: ESL $ED4$ theory, although been an high order and refined theory, miss completely the stresses distribution in the core thickness and makes compulsory the adoption of a more suited LW theory, unless only a rough approximation is sought or the plate is thin. This last condition is of less interest since sandwich plate are widely adopted for theirs peculiar mechanical properties which comes from their intrinsic thickness.

The consideration made for $Problems\ I-VI$ can be used as design parameters to choose the most effective kinematic theory to model a plate taking into account its thickness and also the difference between the mechanical properties of the various layers of the laminate.

7.3 Eigenvalue Analysis

Eigenvalue analysis have been carried out to ensure the capability of the code to get the correct mass and stiffness matrix and then solve the eigenvalue problem of the plates considered, taking into account different lamination schemes and, in particular, different boundary conditions.

The natural frequencies calculated in this thesis are adimensionalized according the following adimensionalizations:

$$
\begin{aligned}
\lambda_1: &\quad \bar{\omega} = \omega h \sqrt{\tfrac{\rho}{E}} \\
\lambda_2: &\quad \bar{\omega} = \omega a \sqrt{\tfrac{\rho}{E}} \\
\lambda_3: &\quad \bar{\omega} = \omega a^2 \sqrt{\tfrac{h\rho}{D}} \\
\lambda_4: &\quad \bar{\omega} = \omega b^2 \sqrt{\tfrac{h\rho}{D}} \\
\lambda_5: &\quad \bar{\omega} = \omega \tfrac{a^2}{h} \sqrt{\tfrac{\rho}{E}} \\
\lambda_6: &\quad \bar{\omega} = \omega \tfrac{b^2}{h} \sqrt{\tfrac{\rho}{E}} \\
\lambda_7: &\quad \bar{\omega} = \omega \tfrac{b^2}{h\pi^2} \sqrt{\tfrac{\rho}{E}} \\
\lambda_8: &\quad \bar{\omega} = \omega \tfrac{a^2}{\pi^2} \sqrt{\tfrac{h\rho}{D}} \\
\lambda_9: &\quad \bar{\omega} = \omega \tfrac{b^2}{\pi^2} \sqrt{\tfrac{h\rho}{D}} \\
\lambda_{10}: &\quad \bar{\omega} = \omega \sqrt{\tfrac{h\rho}{Da^2}}
\end{aligned}
$$

The young modulus and the flexural stiffness used in the adimensianalization are E_2 and D_{12} related to the mechanical properties of the top layer of the plate, unless differently specified in problems description.

7.3.1 Convergence Analysis

The approximation obtained by the Ritz method can be made as accurate as desired by increasing the number of terms in the expansion, but it is truncated to a finite value due to computational time and computer capability. Therefore, the accuracy of the approximate solution is affected by the rate of convergence associated with the choice of the set of trial functions.

First of all a preliminary study has been done to assess the convergence of the solution with respect to the proposed Ritz expansion. The firsts natural frequencies, adimensionalized as λ_1 and reported in the followings tables, are obtained with various boundary conditions, lamination schemes and height to side ratios.

In table 7.16 is shown the variation of the results obtained with different ESL and LW theories, with respect of the order of the Ritz expansion. The plate considered is a simply supported square three layer laminate with an height to side ratio of $\frac{h}{a} = 0.1$. All layers have the same thickness and are made of CFRP1 and, the lamination scheme is (0/90/0).

Theory	P	Adimensionalized natural frequencies					
		$\bar{\omega_1}$	$\bar{\omega_2}$	$\bar{\omega_3}$	$\bar{\omega_4}$	$\bar{\omega_5}$	$\bar{\omega_6}$
ED2	7	0.15242	0.22688	0.24335	0.24335	0.38294	0.39808
	9	0.15242	0.22687	0.24335	0.24335	0.37903	0.39808
	10	0.15242	0.22687	0.24335	0.24335	0.37898	0.39808
	11	0.15242	0.22687	0.24335	0.24335	0.37898	0.39808
	12	0.15242	0.22687	0.24335	0.24335	0.37898	0.39808
	13	0.15242	0.22687	0.24335	0.24335	0.37898	0.39808
LD4	7	0.14696	0.21675	0.24335	0.24335	0.35294	0.37354
	9	0.14696	0.21675	0.24335	0.24335	0.34980	0.37354
	10	0.14696	0.21675	0.24335	0.24335	0.34976	0.37354
	11	0.14696	0.21675	0.24335	0.24335	0.34976	0.37354
	12	0.14696	0.21675	0.24335	0.24335	0.34976	0.37354
	13	0.14696	0.21675	0.24335	0.24335	0.34976	0.37354

Table 7.16: Convergence of first six frequency parameters for different theories

In table 7.17 is shown the variation of the results obtained with two different boundary conditions, for ESL $ED4$ theory, with respect of the order of the Ritz expansion. The plate considered is a rectangular four layer laminate with an height to side ratio of $\frac{h}{a} = 0.1$ and a form factor $\frac{b}{a} = 1.5$. All layers have the same thickness and are made of CFRP4 and the lamination scheme is (0/90/0/90).

In table 7.18 is shown the variation of the results obtained with two different lamination sequences, for LW $LD2$ theory, with respect of the order of the Ritz expansion. The squared, fully clamped plates considered are a five layer laminate with an height to side ratio of $\frac{h}{a} = 0.2$ and a sandwich with an height to side ratio of $\frac{h}{a} = 0.25$. In the first case all layers have the same thickness, are made of CFRP3 and the lamination scheme is $(45/-45/45/-45/45)$. In the second case, the skins of the sandwich are made of RaoF and their thickness is $\frac{1}{10}$ of the thickness of the laminate, while the core is made of RaoC and its thickness is the remaining $\frac{8}{10}$ of the thickness of the laminate.

It can be observed that convergence is monotonic from above as Ritz terms are added and that the trend is similar for all theories selected.

These results indicates that a Ritz expansion of eleventh order is sufficiently to get a good approximation of the first natural frequencies. Go beyond this value does not improve so much the results while the compute became more and more time demanding. A more refined Ritz expansion is required if higher mode shall be well computed, especially in the case of

Boundary conditions	P	Adimensionalized natural frequencies					
		$\bar{\omega_1}$	$\bar{\omega_2}$	$\bar{\omega_3}$	$\bar{\omega_4}$	$\bar{\omega_5}$	$\bar{\omega_6}$
CFSF	7	0.10203	0.10464	0.13953	0.21465	0.22583	0.24952
	9	0.10202	0.10460	0.13946	0.21398	0.22395	0.24947
	10	0.10202	0.10459	0.13946	0.21378	0.22390	0.24946
	11	0.10201	0.10459	0.13944	0.21378	0.22390	0.24946
	12	0.10201	0.10458	0.13944	0.21372	0.22388	0.24945
	13	0.10201	0.10458	0.13943	0.21372	0.22388	0.24945
FCCF	7	0.03532	0.08342	0.14188	0.16626	0.17722	0.23229
	9	0.03531	0.08338	0.14185	0.16617	0.17711	0.23212
	10	0.03531	0.08337	0.14184	0.16616	0.17709	0.23209
	11	0.03531	0.08337	0.14183	0.16615	0.17709	0.23208
	12	0.03531	0.08337	0.14183	0.16614	0.17708	0.23207
	13	0.03531	0.08336	0.14183	0.16614	0.17708	0.23206

Table 7.17: Convergence of first six frequency parameters for different boundary conditions

Lamination scheme	P	Adimensionalized natural frequencies					
		$\bar{\omega_1}$	$\bar{\omega_2}$	$\bar{\omega_3}$	$\bar{\omega_4}$	$\bar{\omega_5}$	$\bar{\omega_6}$
(45/-45/45/-45/45)	7	0.51035	0.78949	0.85270	1.04846	1.18278	1.21759
	9	0.51015	0.78921	0.85238	1.04805	1.18213	1.21696
	10	0.51011	0.78915	0.85232	1.04798	1.18204	1.21686
	11	0.51009	0.78911	0.85228	1.04793	1.18199	1.21681
	12	0.51008	0.78909	0.85226	1.04790	1.18196	1.21678
	13	0.51007	0.78908	0.85225	1.04788	1.18194	1.21676
Sandwich	7	0.14211	0.18681	0.19090	0.22436	0.26752	0.29686
	9	0.14202	0.18644	0.19084	0.22406	0.26702	0.29635
	10	0.14202	0.18623	0.19084	0.22388	0.26700	0.29633
	11	0.14197	0.18621	0.19081	0.22386	0.26662	0.29595
	12	0.14197	0.18609	0.19080	0.22376	0.26660	0.29594
	13	0.14194	0.18608	0.19079	0.22375	0.26640	0.29574

Table 7.18: Convergence of first six frequency parameters for different lamination scheme

clamped boundaries, which are characterized by local displacement gradients near the edge difficult to be well approximated by global polynomials of relatively low order. From now, if not specified differently, all the results presented in this section are calculated using an eleventh order Ritz expansion.

7.3.2 Problem VII - Eigenvalues of laminate square plates with different boundary conditions and lamination schemes

Three different two layer laminated square plates with distinct lamination schemes and boundary conditions involving combinations of clamped and free edges have been analyzed. The cases considered are:

1. a fully clamped (CCCC) plate with layup $(-30/45)$

2. a plate with two opposite edges clamped and the others free (FCFC) having layup (0/45)

3. a cross-ply (0/90) plate with two adjacent edges clamped and two adjacent edges free (FCCF).

All layers are assumed to be of the same thickness and made of CFRP4. A thick plates is considered: the height to side ratio is $\frac{h}{a} = 0.25$.

The resulting first six natural frequencies, adimensionalized with respect of λ_5 are presented in table 7.19, and are compared with those computed by [22] using the same theories, but also in comparison with those computed with the Laminate-5 finite element model.

Case	Theory	Dof	Adimensionalized natural frequencies					
			$\bar{\omega}_1$	$\bar{\omega}_2$	$\bar{\omega}_3$	$\bar{\omega}_4$	$\bar{\omega}_5$	$\bar{\omega}_6$
CCCC	ED4	1815	8.8695	13.6648	14.8498	18.7239	19.6378	21.8654
(−30/45)	ED6	2541	8.7805	13.5256	14.6765	18.5148	19.4287	21.5954
	LD2	1815	8.9607	13.7798	14.9870	18.8702	19.7755	22.0485
	LD3	2541	8.7492	13.4840	14.6422	18.4751	19.3818	21.5622
	ED6 Ref		8.772	13.522	14.667	18.508		
	LD3 Ref		8.740	13.480	14.630	18.467		
FCFC	ED4	1815	4.9440	5.9551	10.0156	10.5876	11.1841	12.8629
(0/45)	ED6	2541	4.9162	5.9270	9.9699	10.5511	11.1177	12.7622
	LD2	1815	4.9646	5.9875	10.0327	10.6080	11.2361	12.9569
	LD3	2541	4.9013	5.9118	9.9518	10.5368	11.0874	12.7319
	ED6 Ref		4.918	5.928	9.972	10.555		
	LD3 Ref		4.903	5.913	9.954	10.541		
FCCF	ED4	1815	2.8044	7.5097	7.7474	11.1051	14.8254	14.8396
(0/90)	ED6	2541	2.7939	7.4537	7.6885	11.0167	14.6948	14.7077
	LD2	1815	2.8211	7.5874	7.8268	11.1862	14.9801	14.9876
	LD3	2541	2.7877	7.4346	7.6668	10.9851	14.6540	14.6647
	ED6 Ref		2.794	7.454	7.689	11.017		
	LD3 Ref		2.788	7.435	7.667	10.986		
	Fem		2.7909	7.5117	7.6953	11.0525	14.8373	14.8423

Table 7.19: First six frequency parameters of square plates with different boundary conditions and lamination schemes

These results confirmed that the present approach is capable of yielding highly accurate results for arbitrary lamination layups and boundary conditions. This statement will be stressed with the following analyses.

7.3.3 Problem VIII - Eigenvalues of a laminate square plate

A three layer laminated square plates with a symmetric lamination scheme of (0/90/0) have been analyzed. All layers are assumed to be of the same thickness and made of CFRP1. Both a thin and thick plates is considered: the height to side ratio is $\frac{h}{a} = 0.05$ for the thin plate and $\frac{h}{a} = 0.2$ for the thick plate. The resulting first natural frequency for each case, adimensionalized with respect of λ_5, is presented in table 7.20 and is compared with those computed by [20]. The values of the classical plate theory, CPT, are also presented as a reference.

Case	Theory	Dof	Boundary conditions					
			SSSS	SSCS	CSCS	FSFS	FSSS	FSCS
	CPT	726	18.8485	28.4371	40.6497	4.4237	5.0950	8.2600
$\frac{h}{a} = 0.05$	ED2	1098	17.7176	24.2542	31.2331	4.4314	5.0355	8.0265
	ED4	1815	17.4859	23.5888	30.0186	4.4209	5.0238	7.9778
	LD2	2541	17.4837	23.5880	30.0220	4.4167	5.0204	7.9755
	LD4	4719	17.4809	23.5759	29.9938	4.4128	5.0168	7.9726
	ED3 Ref		17.488	23.588	30.018	4.423	5.023	7.978
	LD4 Ref		17.483	23.578	29.993	4.413	5.018	7.973
$\frac{h}{a} = 0.2$	ED2	1089	10.8770	11.3636	12.1277	4.1043	4.6059	6.0837
	ED4	1815	10.2665	10.8048	11.5891	3.9779	4.4767	5.9097
	LD2	2541	10.2605	10.8053	11.5936	3.9335	4.4423	5.8838
	LD4	4719	10.2318	10.7487	11.5100	3.8939	4.4083	5.8505
	ED3 Ref		10.269	10.808	11.593	3.978	4.477	5.911
	LD4 Ref		10.232	10.749	11.510	3.894	4.408	5.851

Table 7.20: First frequency parameter of a square plate of three layer (0/90/0). Different boundary conditions

It is shown that the frequency results are all in good agreement for the thin plate while the error of CPT increases rapidly when the plate becomes thicker. Note also that, by comparing results of $ED4$ and $LD4$ theories, the fundamental frequency is well estimated by a fourth order ESL theory without the need of a more computational demanding LW approach.

7.3.4 Problem IX - Eigenvalues of a soft-core sandwich square plate

A simply supported soft-core sandwich plate is considered, the plate has a (0/90/*core*/0/90) layup with the crossply faces made by RaoF and the isotropic core made by RaoC. The ratio of thickness of the core to thickness of the face sheet is assumed to be 10 in this example. Both a thin and moderately thick plates is considered: the height to side ratio is $\frac{h}{a} = 0.01$ for the thin plate and $\frac{h}{a} = 0.1$ for the moderately thick plate.

The resulting first six natural frequency, adimensionalized with respect of λ_5, is presented in table 7.21 for each case and are compared with those computed by [22].

Case	Theory	Dof	Adimensionalized natural frequencies					
			$\bar{\omega_1}$	$\bar{\omega_2}$	$\bar{\omega_3}$	$\bar{\omega_4}$	$\bar{\omega_5}$	$\bar{\omega_6}$
$\frac{h}{a} = 0.01$	ED3	1452	15.5455	39.2599	39.2599	55.1396	73.4883	73.4883
	ED5	2178	12.8426	26.3405	26.3405	35.1669	41.6706	41.6706
	LD2	3993	11.9457	23.4140	23.4140	30.9599	36.1634	36.1634
	LD3	5808	11.9457	23.4140	23.4140	30.9599	36.1634	36.1634
	ED5 Ref		12.8426	26.3405	41.6706	35.1669	47.8077	57.1171
	LD3 Ref		11.9457	23.4140	36.1634	30.9599	41.4706	49.7903
$\frac{h}{a} = 0.1$	ED3	1452	4.9618	8.1928	8.1928	10.5185	11.9857	11.9857
	ED5	2178	2.1587	3.6851	3.6851	4.8601	5.8204	5.8204
	LD2	3993	1.8492	3.2217	3.2217	4.2925	5.2270	5.2270
	LD3	5808	1.8492	3.2217	3.2217	4.2925	5.2267	5.2267
	ED5 Ref		2.1587	3.6851	5.8204	4.8601	6.7667	8.4305
	LD3 Ref		1.8492	3.2217	5.2270	4.2925	6.0989	7.6834

Table 7.21: First six frequency parameters of a square soft-core sandwich plate. Different thickness

In the case of a flexible or soft-core sandwich plate, the large difference in stiffness between the core and the faces, increase the difficulties in representing the correct dynamic behaviour with simple kinematic models. Table 7.21 shows that results computed with ESL theories grossly overestimate the natural frequencies in comparison with LW models both for thin and moderately thick plates. This is due to the large stiffness ratio between the skins and the core. The numerical investigation demonstrates that the discrepancy can be contrasted by the use of layerwise kinematic theories, which appears to be mandatory for sandwich plates with very soft core.

Now, the moderately thick sandwich plate is considered with different boundary conditions. The resulting first six natural frequency, adimensionalized with respect of λ_5, is presented in table 7.22 and are obtained adopting LW $LD3$ theory to be highly accurate. Results are compared with those reported in [22] and also with those calculated with the Sandwich-9 finite element model in the fully clamped case. The number of degrees of freedom is 5808 for the proposed $LD3$ model while the Sandwich-9 model has 100101 elements.

Boundary conditions	Theory	Adimensionalized natural frequencies					
		$\bar{\omega}_1$	$\bar{\omega}_2$	$\bar{\omega}_3$	$\bar{\omega}_4$	$\bar{\omega}_5$	$\bar{\omega}_6$
SCSS	LD3	1.9483	3.2842	3.4890	4.5073	5.2700	5.6795
	LD2 Ref	1.9481	3.2841	3.4885	4.5069	5.2699	5.6786
SCCS	LD3	2.0428	3.5465	3.5476	4.7132	5.7189	5.7200
	LD2 Ref	2.0425	3.5459	3.5471	4.7124	5.7179	5.7190
SCCC	LD3	2.1621	3.6204	3.8522	4.9564	5.7688	6.2166
	LD2 Ref	2.1619	3.6200	3.8500	4.9542	5.7678	6.2162
CCCC	LD3	2.2757	3.9200	3.9200	5.1887	6.2594	6.2650
	LD2 Ref	2.2756	3.9180	3.9180	5.1853	6.2592	6.2647
	FEM	2.2720	3.8603	3.9595	5.1714	6.1627	6.3207
CFFF	LD3	0.6787	1.2308	2.1674	2.5629	2.8120	3.6480
	LD2 Ref	0.6786	1.2311	2.1670	2.5625	2.8120	3.6477
SFCS	LD3	1.5480	2.4915	3.2416	3.8868	4.0517	5.1898
	LD2 Ref	1.5478	2.4914	3.2411	3.8863	4.0514	5.1892

Table 7.22: First six frequency parameters of a square soft-core sandwich plate. Different boundary conditions

Table 7.22 shows that the proposed model is capable to calculate accurate natural frequencies of a soft core sandwich plate not only in the simply supported case, but also with an other arbitrary set of boundary conditions. Note that natural frequency of the modes in the range under investigation get higher, with respect to the simply supported case, as the number of clamped edges increases. This is due to the higher constraints introduced at boundaries.

Results of *Problems* $VII - IX$ shows that the code can create correct dynamical models with any kinematic theory in the selected range. This achievement gives the possibility to solve the eigenvalue problem for any type of plate. Moreover, an accurate solution of the eigenvalue problem gives the possibility of build an accurate reduce order modal model to solve dynamical response problems with less time demanding analysis, theoretically without an appreciable loss of accuracy.

7.4 Dynamic time response

The capability of the code to compute the time response of a dynamically loaded plate is validated comparing the results with those provided in [23]. For both the problems considered, the time response has been calculated with both the direct time integration of the full model, using the Newmark integration scheme, and the time response of the reduced order modal model.

7.4.1 Convergence Analysis

The approximation obtained by the Ritz method can be made as accurate as desired by increasing the number of terms in the expansion, but it is truncated to a finite value due to computational time and computer capability. Therefore, the accuracy of the approximate solution is affected by the rate of convergence associated with the choice of the set of trial functions.

A preliminary study has been done to assess the convergence of the solution with respect to the proposed Ritz expansion and the order of the modal model.

In table 7.23 is shown the variation of the first six natural frequencies, expressed in Hertz, obtained with ESL $ED4$ theory, with respect of the order of the Ritz expansion. The plate considered is a fully clamped square isotropic plate with an height to side ratio of $\frac{h}{a} = 0.05$. The plate is made of Al5086 and is loaded with a unitary pressure of constant spatial distribution and amplitude varied as $p_z(t) = P_z[H(t-0) - H(t-0.02)]$. The relative resulting time responses are shown in figure 7.36 and are calculated for the midplane of the plate at coordinates: $x = y = \frac{1}{3}$.

Theory	P	Dimensional natural frequencies $[Hz]$					
		ω_1	ω_2	ω_3	ω_4	ω_5	ω_6
ED4	7	444.5876	888.6499	888.6499	1285.5276	1545.2548	1555.0919
	10	442.6084	883.3974	883.3974	1277.5841	1539.3895	1549.2362
	13	441.4469	881.6534	881.6534	1275.2490	1535.7511	1545.5411
	14	441.3336	881.2106	881.2106	1274.5832	1535.3695	1545.1569

Table 7.23: Convergence of first six frequency parameters for ESL $ED4$ theory. Fully clamped square isotropic plate

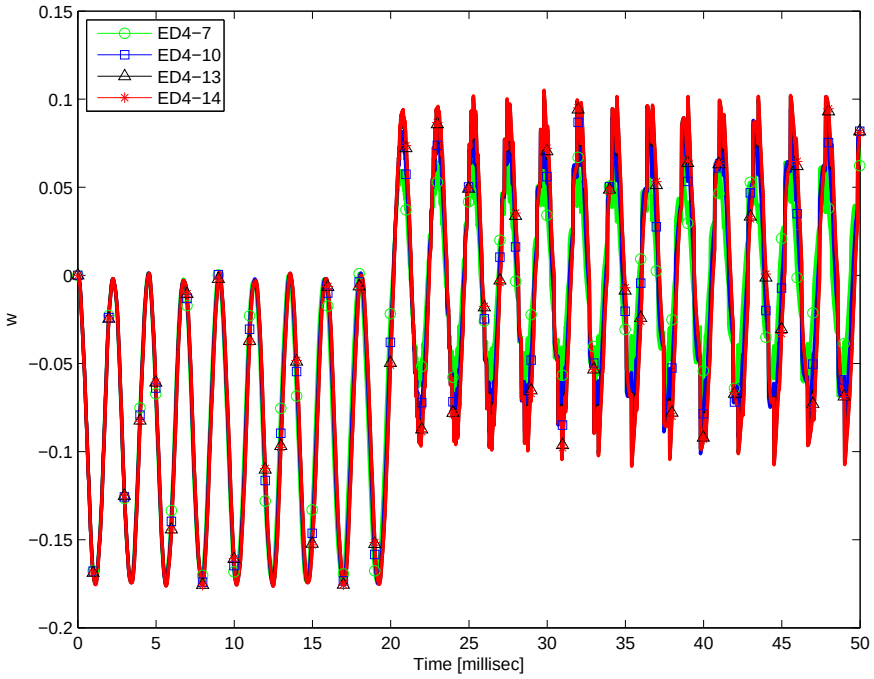

Figure 7.36: $\bar{w}\ (\frac{a}{3}, \frac{b}{3}, 0)$ vs. time for a thin plate under transient load, different Ritz expansion order

Figure 7.36 shows that all the presented model based on different Ritz expansions are capable to predict the behaviour of the plate during the loaded temporal interval, while after the transient, low order Ritz expansion models lack in accuracy and underestimate the displacements of the considered point of the plate.

Now, the convergence of the modal solution is analyzed adopting the same plate, with same load. A Ritz expansion of thirteenth order is selected to create the modal base used to build up modal models of various order. The relative resulting time responses are shown in figure 7.37 and are calculated for the midplane of the plate at coordinates:$x = \frac{1}{5}$ and $y = \frac{3}{4}$.

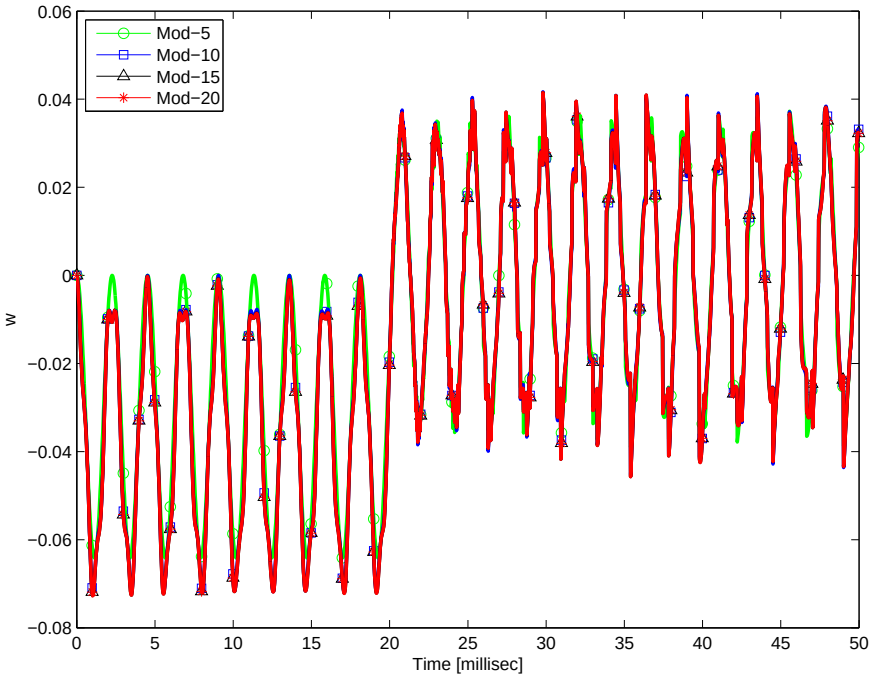

Figure 7.37: $\bar{w}$ $(\frac{a}{5}, \frac{3}{4}b, 0)$ vs. time for a thin plate under transient load, modal models of different order

Figure 7.37 shows that all the presented model based on different modal base order are capable to predict well the behaviour of the plate during the whole temporal interval, however low order models lack in accuracy in the prediction of the displacements in some time intervals. The reason is the lack of information of higher modes caused by the earlier truncation of the associated eigenvectors matrix.

7.4.2 Problem X - Time response of an isotropic plate forced by a sinusoidal load

The plate considered is a fully clamped moderately thick isotropic plate, made of Al5086, with an height to side ratio of $\frac{h}{a} = 0.1$ and side length $a = b = 0.25$. The validation has been carried out only tanking into account this simple plate, since the capability of the code to get the correct dynamic behaviour of laminated or sandwich plates is already validated by the analysis reported previously.

The eigenvalue problem of the plate has been solved prior to conduct the analysis to assure that the model of the plate is good enough to represent the plate used in [23] and to avoid errors which could led to misunderstoodable results. The first six natural frequencies, adimensionalized as λ_1, are

Case	Theory	Adimensionalized natural frequencies					
		$\bar{\omega_1}$	$\bar{\omega_2}$	$\bar{\omega_3}$	$\bar{\omega_4}$	$\bar{\omega_5}$	$\bar{\omega_6}$
$\frac{h}{a} = 0.01$	ED2	0.1010	0.1936	0.1936	0.2718	0.3212	0.3242
	ED3	0.1000	0.1906	0.1906	0.2670	0.3147	0.3178
	ED4	0.0999	0.1905	0.1905	0.2668	0.3145	0.3175
	ED5	0.0999	0.1904	0.1904	0.2667	0.3144	0.3174
	Ref	0.0999	0.1909	0.1909	0.2673	0.3144	0.3171

Table 7.24: First six frequency parameters for different ESL theories. Fully clamped moderately thick isotropic plate

compared with those reported in table 4 of [23] and presented in table 7.24. The results are referred to a twelfth order Ritz expansion.

The plate has been modelled using ESL theories of different order without taking into account LW theories since the plate is a single isotropic lamina and ESL results are good approximation of the real behaviour of a plate of this kind. As it can be seen in table 7.24, ED4 can be choiced since it's capable to get accurate results with a smaller model than ESL theories of higher order. This lead to faster time response analysis, especially in the case of full model time integration, which is more time demanding than the modal time integration since the later is performed onto a reduced order model.

The results of the time response analysis, in terms of displacements ad stresses, are referred to the followings coordinates:

$$\begin{aligned}
\text{Transverse displ.}, \quad & \text{w}, \quad && \text{computed at:} \quad && (\tfrac{a}{2}, \tfrac{b}{2}, 0) \\
\text{Sigma}_x, \quad & \sigma_{xx}, \quad && \text{computed at:} \quad && (\tfrac{a}{2}, \tfrac{b}{2}, \tfrac{h}{2}) \\
\text{Sigmay}_y, \quad & \sigma_{yy}, \quad && \text{computed at:} \quad && (\tfrac{a}{2}, \tfrac{b}{2}, \tfrac{h}{2}) \\
\text{Sigma}_{xy}, \quad & \sigma_{xy}, \quad && \text{computed at:} \quad && (0, 0, -\tfrac{h}{2}) \\
\text{Sigma}_{xz}, \quad & \sigma_{xz}, \quad && \text{computed at:} \quad && (0, \tfrac{b}{2}, 0) \\
\text{Sigma}_{yz}, \quad & \sigma_{yz}, \quad && \text{computed at:} \quad && (\tfrac{a}{2}, 0, 0)
\end{aligned}$$

Then, are adimensionalized as following:

$$
\begin{aligned}
\text{Transverse displ. } \bar{w} &= \frac{100h^3E}{p_z a^4} w \\
S_x &= \frac{h^2}{P_z a^2}\sigma_{xx} \\
S_y &= \frac{h^2}{P_z a^2}\sigma_{yy} \\
S_{xy} &= \frac{h^2}{P_z a^2}\sigma_{xy} \\
S_{xz} &= \frac{h}{P_z a}\sigma_{xz} \\
S_{yz} &= \frac{h}{P_z a}\sigma_{yz}
\end{aligned}
$$

The young modulus used in the adimensionalization is E_2.

The integration parameters γ and β have been set to 0.5 and 0.25 respectively to ensure that the Newmark integration method will be asymptotically stable.

The reduced order modal model has been made adopting a twentieth order modal expansion to be highly accurate whereas the order of the problem is dramatically reduced from thousands to 20 degrees of freedom. For this reason the compute of the dynamic response obtained with the modal model is extremely fast, while the direct integration takes several minutes.

The time of integration has been set to 5 milliseconds with a time step $\Delta t = 2 \cdot 10^{-7}$ seconds as stated in [23], to compare the results with those presented there. The reference results have been calculated with a MLPG method, which are in turn confronted with good approximation, directly with results of a finite element model by the authors.

The plate is loaded with a pressure of constant distribution acting on the top surface of the plate with a sinusoidal temporal behaviour: $p_z(t) = P_z \sin(5000t)$, able to excite the first natural frequency of the plate, which is at 3287 Hertz.

The computed time response, in terms of adimensionalized transverse displacements and stresses, is presented in figures from 7.38 to 7.40.

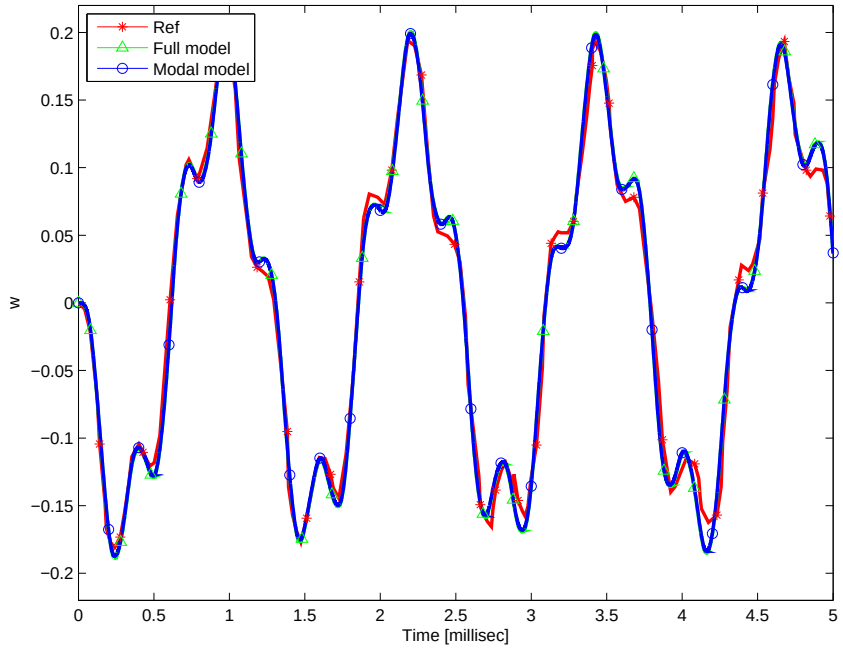

Figure 7.38: $\bar{w}\ (\frac{a}{2}, \frac{b}{2}, 0)$ vs. time for a moderately thick plate under sinusoidal load

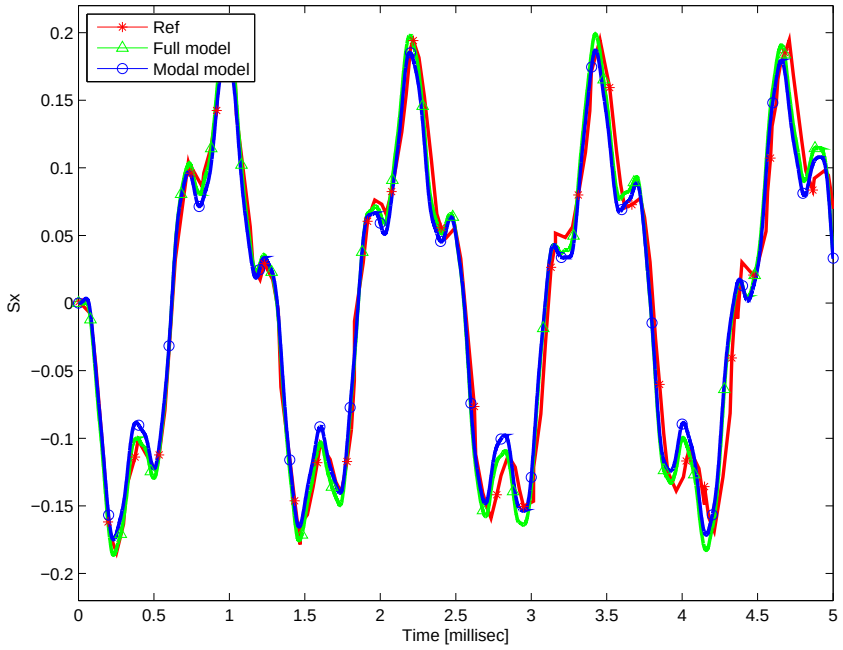

Figure 7.39: $S_x\ (\frac{a}{2}, \frac{b}{2}, \frac{h}{2})$ vs. time for a moderately thick plate under sinusoidal load

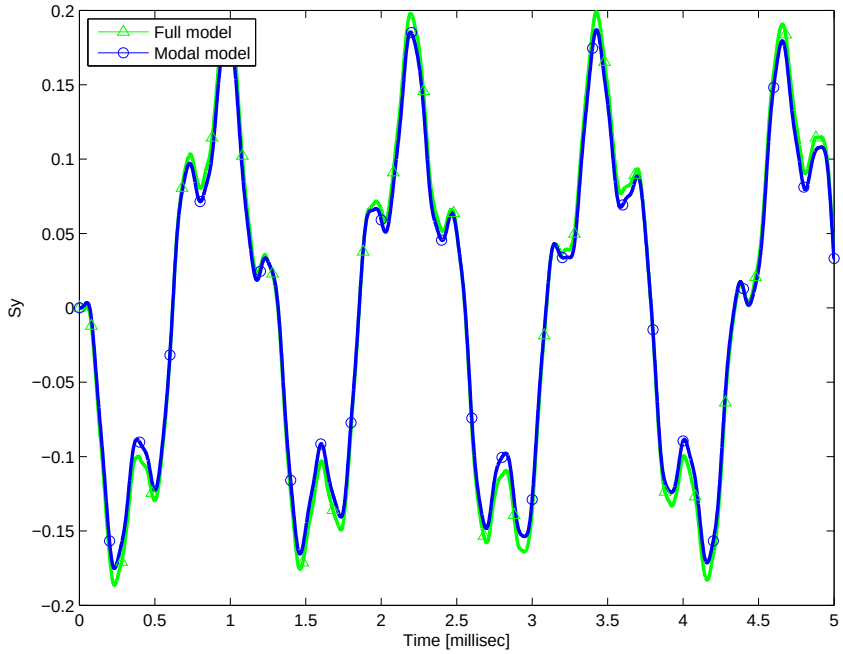

Figure 7.40: S_y $(\frac{a}{2}, \frac{b}{2}, \frac{h}{2})$ vs. time for a moderately thick plate under sinusoidal load

Figures 7.38, 7.39 and 7.40 shows that the proposed models, the full and the modal one, are capable to match the correct dynamic behaviour in therms of displacements and stresses. The full model time integrations shows a better precision in the stress recovery with respect of the results of the modal model, but it will be acquired at the price of an higher computational time.

7.4.3 Problem XI - Time response of an isotropic plate forced by a transient load

The same plate of *problem X* is now loaded with a pressure of constant distribution acting on the top surface of the plate with a transient temporal behaviour: $p_z(t) = P_z[H(t-0) - H(t-0.002)]$, able to excite the first natural frequency of the plate, which is at 3287 Hertz.

The computed time response, in terms of adimensionalized transverse displacements and stresses, is presented in figures from 7.41 to 7.43.

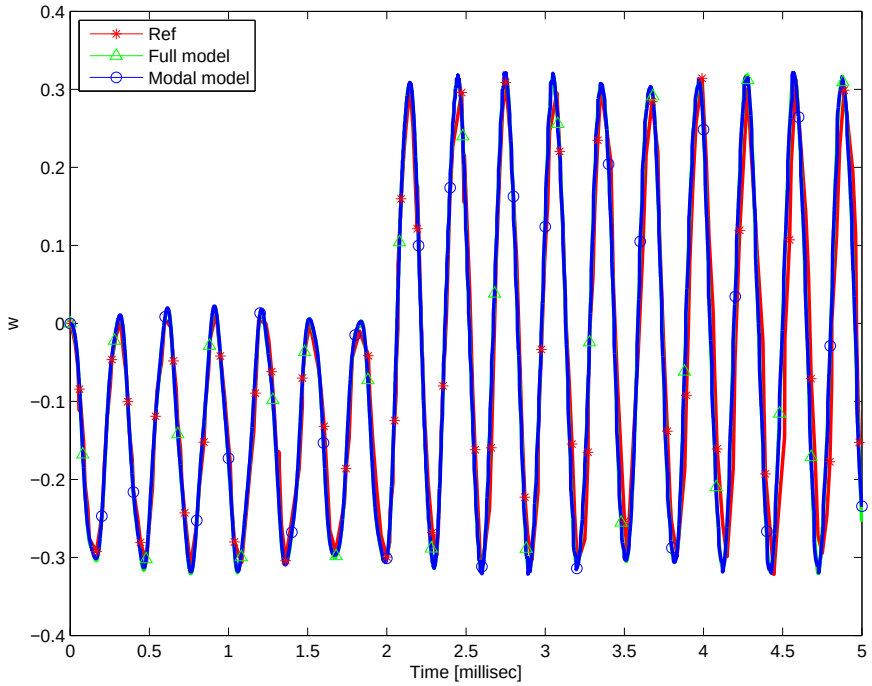

Figure 7.41: $\bar{w}\ (\frac{a}{2}, \frac{b}{2}, 0)$ vs. time for a moderately thick plate under transient load

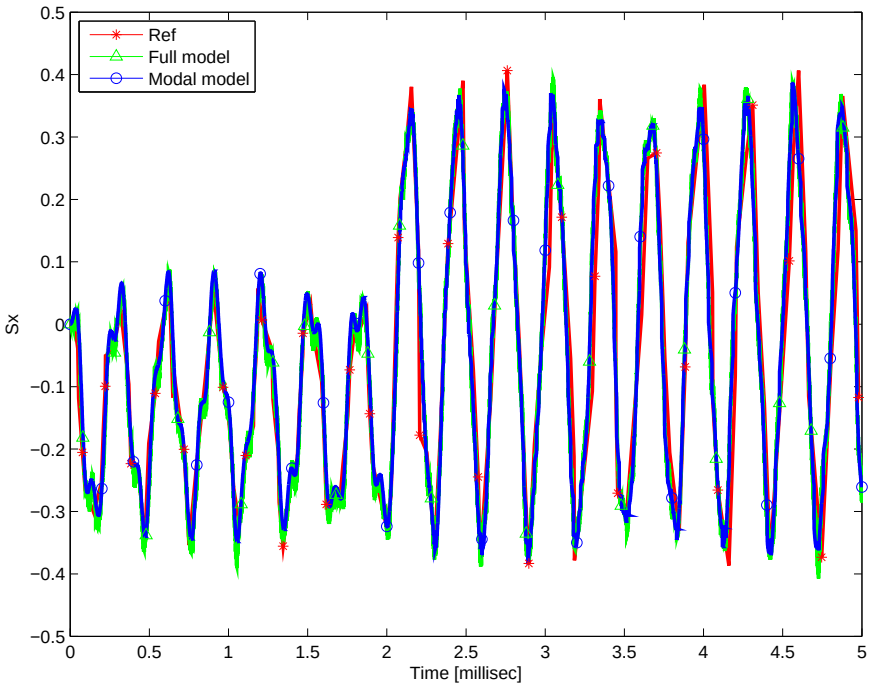

Figure 7.42: $S_x\ (\frac{a}{2}, \frac{b}{2}, \frac{h}{2})$ vs. time for a moderately thick plate under transient load

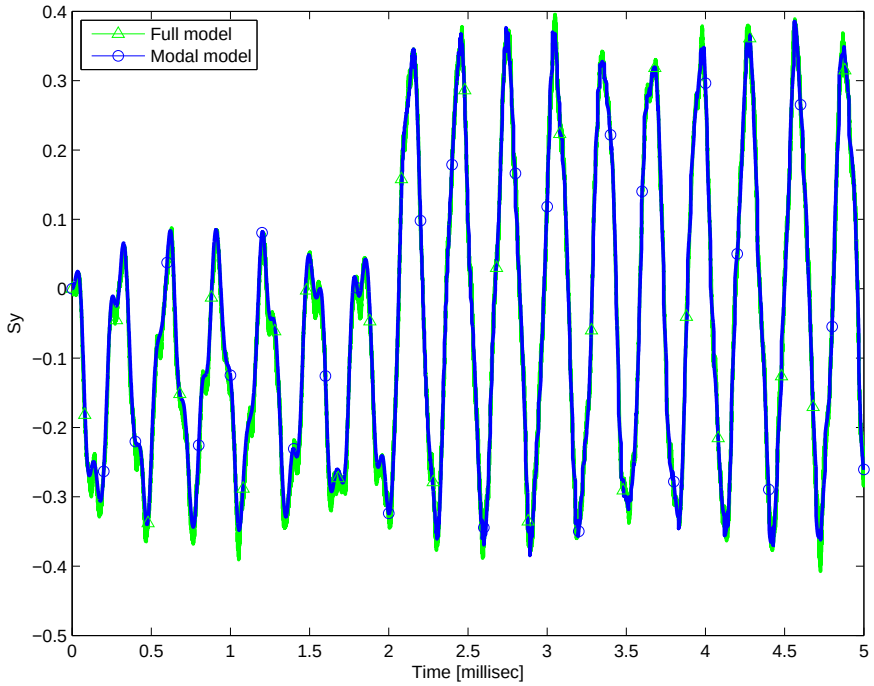

Figure 7.43: S_y $(\frac{a}{2}, \frac{b}{2}, \frac{h}{2})$ vs. time for a moderately thick plate under transient load

Figures 7.41, 7.42 and 7.43 shows that the proposed models, the full and the modal one, are capable to match the correct dynamic behaviour in therms of displacements and stresses. Same consideration of the previous problem can be done.

7.5 Dynamic frequency response

The frequency response of a plate forced by a load with constant amplitude with respect to the range of frequencies selected has been calculated with both the full model and the reduced order modal model.

7.5.1 Convergence Analysis

The approximation obtained by the Ritz method can be made as accurate as desired by increasing the number of terms in the expansion, but it is truncated to a finite value due to computational time and computer capability. Therefore, the accuracy of the approximate solution is affected by the rate of convergence associated with the choice of the set of trial functions.

A preliminary study has been done to assess the convergence of the solution with respect to the proposed Ritz expansion and the order of the modal

model.

In table 7.25 is shown the variation of the first six natural frequencies, expressed in Hertz, obtained with an ESL $ED4$ theory model, with respect of the order of the Ritz expansion. The plate considered is a fully clamped square isotropic plate with an height to side ratio of $\frac{h}{a} = 0.02$ and side length $a = 1$. The plate is made of Al7075 and is loaded with a unitary pressure of constant spatial distribution and constant amplitude for all frequencies. The relative resulting frequency responses are shown in figure 7.44 and are calculated for the midplane of the plate at coordinates:$x = y = \frac{1}{3}$.

Theory	P	Dimensional natural frequencies $[Hz]$					
		ω_1	ω_2	ω_3	ω_4	ω_5	ω_6
ED4	7	177.7628	361.7543	361.7543	531.8238	644.4254	647.6620
	9	177.2437	360.5485	360.5485	529.9513	642.6772	645.8969
	10	177.2187	359.9450	359.9450	528.8788	642.5416	645.7633
	11	176.9472	359.7962	359.7962	528.7924	641.5107	644.7251
	13	176.7636	359.3511	359.3511	528.1074	640.8470	644.0603

Table 7.25: Convergence of first six natural frequencies for ESL $ED4$ theory. Fully clamped isotropic plate

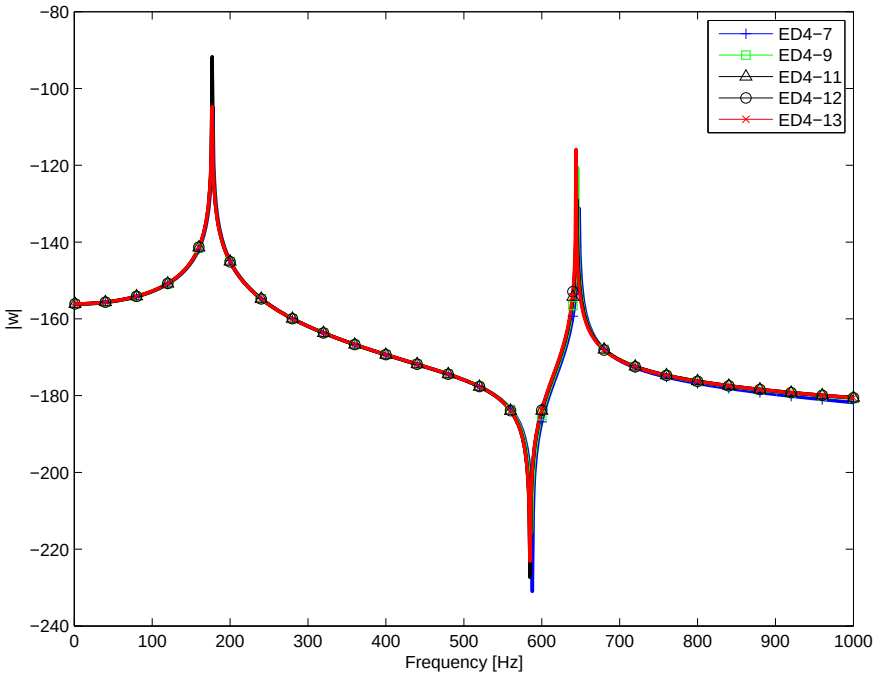

Figure 7.44: $|w|$ $(\frac{a}{3}, \frac{b}{3}, 0)$ vs. frequency for a thin plate, $ED4$ model with different Ritz expansion orders

Figure 7.45 shows that all models are capable to get the correct frequency response with minimal difference between model with expansion of low and high order. To cancel these difference and to ensure the correctness of the response also at higher frequencies an high Ritz expansion shall be preferred, since the higher modes of the plate are less well approximate than the lower modes for low order expansion, as it can be saw in precedence in section 7.3. For this reason the differences reported among the various response around the antiresonance might be much consistent for a second antiresonance at higher frequency.

Therefore the order of the Ritz expansion to reach the convergence of the results shall be selected tacking into account also the frequency range of interest. More it spreads into the high frequencies more the Ritz expansion order shall be higher.

Now, the convergence of the modal solution is analyzed adopting the same plate, with same load. A Ritz expansion of thirteenth order is selected to create the modal base to create a modal model of various order. The relative resulting frequency responses are shown in figure 7.45 and are calculated for the midplane of the plate at coordinates:$x = \frac{1}{5}$ and $y = \frac{3}{4}$.

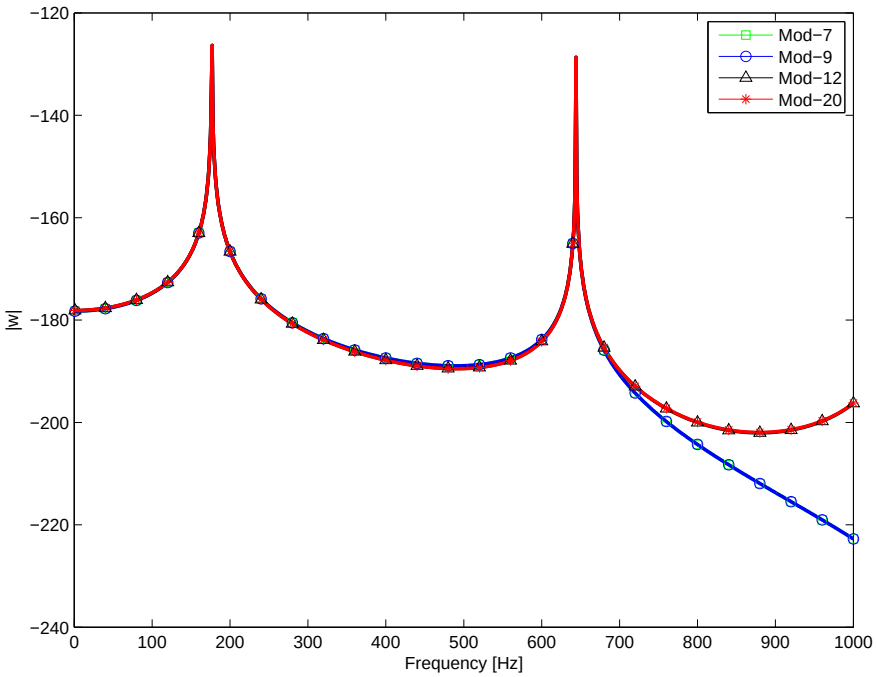

Figure 7.45: $|w|$ $(\frac{a}{5}, \frac{3}{4}b, 0)$ vs. frequency for a thin plate, modal models of different order

Figure 7.45 shows that all the presented model based on different modal

base order are capable to predict well the behaviour of the plate during the low to mid frequency range, however low order models lack in accuracy in the prediction of the response at higher frequencies. The reason is the lack of information of higher modes caused by the earlier truncation of the associated eigenvectors matrix.

7.5.2 Problem XI - Frequency response of an isotropic plate

The plate considered is a fully clamped thin isotropic plate, made of Al7075, with an height to side ratio of $\frac{h}{a} = 0.02$ and side length $a = 1$. The validation has been carried out only tanking into account this simple plate, since the capability of the code to get the correct dynamic behaviour of laminated or sandwich plates is already validated by the analysis reported previously.

The eigenvalue problem of the plate has been solved prior to conduct the analysis to assure that the model of the plate is good enough to represent the plate used in Isotropic-1 finite element model, to avoid errors which could led to misunderstoodable results. The results presented in table 7.26 are referred to a twelfth order Ritz expansion and are expressed in Hertz.

Case	Theory	Dimensional natural frequencies $[Hz]$					
		ω_1	ω_2	ω_3	ω_4	ω_5	ω_6
$\frac{h}{a} = 0.01$	ED2	176.8674	359.7191	359.7191	528.8455	641.8009	644.9982
	ED3	176.7639	359.3516	359.3516	528.1081	640.8495	644.0627
	ED4	176.7636	359.3511	359.3511	528.1074	640.8470	644.0603
	ED5	176.7636	359.3510	359.3510	528.1071	640.8469	644.0602

Table 7.26: First six natural frequencies for different ESL theories. Fully clamped moderately thin isotropic plate

The plate has been modelled using ESL theories of different order without taking into account LW theories since the plate is a single isotropic lamina and ESL results are good approximation of the real behaviour of a plate of this kind. As it can be seen in table 7.26, ED3 can be the better choice since it's capable to get accurate results with a smaller model than ESL theories of higher order. This lead to faster frequency response analysis, especially in the case of full model analysis, which is more time demanding than the modal analysis since the later is performed onto a reduced order model.

The results of the analysis, in terms of displacements, are computed in the center of the midplane of the plate.

The frequency response has been computed for a range of 1000 Hz with a frequency step $\Delta f = 1$ Hz, between 1 Hz and 1000 Hz. This frequency

range has been selected since contains the first six natural frequencies of the plates as an illustrative example.

The reduced order modal model has been made adopting a twentieth order modal expansion to be highly accurate whereas the order of the problem is dramatically reduced from thousands to 20 degrees of freedom. For this reason the compute of the frequency response obtained with the modal model is extremely fast, while the direct integration takes hours.

The load is a punctual force applied at the plate center with constant intensity all over the frequency range. The load temporal behaviour has no influence in this type of analysis, since it will not be taken into account.

In figure 7.46 are presented the frequency responses, calculate directly with the full model, of the plate modelled with the four ESL theories presented in table 7.26, while in figure 7.47 are presented the frequency response obtained with ESL $ED2$ theory, a Ritz expansion of order thirteen, calculated directly on the full model and with the reduced order modal model.

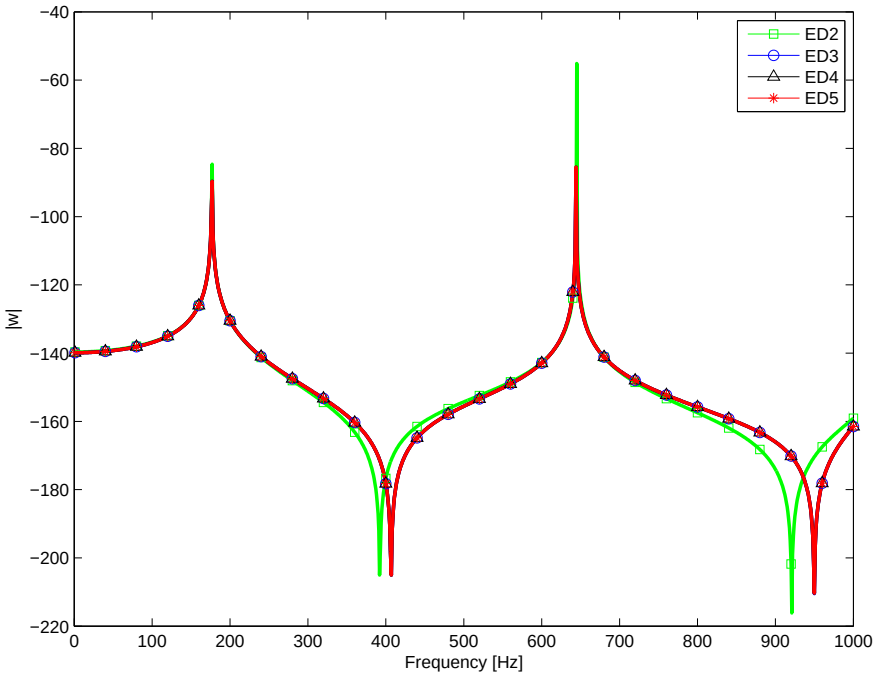

Figure 7.46: $|w|$ $(\frac{a}{2}, \frac{b}{2}, 0)$ vs. frequency for a thin plate, different theory orders

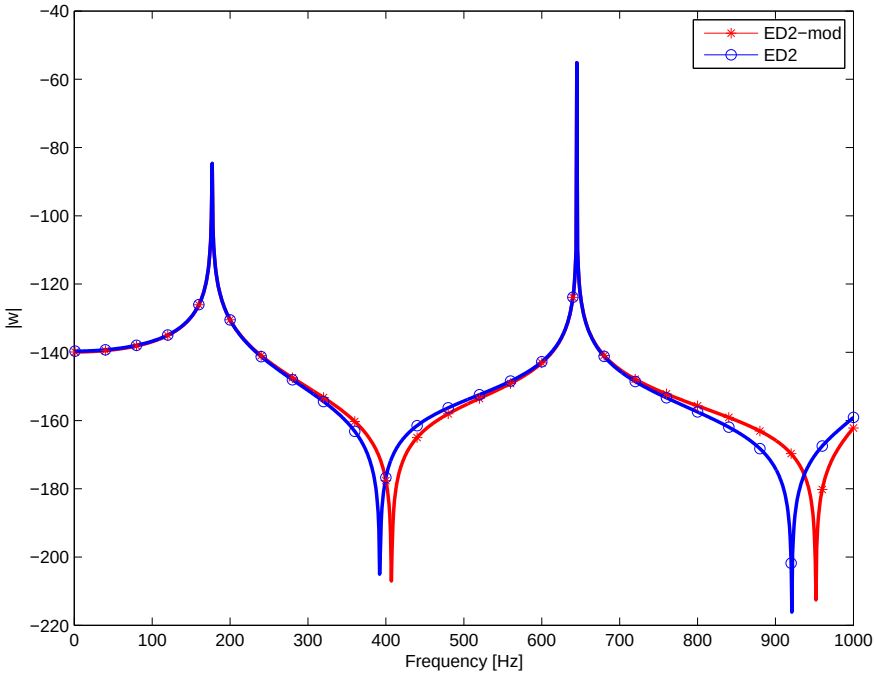

Figure 7.47: $|w|$ $(\frac{a}{2}, \frac{b}{2}, 0)$ vs. frequency for a thin plate, full and modal models differences

Figures 7.46 shows that the resonance frequencies are well displayed, while the amplitude of the respective amplifications are overestimate by lower order theories. A different consideration can be made for antiresonances: low order theories anticipate the antiresonances at lower frequencies and also overestimate theirs amplitudes. Figure 7.47 shows that at low frequencies the response of the full model and the relative modal model are basically the same, whereas increasing the frequency, the difference between the two models increase.

7.6 Attached masses

The capability of the code to compute the correct mass matrix of a plate loaded with various types of attached masses is validated solving the eigenvalue problem of the loaded plate and comparing the resulting natural frequencies with those reported in literature or calculated with validated finite element models. Several cases has been analyzed, with respect of masses definition, dimensions and position onto the plate.

7.6.1 Convergence Analysis

The approximation obtained by the Ritz method can be made as accurate as desired by increasing the number of terms in the expansion, but it is truncated to a finite value due to computational time and computer capability. Therefore, the accuracy of the approximate solution is affected by the rate of convergence associated with the choice of the set of trial functions.

First of all a preliminary study has been done to assess the convergence of the solution with respect to the proposed Ritz expansion. The first natural frequencies, adimensionalized as λ_1 and reported in the followings tables, are obtained with various boundary conditions, lamination schemes and dimension of the attached mass.

In table 7.27 is shown the variation of the results obtained with different ESL and LW theories, with respect of the order of the Ritz expansion. The plate considered is a simply supported square three layer laminate with an height to side ratio of $\frac{h}{a} = 0.1$. All layers have the same thickness and are made of CFRP1 and, the lamination scheme is (0/90/0). The attached mass considered is a punctual mass attached at center of the plate onto the top surface and has a mass equal at the plate's one.

Theory	P	Adimensionalized natural frequencies					
		$\bar{\omega_1}$	$\bar{\omega_2}$	$\bar{\omega_3}$	$\bar{\omega_4}$	$\bar{\omega_5}$	$\bar{\omega_6}$
ED2	7	0.06183	0.11447	0.12928	0.22894	0.27638	0.39452
	9	0.06026	0.10871	0.12699	0.22889	0.26181	0.36399
	10	0.06003	0.10870	0.12698	0.22889	0.25991	0.36393
	11	0.05910	0.10369	0.12499	0.22884	0.25352	0.34192
	12	0.05897	0.10368	0.12499	0.22884	0.25263	0.34189
	13	0.05811	0.09928	0.12321	0.22879	0.24703	0.32658
	14	0.05803	0.09927	0.12321	0.22879	0.24650	0.32656
LD4	7	0.05930	0.11193	0.12820	0.22025	0.25889	0.36944
	9	0.05767	0.10533	0.12534	0.22008	0.24562	0.34788
	10	0.05729	0.10529	0.12533	0.22007	0.24292	0.34772
	11	0.05648	0.09950	0.12272	0.21991	0.23805	0.32676
	12	0.05622	0.09947	0.12271	0.21991	0.23647	0.32667
	13	0.05547	0.09434	0.12027	0.21975	0.23217	0.31219
	14						

Table 7.27: Convergence of first six frequency parameters for different theories. Punctual attached mass

In table 7.28 is shown the variation of the results obtained with two dif-

ferent boundary conditions, for ESL $ED4$ theory, with respect of the order of the Ritz expansion. The plate considered is a rectangular four layer laminate with an height to side ratio of $\frac{h}{a} = 0.1$ and a form factor $\frac{b}{a} = 1.5$. All layers have the same thickness and are made of CFRP4, the lamination scheme is (0/90/0/90). The plate is loaded with a distributed mass attached onto the top surface of the plate and has a mass equal at the plate's one. The mass has sides length equal at $\frac{1}{10}$ of the respective plate sides, its center is positioned at coordinates: $\frac{x_c}{a} = 0.35$, $\frac{y_c}{b} = 0.7$.

Boundary conditions	P	Adimensionalized natural frequencies					
		$\bar{\omega_1}$	$\bar{\omega_2}$	$\bar{\omega_3}$	$\bar{\omega_4}$	$\bar{\omega_5}$	$\bar{\omega_6}$
CFSF	7	0.04874	0.10146	0.11294	0.13014	0.13959	0.16557
	9	0.04727	0.10079	0.11048	0.12329	0.13295	0.15763
	10	0.04713	0.10063	0.11012	0.11764	0.13150	0.15550
	11	0.04671	0.10026	0.10932	0.11613	0.13059	0.15459
	12	0.04631	0.09989	0.10796	0.10991	0.12979	0.15267
	13	0.04623	0.09971	0.10700	0.10916	0.12939	0.15182
	14	0.04594	0.09928	0.10479	0.10832	0.12865	0.15119
FCCF	7	0.02062	0.07465	0.09742	0.13266	0.15440	0.16920
	9	0.02054	0.07417	0.09357	0.12425	0.14864	0.16330
	10	0.02051	0.07381	0.09197	0.12074	0.14465	0.16040
	11	0.02049	0.07367	0.09031	0.11784	0.14314	0.15886
	12	0.02047	0.07351	0.08933	0.11624	0.14095	0.15791
	13	0.02045	0.07328	0.08812	0.11431	0.13900	0.15646
	14	0.02044	0.07319	0.08702	0.11280	0.13800	0.15588

Table 7.28: Convergence of first six frequency parameters for different boundary conditions. Distributed attached mass

In table 7.29 is shown the variation of the results obtained with different mass dimensions, for LW $LD3$ theory, with respect of the order of the Ritz expansion. The squared, fully clamped plates considered are a three layer laminate with an height to side ratio of $\frac{h}{a} = 0.15$. All layers have the same thickness, are made of CFRP3 and the lamination scheme is $(45/0/-45)$. The plate is loaded with a distributed mass attached onto the top surface of the plate and has a mass equal at the plate's one. The mass has side length ratios equal at $\frac{c}{a} = \frac{d}{b} = \frac{1}{20}$ in the first case and $\frac{c}{a} = \frac{d}{b} = \frac{1}{5}$ in the second case. The mass center is positioned at the plate center in both cases.

Mass dimensions	P	Adimensionalized natural frequencies					
		$\bar{\omega_1}$	$\bar{\omega_2}$	$\bar{\omega_3}$	$\bar{\omega_4}$	$\bar{\omega_5}$	$\bar{\omega_6}$
$\frac{c}{a} = \frac{d}{b} = \frac{1}{20}$	7	0.03551	0.05787	0.10816	0.38659	0.41885	0.44917
	9	0.03393	0.05156	0.09656	0.32738	0.34302	0.35890
	10	0.03389	0.05126	0.09524	0.28362	0.29381	0.29792
	11	0.03265	0.04712	0.08843	0.27231	0.27832	0.28149
	12	0.03262	0.04690	0.08744	0.23673	0.23847	0.24075
	13	0.03159	0.04382	0.08244	0.22734	0.22765	0.22948
	14	0.03157	0.04365	0.08167	0.19696	0.19848	0.20007
$\frac{c}{a} = \frac{d}{b} = \frac{1}{5}$	7	0.03946	0.06939	0.12098	0.14556	0.14914	0.16146
	9	0.03896	0.06604	0.10863	0.12559	0.12934	0.13366
	10	0.03893	0.06536	0.10088	0.11406	0.11432	0.11779
	11	0.03875	0.06436	0.09981	0.11175	0.11260	0.11539
	12	0.03874	0.06388	0.09447	0.10279	0.10547	0.10619
	13	0.03870	0.06352	0.09400	0.10140	0.10462	0.10490
	14	0.03869	0.06323	0.09063	0.09616	0.09959	0.10010

Table 7.29: Convergence of first six frequency parameters for different distributed attached mass dimensions

As it can be seen from the previous tables, the attached mass, punctual or distributed, affects negatively the convergence of the Ritz method, since the local effects generated by the presence of the mass are difficultly well approximated by global polynomials of relatively low order. It can also be noted that, between natural frequencies, some are well approximated also by low order expansion: this is due to the position and dimension of the attached mass, since a mass positioned in a modal node does not affect that mode, and then will not affect the convergence of the relate natural frequency.

This behaviour implies that in case of attached mass an eleventh order Ritz expansion might not be sufficiently accurate, as stated before in the *eigenvalue analysis* section, for a not-loaded plate, and an higher order shall be selected. Moreover, high order expansions are required when the presence of attached masses is coupled with clamped boundaries. It can be observed that, also in this case, the convergence is monotonic from above as Ritz terms are added and that the trend is similar for all theories selected.

From now, if not specified differently, all the results presented in this section are calculated using a twelfth order Ritz expansion. Go beyond this value will slightly improve the results while the compute became more and more time demanding.

7.6.2 Problem XII - Natural frequencies of an isotropic plate with a concentrate mass

A thin, simply supported isotropic square plate is considered, it's made of Steel with an height to side ratio of $\frac{h}{a} = 0.0025$. The plate is loaded with a point mass of $50kg$ positioned onto the top surface at $x_m = y_m = \frac{1}{4}a$. The computed first five natural frequencies are confronted with those reported in [27], and are reported in $\frac{rad}{sec}$ in table 7.30. The results of the loaded plate has been modelled using only ESL theories, since LW theories have not been taken into account since the plate is thin and isotropic.

Case	Theory	Dof	Natural frequencies $[\frac{rad}{sec}]$				
			ω_1	ω_2	ω_3	ω_4	ω_5
Plate loaded	ED2	1296	31.7679	62.8709	95.4097	127.0926	180.2334
with a	ED3	1728	31.7678	62.8701	95.4093	127.0913	180.2315
point mass	ED4	2160	31.7677	62.8706	95.4093	127.0915	180.2314
	ED5	2592	31.7672	62.8708	95.4089	127.0914	180.2312
	Ref		31.8536	63.5505	95.4149	128.0735	180.8910

Table 7.30: First six natural frequencies of a square isotropic plate with different ESL theories. Punctual attached mass

As it can be seen, the computed frequencies are in good agreement with those of reference even for lower order theories, mainly because the plate considered is very thin and isotropic.

The effect of the mass is seen in the general lowering of the natural frequencies of the plate, except for those frequencies associated with modal shapes which contains the location of the concentrate mass in a nodal point.

7.6.3 Problem XIII - Natural frequencies of an isotropic plate with a distribute mass

A thin, simply supported isotropic rectangular plate is considered, it's made of Steel with an height to side ratio of $\frac{h}{a} = 0.005$ and an aspect ratio: $\lambda = \frac{b}{a} = 1.5$. The plate is loaded by three different distributed mass, shown in figure 7.48, to investigate the effect of size and location of distributed mass loading on the transverse vibration of the plate itself. The additional mass loading in all three cases is 10% of the mass of the unloaded plate. The loaded mass in both cases (a) and (b) is distributed around the center of the plate while that in case (c) is closer to one of the corners of the plate. The loaded area in case (a) is the 25% of the total plate surface area while, in case (b) and (c) it is the 1%.

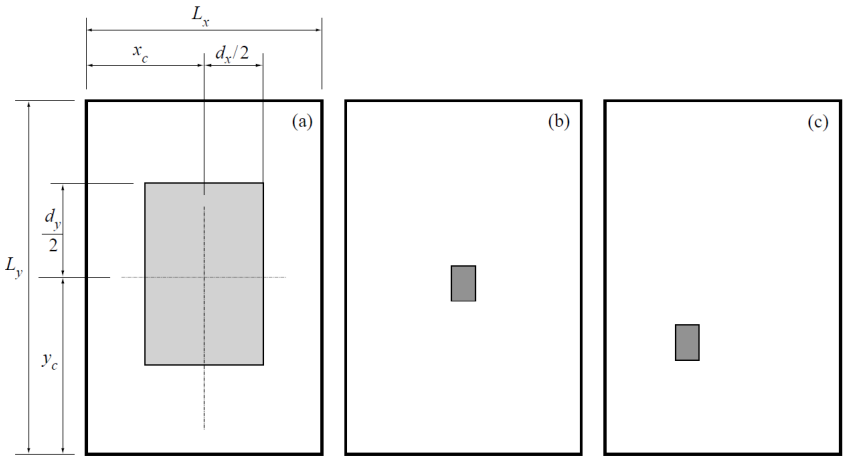

Figure 7.48: Position and dimensions of attached distributed masses of case (a) (left), case (b) (center) and case (c) (right)

The computed natural frequencies are adimensionalized with respect to λ_{10} to be confronted with those reported in [27], and are reported in table 7.31. LW theories have not been taken into account since the plate is thin and isotropic.

The maximum kinetic energy of the vibrating plate is affected most if the mass loading is added on an antinode of the plate in which case a large change of natural frequency of the corresponding vibration mode will be effected. This prediction is substantiated by observing the change of frequency in loading case (b) as shown in table 7.31. Vibration modes with mass loading on an antinode, such as $\bar{\omega_2}$ and $\bar{\omega_3}$ of case (b), have relatively larger changes of natural frequency than the modes with mass loading about a node, such as $\bar{\omega_1}$ and $\bar{\omega_4}$ of the same case. Since the mass loading in case (b) is more concentrated than that in case (a), the effects of the loading on the maximum kinetic energy of the plate for some vibration modes are more dramatic in case (b) than that in case (a). Therefore, the frequency changes in case (a) is generally not as great as that in case (b). In loading case (c), the added mass is moved closer to a corner of the plate. The change of natural frequencies is more significant for modes with the mass added on an antinode such as $\bar{\omega_2}$ and $\bar{\omega_3}$.

7.6.4 Problem XIV - Natural frequencies of a sandwich plate with a distribute mass

The moderately thick sandwich plate of *Problem IX* is now considered with different boundary conditions. The results are obtained adopting LW theo-

Case	Theory	Adimensionalized natural frequencies				
		$\bar{\omega_1}$	$\bar{\omega_2}$	$\bar{\omega_3}$	$\bar{\omega_4}$	$\bar{\omega_5}$
Case 0	ED2	14.2553	27.4125	43.8572	49.3382	57.0113
Unloaded	ED3	14.2552	27.4122	43.8564	49.3372	57.0099
plate	ED4	14.2551	27.4122	43.8564	49.3372	57.0099
	ED5	14.2552	27.4122	43.8564	49.3372	57.0099
	Ref	14.2561	27.4156	43.8649	49.3480	57.0244
Case (a)	ED2	12.6552	25.3840	40.6031	46.5640	54.2691
	ED3	12.6551	25.3837	40.6024	46.5630	54.2678
	ED4	12.6551	25.3837	40.6024	46.5630	54.2678
	ED5	12.6551	25.3837	40.6024	46.5630	54.2678
	Ref	12.6559	25.3867	40.6104	46.5741	54.2811
Case (b)	ED2	12.0062	27.2360	43.1325	43.5724	56.9993
	ED3	12.0062	27.2357	43.1315	43.5715	56.9979
	ED4	12.0061	27.2357	43.1315	43.5715	56.9979
	ED5	12.0062	27.2357	43.1315	43.5715	56.9979
	Ref	12.0753	26.8918	41.9978	45.3518	56.8956
Case (c)	ED2	13.0481	24.7482	39.9342	48.5171	53.1302
	ED3	13.0480	24.7479	39.9334	48.5161	53.1289
	ED4	13.0480	24.7479	39.9334	48.5161	53.1289
	ED5	13.0480	24.7479	39.9334	48.5160	53.1289
	Ref	13.0495	24.7544	39.9536	48.5313	53.1536

Table 7.31: First six frequency parameters of a rectangular isotropic plate with different ESL theories. Distributed attached mass

ries $LD2$ and $LD4$ to be capable of get the correct behaviour of a softcore sandwich plate, as been stated in the consideration of *Problem IX*, and are compared with those calculated using the Sandwich-9 finite element model, already validated in *Problem IX*. The distributed mass is positioned onto the top face at the plate center and has a surface of 1% of the surface area of the plate. Several boundary conditions are considered and the results are reported in table: 7.32 and are expressed in Hertz. To see the effect of the mass on the natural frequencies of the plate, in table are presented also the first frequencies of the plate without the mass attached, calculated with LW $LD4$ theory and are marked as *Plate*.

The attached mass considered has a surface of 1% of the total plate surface

area, an assumed height ratio with plate thickness of $\frac{h_m}{h} = 0.3$ and a density of $\rho_m = 10000\ \frac{Kg}{m^3}$. The mass is distributed around the center of the plate onto the top surface of the sandwich.

The number of degrees of freedom of the proposed $LD2$ model is 4752, while the degrees of freedom rises to 9072 for the proposed $LD4$ model while the Sandwich-9 model has 100101 elements.

Boundary conditions	Theory	Dimensional natural frequencies $[Hz]$					
		ω_1	ω_2	ω_3	ω_4	ω_5	ω_6
CCCC	*Plate*	91.2956	157.1810	157.1810	208.0211	251.0847	251.3084
	LD2	73.5984	155.5946	155.6646	187.8739	207.9654	251.0537
	LD4	73.5939	155.5781	155.6481	187.8361	207.9403	251.0065
	FEM	73.4492	153.2220	157.0500	186.5601	207.3806	250.2000
CFFF	*Plate*	27.2257	49.3726	86.9155	102.7856	112.7519	146.2908
	LD2	26.1995	49.3426	79.8732	102.7134	105.3166	134.6323
	LD4	26.1980	49.3371	79.8476	102.6853	105.2627	134.5761
	FEM	25.2844	50.0606	77.5522	101.2431	107.2138	135.2726
FCCF	*Plate*	38.7562	91.8611	92.0176	128.2759	164.9609	165.1030
	LD2	37.3507	80.7648	91.7722	119.3720	160.7237	164.5115
	LD4	37.3487	80.7429	91.7445	119.3399	160.6563	164.4099
	FEM	37.3356	80.2619	92.0033	119.1614	158.1700	165.8625

Table 7.32: First six natural frequencies of a square sandwich plate with different theories. Distributed attached mass

As shown in table: 7.32, the resulting first natural frequency are in agreement with those calculate with the Sandwich-9 finite element model, with a very smaller model, in all the proposed boundary conditions. The effect of the distribute mass is clearly visible in the systematic lowering of the natural frequencies. However, also in this case, some modes feels more the effect of the mass presence since the mass is nearer to theirs modal antinode.

7.7 Suspended masses

The capability of the code to compute correct mass and stiffness matrices of a plate loaded with of suspended masses is validated solving the eigenvalue problem of the augmented system and comparing the resulting natural frequencies with those reported in literature. Several configurations of plates with suspended mass have been adopted, with respect of mass values, stiffness ratios and position onto the plate.

7.7.1 Convergence Analysis

The approximation obtained by the Ritz method can be made as accurate as desired by increasing the number of terms in the expansion, but it is truncated to a finite value due to computational time and computer capability. Therefore, the accuracy of the approximate solution is affected by the rate of convergence associated with the choice of the set of trial functions.

First of all a preliminary study has been done to assess the convergence of the solution with respect to the proposed Ritz expansion. The first natural frequencies, adimensionalized as λ_1 and reported in the followings tables, are obtained with various boundary conditions, lamination schemes and dimension of the attached mass.

In table 7.33 is shown the variation of the results obtained with different ESL and LW theories, with respect of the order of the Ritz expansion. The plate considered is a simply supported square three layer laminate with an height to side ratio of $\frac{h}{a} = 0.1$. All plies have the same thickness and are made of CFRP1 and, the lamination scheme is (0/90/0). The suspended mass is located at the center of the plate onto the top surface and has a mass equal at that of the plate. The relative stiffness of the spring is:

$$K_0 = \frac{12ab(1-\nu^2)}{E_1 h^3} k_0 = 0.5$$

In table 7.34 is shown the variation of the results obtained with two different boundary conditions, for ESL $ED4$ theory, with respect of the order of the Ritz expansion. The plate considered is a rectangular four layer laminate with an height to side ratio of $\frac{h}{a} = 0.1$ and a form factor $\frac{b}{a} = 1.5$. All layers have the same thickness, are made of CFRP4 and the lamination scheme is (0/90/0/90). The suspended mass is located at coordinates: $\frac{x_m}{a} = 0.3$, $\frac{y_m}{b} = 0.5$ onto the top surface and has a mass equal at that of the plate. The relative stiffness of the spring is:

$$K_0 = \frac{12ab(1-\nu_1\nu_2)}{E_1 h^3} k_0 = 0.8$$

In table 7.35 is shown the variation of the results obtained with different relative spring stiffness, for LW $LD2$ theory, with respect of the order of the Ritz expansion. The squared, fully clamped plates considered are a three layer laminate with an height to side ratio of $\frac{h}{a} = 0.15$. All layers have the same thickness, are made of CFRP3 and the lamination scheme is $(45/0/-45)$. The suspended mass is located at coordinates: $\frac{x_m}{a} = 0.7$, $\frac{y_m}{b} = 0.6$ onto the top surface and has a mass equal at that of the plate. The

Theory	P	Adimensionalized natural frequencies					
		$\bar{\omega_1}$	$\bar{\omega_2}$	$\bar{\omega_3}$	$\bar{\omega_4}$	$\bar{\omega_5}$	$\bar{\omega_6}$
ED2	7	0.01307	0.11447	0.12928	0.15468	0.22894	0.38373
	9	0.01305	0.10871	0.12699	0.15467	0.22889	0.36399
	10	0.01305	0.10870	0.12698	0.15467	0.22889	0.36393
	11	0.01304	0.10369	0.12499	0.15467	0.22884	0.34192
	12	0.01304	0.10368	0.12499	0.15467	0.22884	0.34189
	13	0.01303	0.09928	0.12321	0.15467	0.22879	0.32658
	14	0.01303	0.09927	0.12321	0.15467	0.22879	0.32656
LD4	7	0.01305	0.11193	0.12820	0.14931	0.22025	0.35379
	9	0.01303	0.10533	0.12534	0.14930	0.22008	0.34788
	10	0.01302	0.10529	0.12533	0.14930	0.22007	0.34772
	11	0.01301	0.09950	0.12272	0.14930	0.21991	0.32676
	12	0.01301	0.09947	0.12271	0.14930	0.21991	0.32667
	13	0.01300	0.09434	0.12027	0.14929	0.21975	0.31219
	14	0.01299	0.09432	0.12027	0.14929	0.21975	0.31213

Table 7.33: Convergence of first six frequency parameters for different theories. Punctual suspended mass

Boundary conditions	P	Adimensionalized natural frequencies					
		$\bar{\omega_1}$	$\bar{\omega_2}$	$\bar{\omega_3}$	$\bar{\omega_4}$	$\bar{\omega_5}$	$\bar{\omega_6}$
CFSF	7	0.01075	0.10143	0.10405	0.13717	0.13781	0.18886
	9	0.01074	0.10114	0.10397	0.13443	0.13448	0.16015
	10	0.01073	0.10110	0.10392	0.13207	0.13387	0.15753
	11	0.01072	0.10068	0.10388	0.12715	0.13055	0.14662
	12	0.01072	0.10067	0.10385	0.12699	0.12912	0.14651
	13	0.01071	0.09998	0.10377	0.11889	0.12634	0.14338
	14	0.01071	0.09964	0.10377	0.11643	0.12625	0.14285
FCCF	7	0.01040	0.03603	0.08330	0.12911	0.15162	0.17159
	9	0.01039	0.03601	0.08302	0.12202	0.14851	0.16840
	10	0.01038	0.03601	0.08283	0.11674	0.14715	0.16661
	11	0.01038	0.03600	0.08271	0.11378	0.14652	0.16368
	12	0.01037	0.03600	0.08247	0.10932	0.14575	0.16172
	13	0.01037	0.03600	0.08234	0.10738	0.14545	0.15942
	14	0.01036	0.03599	0.08184	0.10186	0.14472	0.15455

Table 7.34: Convergence of first six frequency parameters for different boundary conditions. Punctual suspended mass

relative stiffness of the spring are in the first case:

$$K_0 = \frac{12ab(1-\nu_1\nu_2)}{E_1 h^3} k_0 = 0.3$$

and $K_0 = 1$ in the second case.

Relative stiffness	P	Adimensionalized natural frequencies					
		$\bar{\omega_1}$	$\bar{\omega_2}$	$\bar{\omega_3}$	$\bar{\omega_4}$	$\bar{\omega_5}$	$\bar{\omega_6}$
$K_0 = 0.3$	7	0.01541	0.21832	0.32824	0.43346	0.52771	0.53552
	9	0.01540	0.19650	0.32294	0.38781	0.52684	0.53156
	10	0.01539	0.18179	0.32044	0.36112	0.52650	0.53018
	11	0.01539	0.17640	0.31964	0.35010	0.52637	0.52971
	12	0.01539	0.16950	0.31853	0.33534	0.52623	0.52917
	13	0.01538	0.15937	0.31523	0.32132	0.52609	0.52862
	14	0.01538	0.15859	0.31212	0.31957	0.52606	0.52852
$K_0 = 1$	7	0.02780	0.21841	0.32962	0.43347	0.52903	0.53568
	9	0.02774	0.19654	0.32434	0.38781	0.52801	0.53188
	10	0.02769	0.18182	0.32183	0.36113	0.52757	0.53061
	11	0.02768	0.17642	0.32102	0.35013	0.52739	0.53018
	12	0.02765	0.16952	0.31986	0.33540	0.52719	0.52971
	13	0.02760	0.15938	0.31587	0.32208	0.52698	0.52924
	14	0.02760	0.15860	0.31236	0.32073	0.52692	0.52916

Table 7.35: Convergence of first six frequency parameters for a square plate loaded with a punctual suspended mass with different relative spring stiffness

As it can be seen from the previous tables, the presence of a suspended mass affects negatively the convergence of the Ritz method, since the local effects generated by the presence of the mass are difficultly well approximated by global polynomials of relatively low order. This implies that in case of suspended mass an eleventh order Ritz expansion might not be sufficiently accurate, as stated before in the *eigenvalue analysis* section for a not-loaded plate, and an higher order shall be selected as stated for attached masses, especially if higher frequencies have to be calculated with very good approximation. In can be observed that, also in this case, the convergence is monotonic from above as Ritz terms are added and that the trend is similar for all theories selected.

From now, if not specified differently, all the results presented in this section are calculated using a thirteen order Ritz expansion. Go beyond this value will slightly improve the results while the compute became more and more time demanding.

7.7.2 Problem XV - Natural frequencies of an isotropic plate with spring-mass system

An isotropic square simply supported thin plate has been considered. The plate is made of Al7075, with an height to side ratio of $\frac{h}{a} = 0.005$. The suspended mass is located at $x_m = y_m = \frac{3}{4}$ and the relative stiffness of the spring K_0 and the mass ratio $M_r = \frac{m_{mass}}{m_{plate}}$ are varied in a range of values for the sake of comparison with [3].

The resulting first six natural frequencies, adimensionalized with respect to λ_8, are presented in table 7.36. The results of the plate without suspended mass has been modeled using various ESL theories to select the better model to conduct the subsequent analysis, which is $ED3$, since higher order theories not improve the results consistently whereas increase the degrees of freedom of the model and the computing time. LW theories have not been taken into account since the plate is thin and isotropic.

The case of spring of infinite stiffness has also been modeled adopting a punctual attached mass to validate in an other way both the capability of the code, since the results of both model shall be almost equal. The results of these analysis are marked as $E\bar{D}3$.

It is important to notice that for some normal modes exists an effective decoupling of the spring-mass system from the plate. This happens when a nodal line of the plate oscillation contains the position of the attached system. In that case the mass does not disturb neither the mode nor the frequency of vibration.

It is appreciated that when the relative rigidity of the spring is small, the first natural frequency practically coincides with the frequency of the one degree spring-mass system with a negligible influence of the plate on it. For higher values of relative stiffness $K0$, the frequency coefficient of the discrete system is strongly modified by the influence of the plate. The remaining values show the natural frequency of the system modified by the presence of the spring-mass system, when the spring-mass system is not located at a nodal line.

The validation has been carried out only tanking into account this simple plates, since the capability of the code to get the correct dynamic behaviour of laminated or sandwich plates is already validated by the analysis reported previously.

Relative stiffness	Mass Ratio	theory	Adimensionalized natural frequencies					
			$\bar{\omega_1}$	$\bar{\omega_2}$	$\bar{\omega_3}$	$\bar{\omega_4}$	$\bar{\omega_5}$	$\bar{\omega_6}$
Unloaded plate		ED2	19.7377	49.3383	49.3383	78.9319	98.6571	98.6571
		ED3	19.7375	49.3372	49.3372	78.9292	98.6529	98.6529
		ED4	19.7375	49.3372	49.3372	78.9292	98.6529	98.6529
		ED5	19.7375	49.3373	49.3373	78.9292	98.6529	98.6529
$K_0 = 0.5$	$M_r = 0.25$	ED3	1.4123	19.7499	49.3365	49.3567	78.9419	98.6407
		Ref	1.4128	19.752		49.368	78.969	98.696
	$M_r = 0.5$	ED3	0.9987	19.7496	49.3357	49.3560	78.9419	98.6283
		Ref	0.9990	19.752		49.368	78.969	98.696
	$M_r = 1$	ED3	0.7059	19.7489	49.3342	49.3544	78.9419	98.6029
		Ref	0.7071	19.752		49.368	78.969	98.696
$K_0 = 5$	$M_r = 0.25$	ED3	4.4092	19.8678	49.3365	49.5389	79.0562	98.6407
		Ref	4.4084	19.869		49.550	79.083	98.696
	$M_r = 0.5$	ED3	3.1184	19.8642	49.3357	49.5373	79.0560	98.6283
		Ref	3.1180	19.866		49.549	79.083	98.696
	$M_r = 1$	ED3	2.2053	19.8620	49.3342	49.5353	79.0559	98.6029
		Ref	2.2050	19.865		49.549	79.083	98.696
$K_0 = \inf$	$M_r = 0.25$	ED3	17.1149	34.0855	49.3365	66.2700	93.3565	98.6407
		$E\bar{D}3$	17.1165	34.1022	49.3365	66.2943	93.3723	98.6407
		Ref	17.103	33.954		66.091	93.267	98.696
	$M_r = 0.5$	ED3	14.8139	30.0627	49.3357	64.8788	92.8900	98.6283
		$E\bar{D}3$	14.8175	30.0799	49.3357	64.9043	92.9076	98.6283
		Ref	14.785	29.928		64.692	92.791	98.696
	$M_r = 1$	ED3	11.8166	27.7553	49.3342	64.1378	92.6289	98.6029
		$E\bar{D}3$	11.8218	27.7701	49.3342	64.1635	92.6473	98.6029
		Ref	11.776	27.640		63.953	92.532	98.696

Table 7.36: First six frequency parameters for different theories. Punctual suspended mass with different relative stiffness and mass ratios

7.8 Patches

The capability of the code to compute the correct mass and stiffness matrices of a plate equipped with various types of patches is validated solving the eigenvalue problem of the equipped plate and comparing the resulting natural frequencies with those calculated with various finite element models designed for this scope. The patches has been considered with and without their stiffness effects: in this later case their contribution can be seen as the same contribution made by a distributed attached mass.

7.8.1 Convergence Analysis

The approximation obtained by the Ritz method can be made as accurate as desired by increasing the number of terms in the expansion, but it is truncated to a finite value due to computational time and computer capability. Therefore, the accuracy of the approximate solution is affected by the rate of convergence associated with the choice of the set of trial functions.

First of all a preliminary study has been done to assess the convergence of the solution with respect to the proposed Ritz expansion. The first natural frequencies, adimensionalized as λ_1 and reported in the followings tables, are obtained with various ESL theories, boundary conditions and patches dimension.

In table 7.37 is shown the variation of the results obtained with different ESL theories, with respect of the order of the Ritz expansion. The plate considered is a simply supported square three layer laminate with an height to side ratio of $\frac{h}{a} = 0.1$. All plies have the same thickness and are made of CFRP1 and, the lamination scheme is (0/90/0).

The squared patch considered has sides length equal at $\frac{1}{10}$ of the respective plate sides, its center is positioned at plate center, onto the top surface. The patch is made of an isotropic material similar to Isot2 but with a density 100 times higher. The ratio between patch and plate height is: $\frac{h_m}{h} = 0.1$

Theory	P	Adimensionalized natural frequencies					
		$\bar{\omega_1}$	$\bar{\omega_2}$	$\bar{\omega_3}$	$\bar{\omega_4}$	$\bar{\omega_5}$	$\bar{\omega_6}$
ED3	9	0.1230	0.2065	0.2204	0.2264	0.3112	0.3698
	10	0.1229	0.2065	0.2204	0.2264	0.3101	0.3697
	11	0.1227	0.2058	0.2201	0.2261	0.3083	0.3696
	12	0.1227	0.2058	0.2201	0.2261	0.3079	0.3695
	13	0.1226	0.2053	0.2199	0.2259	0.3066	0.3695
	14	0.1226	0.2053	0.2199	0.2259	0.3064	0.3694
ED5	9	0.1229	0.2057	0.2202	0.2259	0.3071	0.3697
	10	0.1228	0.2057	0.2202	0.2259	0.3059	0.3696
	11	0.1226	0.2049	0.2200	0.2256	0.3042	0.3695
	12	0.1226	0.2049	0.2200	0.2256	0.3037	0.3694
	13	0.1225	0.2043	0.2198	0.2254	0.3024	0.3694
	14	0.1225	0.2043	0.2198	0.2254	0.3021	0.3692

Table 7.37: Convergence of first six frequency parameters for different theories. Isotropic patch attached

In table 7.38 is shown the variation of the results obtained with two different boundary conditions, for ESL $ED4$ theory, with respect of the order of the Ritz expansion. The plate considered is a rectangular four layer laminate with an height to side ratio of $\frac{h}{a} = 0.1$ and a form factor $\frac{b}{a} = 1.5$. All plies have the same thickness and are made of CFRP4 and the lamination scheme is (0/90/0/90).

The rectangular patch considered has sides length equal at $\frac{1}{10}$ of the respective plate sides, its center is positioned at coordinates: $\frac{x_c}{a} = 0.35$, $\frac{y_c}{b} = 0.7$, onto the top surface. The patch is made of an isotropic material similar to Isot2 but with a density 100 times higher. The ratio between patch and plate height is: $\frac{h_m}{h} = 0.1$

Boundary conditions	P	Adimensionalized natural frequencies					
		$\bar{\omega}_1$	$\bar{\omega}_2$	$\bar{\omega}_3$	$\bar{\omega}_4$	$\bar{\omega}_5$	$\bar{\omega}_6$
CFSF	9	0.0920	0.1037	0.1364	0.1889	0.1970	0.2349
	10	0.0920	0.1037	0.1363	0.1886	0.1967	0.2347
	11	0.0919	0.1037	0.1363	0.1878	0.1965	0.2345
	12	0.0919	0.1037	0.1362	0.1869	0.1963	0.2341
	13	0.0918	0.1037	0.1362	0.1868	0.1963	0.2340
	14	0.0918	0.1037	0.1362	0.1862	0.1961	0.2338
FCCF	9	0.0325	0.0821	0.1334	0.1614	0.1676	0.2225
	10	0.0325	0.0821	0.1333	0.1611	0.1675	0.2220
	11	0.0325	0.0821	0.1332	0.1609	0.1674	0.2216
	12	0.0325	0.0821	0.1331	0.1609	0.1674	0.2213
	13	0.0325	0.0821	0.1330	0.1607	0.1674	0.2211
	14	0.0325	0.0821	0.1329	0.1606	0.1674	0.2208

Table 7.38: Convergence of first six frequency parameters for different boundary conditions. Isotropic patch attached

In table 7.39 is shown the variation of the results obtained with different patch dimensions, for ESL $ED3$ theory, with respect of the order of the Ritz expansion. The squared, fully clamped plates considered are a three layer laminate with an height to side ratio of $\frac{h}{a} = 0.15$. All plies have the same thickness, are made of CFRP3 and the lamination scheme is $(45/0/-45)$.

The squared patches are attached onto the top surface and their center are positioned at the plate center in both cases. The patch has sides length equal at $\frac{1}{20}$ of the respective plate sides in the first case and equal at $\frac{1}{5}$ in the second case. The patches are made of an isotropic material similar to Isot2 but with a density 100 times higher. The ratio between patches and plate

height is: $\frac{h_m}{h} = 0.2$ in both cases.

Patch dimensions	P	Adimensionalized natural frequencies					
		$\bar{\omega_1}$	$\bar{\omega_2}$	$\bar{\omega_3}$	$\bar{\omega_4}$	$\bar{\omega_5}$	$\bar{\omega_6}$
side length ratio $\frac{1}{20}$	9	0.2785	0.4665	0.5261	0.6266	0.6369	0.7142
	10	0.2784	0.4650	0.5261	0.6229	0.6367	0.7142
	11	0.2775	0.4492	0.5256	0.5961	0.6175	0.7142
	12	0.2774	0.4475	0.5256	0.5941	0.6172	0.7142
	13	0.2766	0.4328	0.5251	0.5792	0.6006	0.7142
	14	0.2765	0.4310	0.5250	0.5779	0.6002	0.7142
side length ratio $\frac{1}{5}$	9	0.1356	0.2227	0.3195	0.4032	0.4222	0.4260
	10	0.1356	0.2212	0.3113	0.3772	0.4013	0.4044
	11	0.1354	0.2206	0.3101	0.3719	0.3966	0.3995
	12	0.1354	0.2200	0.3050	0.3607	0.3829	0.3876
	13	0.1353	0.2192	0.3043	0.3576	0.3809	0.3832
	14	0.1353	0.2190	0.3017	0.3539	0.3731	0.3778

Table 7.39: Convergence of first six frequency parameters for a square plate with an isotropic patch attached with different dimensions

As it can be seen from the previous tables, the presence of the patch does not affects the convergence of the Ritz method, since the patches as theoretically handled as layers of reduced surface, instead of add mass a posteriori as done for the attached masses. Again, with fully clamped boundary conditions convergence is slower than in other cases. Same consideration can be made for this issue as done for previous convergence problems. From now, if not specified differently, all the results presented in this section are calculated using a twelfth order Ritz expansion.

7.8.2 Problem XVI - Natural frequencies of an isotropic plate equipped with an isotropic patch

An isotropic square fully clamped plate has been considered. The plate is made of Al7075, with an height to side ratio of $\frac{h}{a} = 0.02$ and a side length $a = 1$ meter. The patch is located onto the top face at the plate center and has a surface of 1% of the surface area of the plate. The ratio between patch and plate height is: $\frac{h_m}{h} = 0.1$ and the patch is made by an isotropic material which has the same characteristics of Al7075 with a density 100 times higher. To not consider the stiffness effect of the patch, the young and shear modulus

have been set as 10, to let the stiffness of the patch be negligible with respect to the stiffness of the plate.

The first six natural frequencies are presented in table 7.40 and are expressed in Hertz. Case 0 refers to the plate without the patch, Case 1 refers to the plate with the patch attached but without consider the stiffness effect of the patch, which is considered in Case 2. Results obtained are confronted with those of finite element model Isotropic-1

Case	Theory	Dimensional natural frequencies $[Hz]$					
		ω_1	ω_2	ω_3	ω_4	ω_5	ω_6
Case 0	ED2	177.0411	359.8006	359.8006	528.8686	642.4252	645.6243
	ED3	176.9266	359.4498	359.4498	528.1782	641.4200	644.6360
	ED4	176.9265	359.4491	359.4491	528.1767	641.4191	644.6351
	ED5	176.9265	359.4491	359.4491	528.1766	641.4189	644.6350
	FEM	176.4279	358.5992	358.5992	526.9542	639.7706	642.9764
Case 1	ED2	138.8601	354.8723	354.8723	512.2447	528.5583	642.0435
	ED3	138.7752	354.5279	354.5279	511.4945	527.8685	641.0402
	ED4	138.7752	354.5273	354.5273	511.4934	527.8670	641.0393
	ED5	138.7751	354.5272	354.5272	511.4906	527.8669	641.0391
	FEM	138.1562	353.1300	353.1300	506.8442	525.9879	638.9488
Case 2	ED2	140.0848	355.0246	355.0246	520.0070	529.9483	644.1652
	ED3	140.0029	354.6792	354.6792	519.2895	529.2603	643.1602
	ED4	140.0026	354.6783	354.6783	519.2849	529.2585	643.1587
	ED5	140.0023	354.6779	354.6779	519.2817	529.2582	643.1580
	FEM	139.5271	353.7638	353.7638	516.6157	527.9115	641.3209

Table 7.40: First six natural frequencies of a square isotropic plate with different ESL theories and an isotropic patch attached

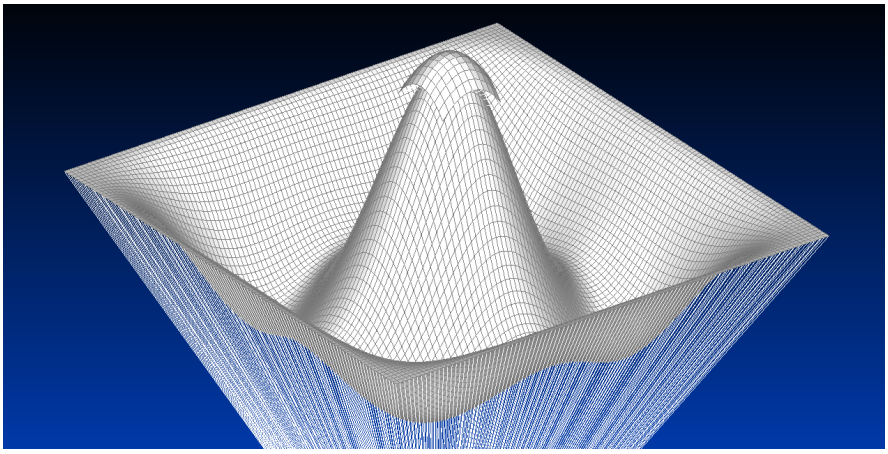

Figure 7.49: Fourth modal shape of Isotropic-1 finite element model

In in table 7.40 the stiffening effect of the patch can be seen looking at the general increasing of the natural frequencies, which is quite negligible for lower frequency, while become considerable for ω_4. This is due to the relative mode shape: if the mode shape deforms considerably the patch, its stiffness become more effective and then increase more that natural frequency than others. This effect can be predicted looking at the mode shapes presented in figure 7.49, relative at the fourth natural frequency of the Isotropic-1 finite element model. It can be seen that at this frequency the modal shape deforms the patch considerably, then, also its stiffness became comparable with that of the plate.

7.8.3 Problem XVII - Natural frequencies of an orthotropic laminate equipped with an isotropic patch

The crossply laminate of *Problem VII* is now considered. The laminate has a stack sequence of (0/90), is made of CFRP4, with an height to side ratio of $\frac{h}{a} = 0.25$ and a side length $a = 1$. The plate has two adjacent edges clamped and two adjacent edges free (FCCF). The patch is located onto the top face at the plate center and has a surface of 1% of the surface area of the plate. The ratio between patch and plate height is: $\frac{h_m}{h} = 0.1$ and the patch is made by an isotropic material which has the same characteristics of Isot with a density 100 times higher. To not consider the stiffness effect of the patch, the young and shear modulus have been set as 10^{-5}, to let the stiffness of the patch be negligible with respect to the plate.

The first six natural frequencies presented in table 7.41 are the adimensional frequencies ω_n, proposed here without an adimensionalization, but still adimensional since the materials properties are adimensional.

Case	Theory	Adimensional natural frequencies					
		ω_1	ω_2	ω_3	ω_4	ω_5	ω_6
Case 0	ED2	0.1132	0.3058	0.3157	0.4502	0.6091	0.6096
	ED3	0.1119	0.3003	0.3097	0.4429	0.5946	0.5952
	ED4	0.1116	0.2988	0.3083	0.4418	0.5899	0.5904
	ED5	0.1112	0.2967	0.3061	0.4386	0.5853	0.5859
	FEM	0.1110	0.2987	0.3060	0.4395	0.5900	0.5902
Case 1	ED2	0.1104	0.2648	0.2902	0.3489	0.4025	0.5372
	ED3	0.1090	0.2553	0.2662	0.3139	0.3899	0.5127
	ED4	0.1087	0.2326	0.2561	0.3038	0.3841	0.4526
	ED5	0.1082	0.2028	0.2498	0.2976	0.3582	0.3766
Case 2	ED2	0.1105	0.2681	0.2925	0.4095	0.5528	0.6068
	ED3	0.1091	0.2627	0.2823	0.4005	0.5363	0.5683
	ED4	0.1088	0.2614	0.2802	0.3988	0.5175	0.5497
	ED5	0.1084	0.2596	0.2785	0.3958	0.5054	0.5428
	FEM	0.1086	0.2659	0.2977	0.4053	0.5591	0.5884

Table 7.41: First six natural frequencies of a square orthotropic plate with different ESL theories and an isotropic patch attached

In in table 7.41 the stiffening effect of the patch can be seen looking at the general increasing of the natural frequencies, which is quite negligible for ω_1, while become considerable for higher frequencies. This is due to the relative mode shape: if the mode shape deforms considerably the patch, its stiffness become more effective and then increase more that natural frequency than others.

7.8.4 Problem XVIII - Natural frequencies of an orthotropic laminate equipped with isotropic patches

The crossply laminate of *Problems VII* and *XVII* is again considered. The laminate has a stack sequence of (0/90), is made of CFRP4, with an height to side ratio of $\frac{h}{a} = 0.25$ and a side length $a = 1$. The plate has two adjacent edges clamped and two adjacent edges free (FCCF). The patches are located onto the top face of the plate and the first has a surface of 1% of the surface area of the plate, while the second has a surface of 4%. The center of the first patch is located at: $\frac{x_c}{a} = 0.35$, $\frac{y_c}{b} = 0.7$, while the center of the second patch is located at: $\frac{x_c}{a} = 0.3$, $\frac{y_c}{b} = 0.4$. The ratio between both patches and plate height is: $\frac{h_m}{h} = 0.1$ and the patches are made by an isotropic material which

has the same characteristics of Isot with a density 100 times higher. To not consider the stiffness effect of the patches, the young and shear modulus have been set as 10^{-5}, to let the stiffness of the patches be negligible with respect to the plate.

The first six natural frequencies presented in table 7.42 are the adimensional frequencies ω_n, proposed here without an adimensionalization, but still adimensional since the materials properties are adimensional.

Case	Theory	Adimensional natural frequencies					
		ω_1	ω_2	ω_3	ω_4	ω_5	ω_6
Case 0	ED2	0.1132	0.3058	0.3157	0.4502	0.6091	0.6096
	ED3	0.1119	0.3003	0.3097	0.4429	0.5946	0.5952
	ED4	0.1116	0.2988	0.3083	0.4418	0.5899	0.5904
	ED5	0.1112	0.2967	0.3061	0.4386	0.5853	0.5859
	FEM	0.1110	0.2987	0.3060	0.4395	0.5900	0.5902
Case 1	ED2	0.0920	0.1845	0.1961	0.2749	0.3366	0.3467
	ED3	0.0905	0.1637	0.1899	0.2439	0.2714	0.2960
	ED4	0.0900	0.1502	0.1863	0.2150	0.2260	0.2327
	ED5	0.0892	0.1351	0.1774	0.1836	0.1911	0.1964
Case 2	ED2	0.0925	0.1986	0.2882	0.3773	0.3951	0.3971
	ED3	0.0911	0.1935	0.2753	0.3592	0.3619	0.3754
	ED4	0.0908	0.1908	0.2729	0.3539	0.3595	0.3657
	ED5	0.0904	0.1886	0.2703	0.3493	0.3548	0.3607
	FEM	0.0842	0.1808	0.2730	0.3394	0.3466	0.5884

Table 7.42: First six natural frequencies of a square orthotropic plate with different ESL theories and two different isotropic patches attached

In in table 7.42 the stiffening effect of the patch can be seen looking at the general increasing of the natural frequencies, which is quite negligible for ω_1, while become considerable for higher frequencies, as seen before for *Problems* $XVI - XVII$. In fact, the positions and the dimensions of the two patches led to less deformation for the first mode with respect to deformations due to higher modes, which will involve one or both patches. This is the case of ω_3 and ω_4 which are remarkably increased by the stiffness of the patches, with respect to the case of patches without stiffness, to a value near to the respective value of Case 0.

7.9 Novel results

7.9.1 Problem XIX - Frequency response of an orthotropic laminate equipped with orthotropic patches and a suspended mass

A composite rectangular laminate plate is considered. The laminate present a symmetric stack sequence of (0/90/0), is made of CFRP7 and has an height to side ratio of $\frac{h}{a} = 0.1$. The aspect ratio of the plate is $\lambda = \frac{b}{a} = 0.66667$ with a side length $a = 1.5$ meters. The plate has two opposite edges free, one of the two others edges is clamped and the last one is simply supported (FSFC). The patches are located onto the top face of the plate, as sketched in figure 7.50. The first patch center is located at coordinates: $\frac{x_{c1}}{a} = 0.325$, $\frac{y_{c1}}{b} = 0.225$, while the center of the second patch is at $\frac{x_{c2}}{a} = 0.25$, $\frac{y_{c2}}{b} = 0.7$. The dimensions of the first patch are $\frac{c_1}{a} = 0.4$, $\frac{d_1}{b} = 0.25$, while the dimension of the second are $\frac{c_2}{a} = 0.2$, $\frac{d_2}{b} = 0.3$. Both patches have the same height: $h_{patches} = 0.02$, and are made of orthotropic material CFRP8 with theirs fiber direction parallel to the fiber direction of the central, 90^{deg}, layer.

The plate is equipped with a suspended mass located at coordinates: $\frac{x_m}{a} = 0.7$, $\frac{y_m}{b} = 0.75$ onto the top surface with a mass of 30 kg, while the plate weights around 355 kg. The relative stiffness of the spring is:

$$K_0 = \frac{12ab(1-\nu_1\nu_2)}{E_1 h^3} k_0 = 1$$

.

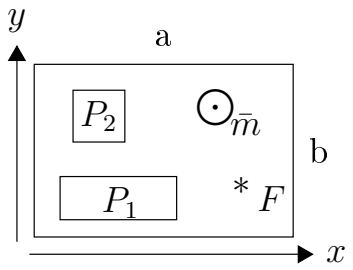

Figure 7.50: Geometrical representation of loaded plate of *Problem XIX*

The first eight natural frequencies presented in table 7.43 are expressed in Hertz and are relative to various ESL kinematic theories with a Ritz expansion of the thirteenth order. Case 0 refers to the plate without nor the patches and nor the masses, Case 1 refers to the plate with the patches attached but without the suspended mass, which is then considered in Case 2.

Case	Theory	Dimensional natural frequencies $[Hz]$							
		ω_1	ω_2	ω_3	ω_4	ω_5	ω_6	ω_7	ω_8
Case 0	ED2	313.6965	368.2526	769.1370	894.6705	950.1703	993.1423	1220.0791	1418.2066
	ED4	311.0547	364.8768	737.0668	880.1543	934.1170	991.2114	1180.0548	1293.8764
	ED5	310.9557	364.4317	731.1476	879.7249	933.0420	991.2059	1173.8537	1277.1399
	ED6	310.9534	364.4291	731.1438	879.7020	933.0215	991.1642	1173.8402	1277.1257
Case 1	ED2	322.9163	376.0834	772.9476	924.2083	988.7559	999.3861	1242.0934	1414.9663
	ED4	318.6804	371.5912	740.1971	908.7551	983.6508	986.7150	1201.5730	1288.8055
	ED5	318.3557	370.9660	734.1853	907.7959	981.1904	986.6685	1194.9114	1271.8578
	ED6	318.2283	370.8494	733.8548	907.6349	980.5692	986.6035	1194.2820	1271.1510
Case 2	ED2	210.6863	326.2139	376.6755	771.8846	926.6410	957.9846	999.2091	1238.8413
	ED4	210.1756	321.9996	372.2648	739.1633	911.1253	954.6330	983.8901	1197.9289
	ED5	210.1224	321.6734	371.6527	733.1991	910.2035	954.3660	981.5399	1191.4186
	ED6	210.1166	321.5418	371.5416	732.8690	910.0479	954.2482	980.9516	1190.7834

Table 7.43: First eight natural frequencies of a rectangular orthotropic plate with different ESL theories equipped with patches and a suspended mass

As shown in table 7.43, all the selected theories are capable to get the same approximate results in terms of natural frequencies, except for $ED2$ theory which overestimate all natural frequencies calculated and so it will be discarded prior to perform dynamic analyses. In fact it can be appreciated how $ED5$ can get results near $ED6$ in the whole frequency range, while $ED4$ fails when frequencies goes higher than 1000 Hz. For this reason $ED4$ will be also discarded and $ED5$ will be choose to be the model on which performs the frequency response analysis, thanks to the good performances with an important degrees of freedom reduction with respect to $ED6$.

The effect of the patches is seen as an increment of all the natural frequencies, due to the stiffening of the plate. However some frequencies are increase more than others since the relative mode shape is more influenced by the stiffening effect of the patches, as seen in $Problems\ XVI - XVIII$.

The effect of the suspended mass is seen in Case 2, where the first natural frequency became the natural frequency of the spring-mass system. In fact, that frequency is almost equal to the natural frequency that the suspended mass will have if grounded: $217,75$ Hz. The other frequencies are slightly increased if the suspended mass is nearer to one node of the respective mode shape, while at the contrary are decreased if the suspended mass is nearer to one respective antinode.

The model based onto $ED5$ theory is used to create a modal model of the thirtieth order, to be a very accurate representation of the full model since takes all natural modes till the thirty. This mode is relative to a frequency of 3087 Hz for the not equipped plate, so well above the upper end of the frequency range of interest for the analysis. In fact, the frequency range

selected is from 1 Hz to 1500 Hz, to include the first eight natural frequencies of the plate, with a frequency step $\Delta f = 1\ Hz$. The modal model is used to get the frequency response for the three cases mentioned above.

The plate is forced by a punctual force located at coordinates: $\frac{x_f}{a} = 0.8$, $\frac{y_f}{b} = 0.3$, acting onto the top of the plates in transverse direction, which has constant unitary amplitude all over the whole frequency range. Frequency responses have been calculated at the centroidal point of the plate and at the midplate at coordinates at which the suspended mass has been located in case 3: $\frac{x}{a} = 0.7$, $\frac{y}{b} = 0.75$. Resulting plots are presented in figures 7.51 and 7.52 respectively. For case 3 also the frequency response of the suspended mass is provided, not only with the modal model but also with the full model, and, it is shown in figure 7.53.

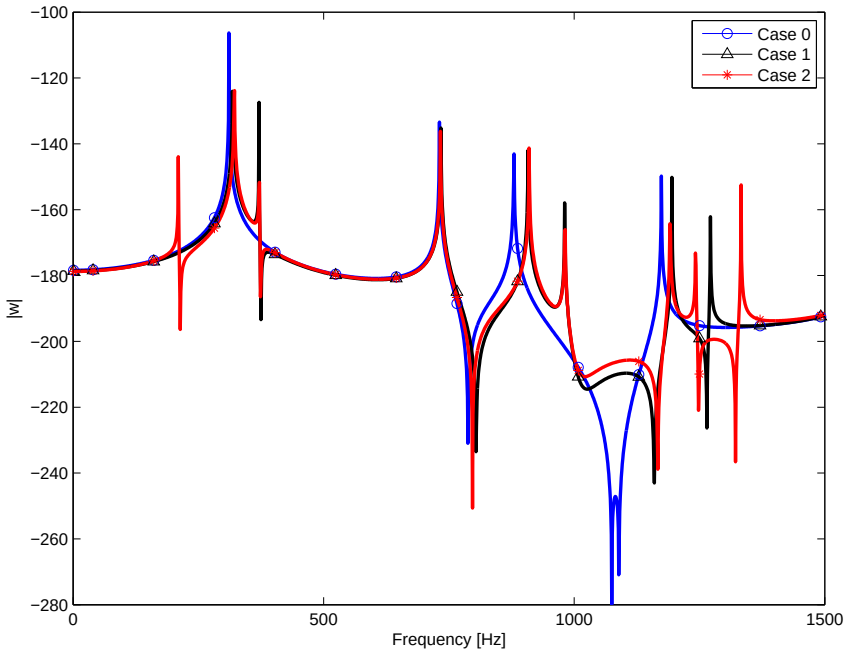

Figure 7.51: $|w|$ $(\frac{a}{2}, \frac{b}{2}, 0)$ vs. frequency for an equipped rectangular plate, different equipement cases

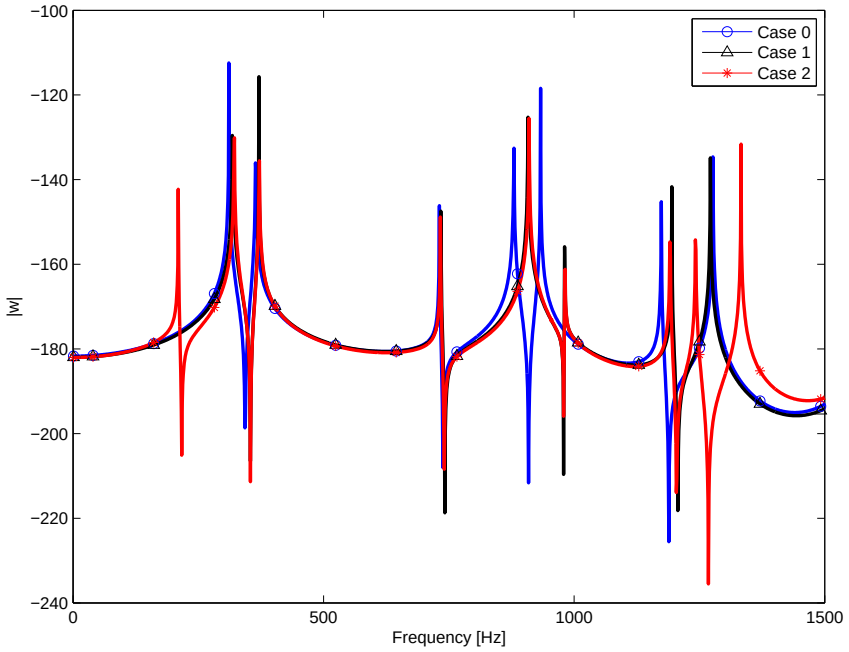

Figure 7.52: $|w|$ $(x_m, y_m, 0)$ vs. frequency for an equipped rectangular plate, different equipement cases

The frequency response plots shows how the stiffening effects of the patches influence the behaviour of the plate: all natural frequencies are slightly higher, as expected after the solution of the eigenvalue problem, while the stiffening effect led to a decrement of the peak response at the respective shifted natural frequencies. This effects can be seen looking at the differences between blue with circle and black with triangle lines in previous plots.

Taking into account the difference between the black with triangle and the red with stars lines the effect of the suspended mass can be recognized. The first thing noticeable is the presence of the natural frequency of the suspended mass before the first of the plate. Then, the presence of the suspended mass further attenuate all peaks response at the other natural frequencies of the plates which does not differs so much from that of the plate in Case 1.

At higher frequencies, not considered in table 7.43, the response becomes more different from the response of the non loaded plate. This is due to the mode shapes relative to those frequencies: deformation related to higher modal shapes are more complicated than the lower ones and present an higher number of nodes and antinodes. Then, the presence of the patches and the suspended mass influence more such mode shapes since it is more probable that they are positioned near an antinode, hence modifying markedly those

modes.

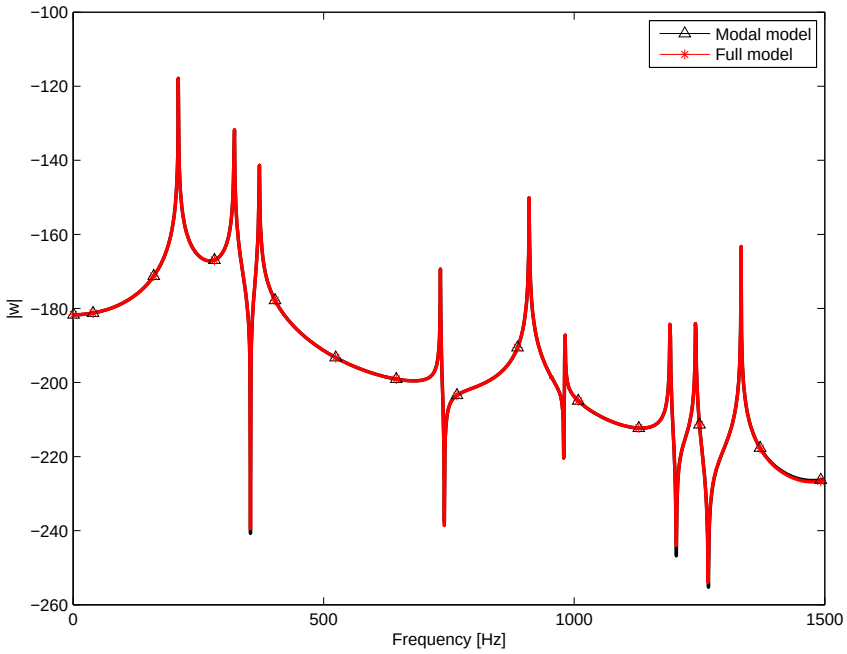

Figure 7.53: $|w|$ vs. frequency for the suspended mass, full model vs. modal model

The frequency response of the mass can be directly confronted with that retrieved for the plate at the same coordinates, shown in figure 7.52, to find that the first peak is amplified by the spring as expected, since its relative at the suspended mass natural frequency, whereas the subsequent peaks, relative to the plate, are then attenuated. The attenuation becomes higher at higher frequencies. This behaviour is characteristic of the spring mass systems which after the amplification at their natural frequency starts to attenuate theirs output.

Figure 7.53 shows the responses of both the full model and the modal model which are practically identical for the all frequency range. This is the proof that the modal model adopted has been build up in the correct way and can represent the system with only 30 degrees of freedom in the frequency range selected.

Now, the same analysis are repeated for a different loading condition: the plate is loaded by a distributed pressure acting onto the top of the plates in transverse direction with uniform distribution and constant unitary amplitude allover the whole frequency range. Also in this case the frequency responses have been calculated at the centroidal point of the plate and at the midplate at coordinates at which the suspended mass has been located in

case 3: $\frac{x}{a} = 0.7$, $\frac{y}{b} = 0.75$. Resulting plots are presented in figures 7.54 and 7.55 respectively. For case 3 also the frequency response of the suspended mass is provided, not only with the modal model but also with the full model, and, it is shown in figure 7.56.

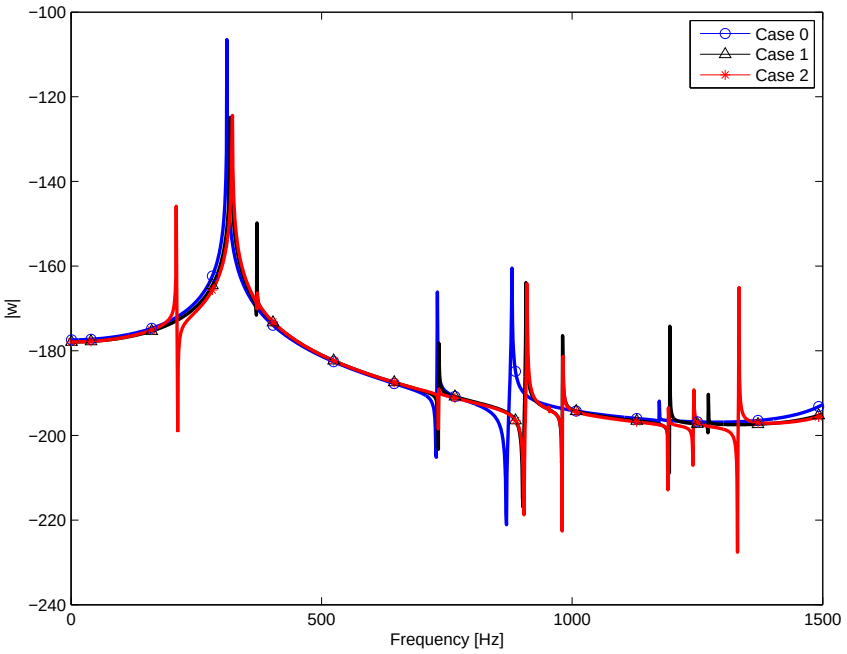

Figure 7.54: $|w|$ $(\frac{a}{2}, \frac{b}{2}, 0)$ vs. frequency for an equipped rectangular plate, different equipement cases

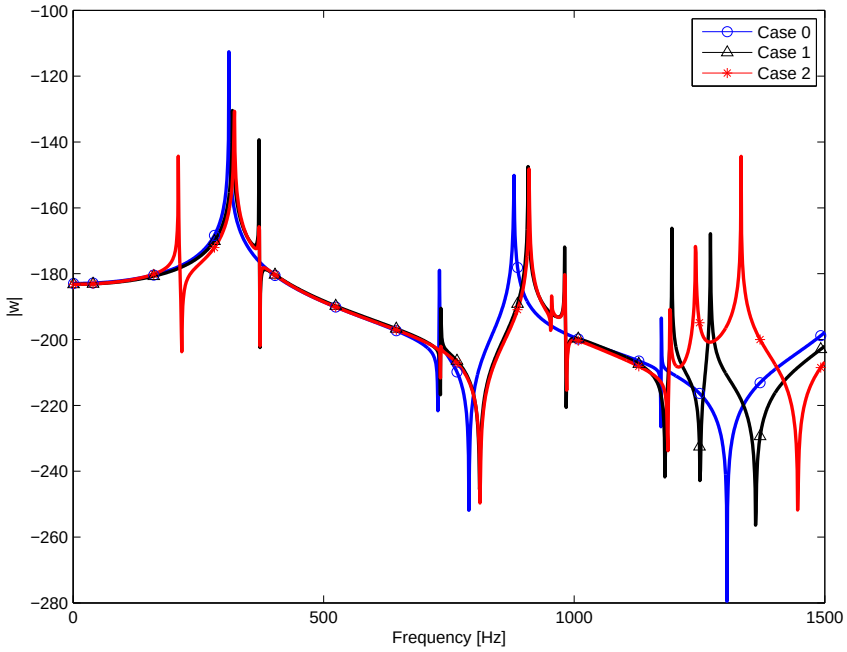

Figure 7.55: $|w|$ $(x_m, y_m, 0)$ vs. frequency for an equipped rectangular plate, different equipement cases

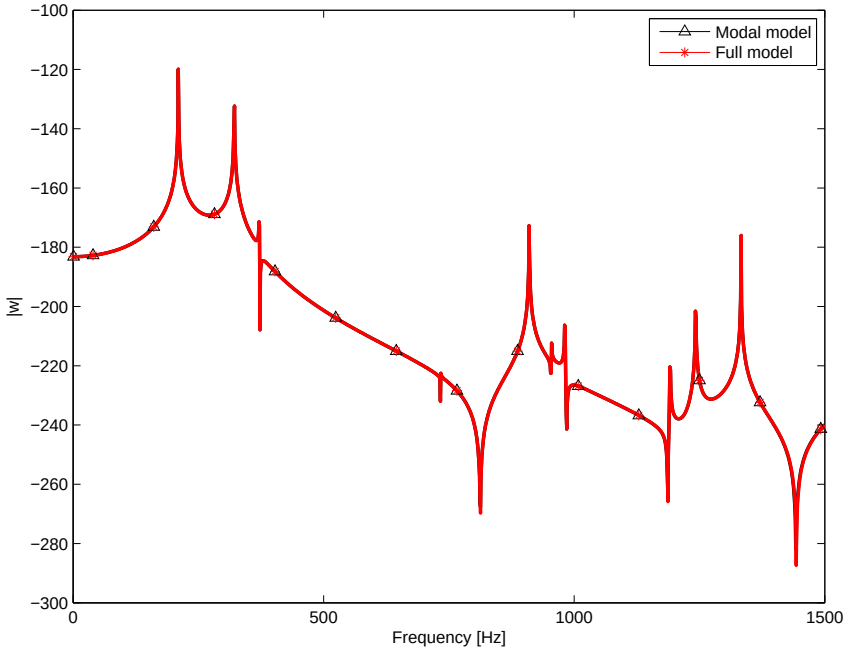

Figure 7.56: $|w|$ vs. frequency for the suspended mass, full model vs. modal model

The consideration made before for the punctual force are still valid in this case with the plate loaded by a distribute pressure. It can be noticed that the response is characterized by less peaks and antiresonances, this is due to the load distribution that in this case is uniform and so can not excite as well the modes of the plate.

Also in this case the modal model is capable to get the correct dynamical behaviour of the system.

7.9.2 Problem XX - Time and frequency responses of a soft core sandwich plate equipped with distribute masses

A fully clamped sandwich plate is considered, the plate has a (0/90/*core*/0/90) layup with the crossply faces made by orthotropic RaoF composite material and the isotropic, very soft core made by RaoC. The ratio of thickness of the core to thickness of the face sheet is assumed to be 14 in this example. A moderately thick plates is considered: the height to side ratio is $\frac{h}{a} = 0.1$. The aspect ratio of the plate is $\lambda = \frac{b}{a} = 0.75$ with a side length $a = 0.8$ meters.

This illustrative case has been designed to analyze an equipped sandwich plate which seems like a plate adopted as side wall of a moderately small spacecraft equipped with instruments on both sides of the plate ad subjected to a distribuite transient load. The equipments to be modelled as attached to the plate have been selected among real scientific equipments mounted on spacecrafts and have been modelled as distributed masses of dimension and mass comparable with those used in an hypothetical feasibility study of a scientific spacecraft. The equipements modelled are:

1. a magnetometer, mass 5 kg with dimensions of 0.5 and 0.3 meters

2. a spectrometer, mass 3 kg with dimensions of 0.3 and 0.2 meters

3. a camera, mass 0.6 kg with dimensions of 0.2 and 0.1 meters

The equipments are mounted on the plate as sketched in figure 7.57, where the grey colour indicate that the mass is locate under the lower surface of the plate. The first mass has its center located at coordinates: $\frac{x_{c1}}{a} = 0.2875$, $\frac{y_{c1}}{b} = 0.4625$, the second at: $\frac{x_{c2}}{a} = 0.7125$, $\frac{y_{c2}}{b} = 0.675$ and the third at: $\frac{x_{c3}}{a} = 0.675$, $\frac{y_{c3}}{b} = 0.3625$. It shall be noted that the plate without any equipment weights only 11.06 kg, so the overall mass has been almost doubled.

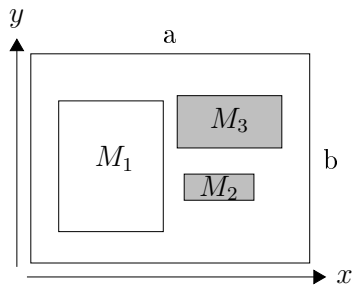

Figure 7.57: Geometrical representation of loaded plate of *Problem XIX*

The eigenvalue problem have been solved both for the equipped plate and for the plate only. The first eight natural frequencies presented in table 7.44 are expressed in Hertz and are relative to various ESL and LW kinematic theories with a Ritz expansion of the thirteenth order. Case 0 refers to the plate without masses while Case 1 refers to the equipped plate.

Case	Theory	Dimensional natural frequencies $[Hz]$							
		ω_1	ω_2	ω_3	ω_4	ω_5	ω_6	ω_7	ω_8
Case 0	ED3	255.1642	369.0709	448.9233	514.4406	525.7752	640.6315	676.7361	679.6144
	ED5	156.8686	229.8464	287.5208	329.4447	337.7298	418.2048	451.7809	455.4733
	LD2	138.4809	204.0126	257.9710	295.8834	303.3615	378.0710	411.4621	416.3153
	LD3	138.4695	203.9943	257.9367	295.8480	303.3219	378.0175	411.3917	416.2280
Case 1	ED3	174.0410	253.3317	298.2467	351.4821	392.5600	434.9577	478.6907	491.3193
	ED5	106.8448	157.5984	188.5476	224.3230	251.5739	281.7945	318.8949	326.6011
	LD2	94.2136	139.6308	168.0293	200.5848	225.1514	253.1522	288.7262	295.8579
	LD3	94.2057	139.6172	168.0080	200.5575	225.1190	253.1111	288.6638	295.7941

Table 7.44: First eight natural frequencies of a rectangular sandwich plate equipped with different distribute masses

As expected, table 7.44 shows that ESL theories overestimate the natural frequencies of the sandwich since they overestimate its stiffness. Note also that $ED3$ gives results with errors over the 70% with respect to the results of the LW theory of the same order: $LD3$. $ED5$ gives better results than its smaller order relative, but is however far away from resulting frequencies of LW models, as also recognized after the analysis of *Problem IX*. This indicates that, a priori, ESL theories should not be adopted to model sandwich plates in dynamical analysis, as also stated in considerations of *Problem VI* for static analysis. Shall be stressed that, in static response ESL theories can however give a rough approximation of the response of the sandwich, while in dynamic analysis they fail completely. To emphasize that, both ESL and LW theories will be used to perform the subsequent time and frequency response analysis.

The $ED5$ and $LD3$ plate models have been selected to create two modal models of the thirtieth order, to be an accurate representation of the respective full model. The models, both full and modal of each of the two theories, are then used to calculate the time response of the equipped plate forced by a transient distribute load $p_z(t) = P_z[H(t-0) - H(t-0.02)]$.

The integration parameters γ and β have been set to 0.5 and 0.25 respectively to ensure that the Newmark integration method will be asymptotically stable.

The reduced order modal model has been made adopting a thirtieth order, to be an accurate representation of the full model since takes all natural modes till the thirty which is relative to a frequency of 693 Hz. The time of integration has been set to 0.04 milliseconds with a time step $\Delta t = 10^{-5}$ seconds. The computed time response, in terms of adimensionalized transverse displacements w for both Case 0 and Case 1, have been evaluate for the central point of the plate, figures 7.58 and 7.58, then at coordinates: $\frac{x}{a} = 0.2875$, $\frac{y}{b} = 0.4625$, at which is located the center of the first equipment mounted onto the plate, figures 7.60 and 7.61.

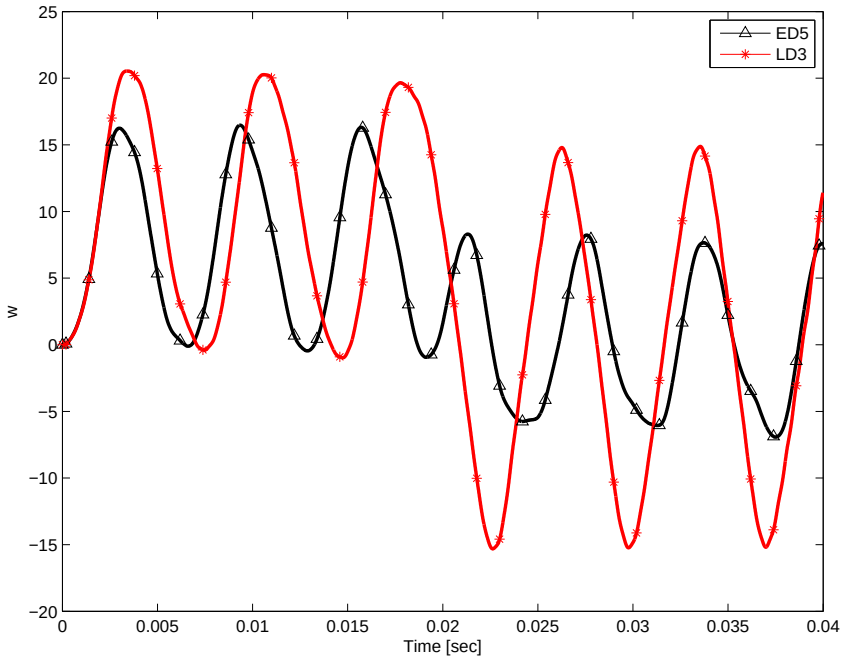

Figure 7.58: $\bar{w}$ $(\frac{a}{2}, \frac{b}{2}, 0)$ vs. time for a sandwich plate under transient load

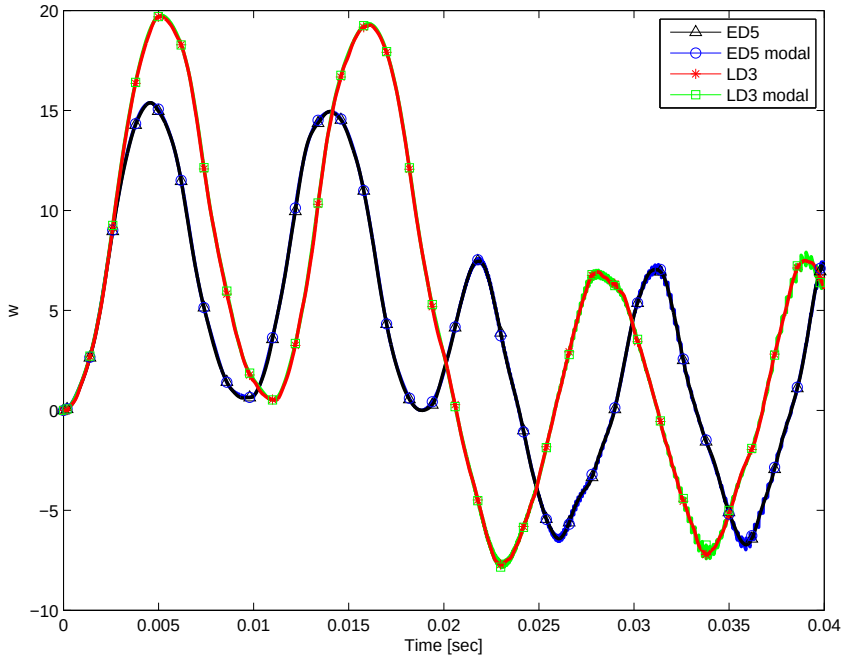

Figure 7.59: $\bar{w}\ (\frac{a}{2}, \frac{b}{2}, 0)$ vs. time for a sandwich equpped plate under transient load

As expected after the eigenvalue analysis, the time responses of $ED5$ are completely different from those of $LD3$, since $ED5$ overestimate the plate stiffness. This overestimation led to a response which is faster and with a smaller amplitude, since the stiffer plate has higher natural frequencies and obviously a lower deformation when loaded.

The effect of the equipments is seen as a slower response, since the natural frequencies are lower than in Case 0, and with a slightly more irregular response, since more modes are now involved in the response after they had been modified in theirs geometry by the presence of the masses.

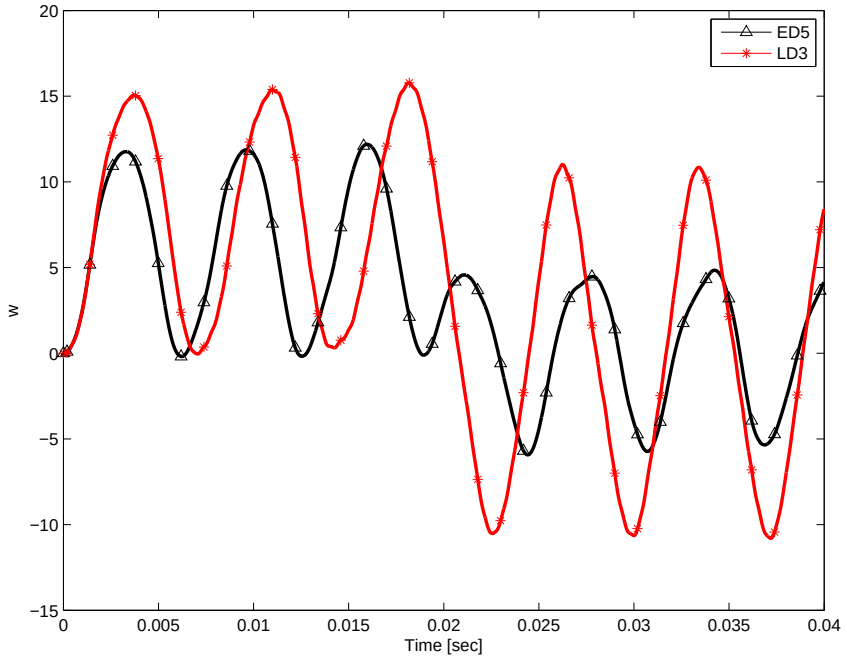

Figure 7.60: $\bar{w}\ (x_m, y_m, 0)$ vs. time for a sandwich plate under transient load

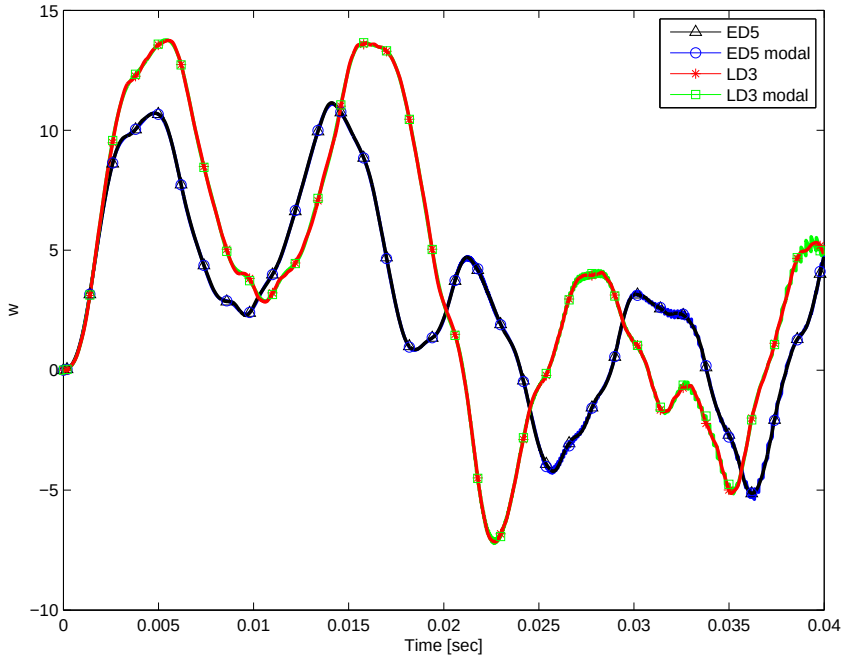

Figure 7.61: $\bar{w}\ (x_m, y_m, 0)$ vs. time for a sandwich equpped plate under transient load

Considerations made for the response in the centroidal point of the plate are still valid for the point at which the center of the first mass is located, $(x_m, y_m, 0)$, for both theories differences and for the effects of the equipments, which now is extremely visible with a very irregular time response for Case 1.

It can be noticed that modal models exhibit problems of convergence in the last peaks of Case 1 the time responses, this is due to the not-so-high frequency associated to the thirtieth mode if relate to the first eight frequencies of the plate, presented in table 7.44. Nevertheless thirty modes have been adopted, there are other many modes with frequencies almost comparable with those included in the reduced order model, leading to this bad behaviour of the response. This suggest to employ more modes in the modal base used to create the modal model.

Then, modal models have been used to get the frequency response in the two cases mentioned above, and resulting plots are presented in figures 7.62 for Case 0 and 7.63 for case 1. The plate is is loaded by a distributed pressure acting onto the top of the plates in transverse direction with uniform distribution and constant unitary amplitude allover the whole frequency range. The frequency range selected is from 1 Hz to Hz, to include the first eight natural frequencies of the plate, with a frequency step $\Delta f = 1\ Hz$. Frequency responses have been calculated for the centroidal point of the plate.

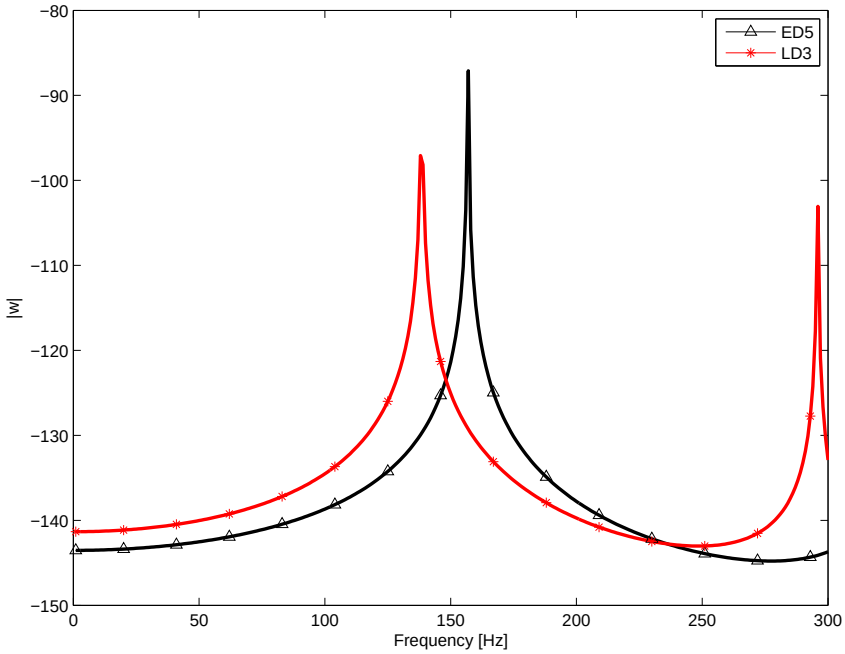

Figure 7.62: $|w|$ $(\frac{a}{2}, \frac{b}{2}, 0)$ vs. frequency for a rectangular sandwich plate

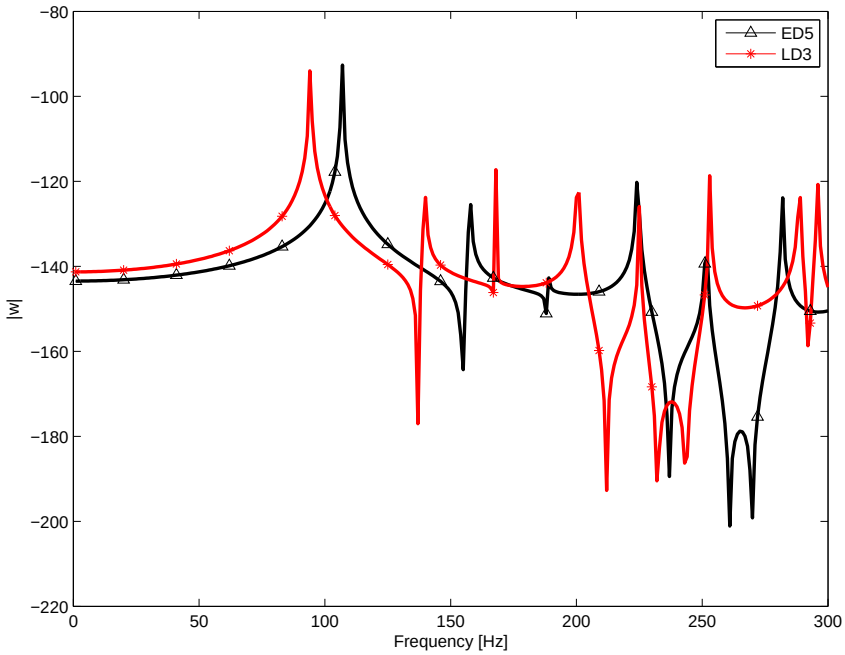

Figure 7.63: $|w|$ $(\frac{a}{2}, \frac{b}{2}, 0)$ vs. frequency for an equipped rectangular sandwich plate

The difference between the ESL and LW theories are again confirmed

looking at frequency responses: the frequencies are shifted at higher frequencies and the quasi static response, characteristic of the frequency ranges away from the natural frequencies, is lower. Moreover the peak at resonance of the not loaded plate in figure 7.62 is higher. Those behaviours are characteristic signs of a stiffer plate. Hence, the adoption of LW theories should be mandatory in dynamical analysis of sandwich plates, even if the plate is not so thicker, because of the great difference between faces and core mechanical properties which can not correctly and exhaustively described only by means of global coordinates proper of ESL theories.

Figure 7.63, relative to the response of the loaded plate, shows how many modes have been modified by the presence of the equipments. First of all can be noticeable that the first peak of resonance has a similar amplitude but is at a lower frequency. Then, the second peak, visible in figure 7.62, has been cancelled and substituted with a dense series of resonances and antiresonances. However all peaks have a smaller maximum amplitude than the one cancelled.

Those considerations suggest that in the design of the configuration of an equipped plate the equipments positions should be defined taking also in the account the fine dynamical behaviour of the plate among the other design parameters coming from the not structural aspects involved in the project of which the plate is a part. This aspect become more and more crucial when the vibrations transmitted through the structure have to be minimized, since a proper configuration might reduce the need of external vibration suppression systems.

Chapter 8

Conclusions

The results found simulating an testing the implemented software are completely in accordance with the theoretical expectations and with benchmark results given in literature and obtained with self developed fem models. The software has been implemented in order to model rectangular and skew plates with arbitrary lamination schemes, arbitrary combination of clamped, free and simply supported boundary conditions and made of a large variety of materials. Moreover, the software has been implemented to model such plates using a *vk*-Ritz formulation under CUF assumptions to have the possibility to choose the more suited kinematic theory case by case. Theories can be choose from the very simple CPT to the quasi-3D $LD4$ passing trough a wide choice of ESL and lover order LW theories.

The presence of equipments onto the plate surfaces has been modelled as attached punctual or distributed masses, which influence only the mass properties of the plate, or at the contrary as patches which also have proper stiffness. Moreover, suspended masses has been implemented as a model of equipments not rigidly constrained to the plate.

The software has been implemented to be capable to solve static and dynamic problems, in terms of time and frequency response. This possibility, with the possibility to make different models of the same plate adopting different plate theories and different theory order for each family of theories had given the possibility to make a wide research to get the peculiar differences among advanced plate theories and to make some consideration useful to choose wisely what theory suits better a determined problem.

All the analyses had shown that, the more the plate is thin, also by a dynamical point of view, the more the mechanical displacements and stresses

distributions along the thickness of the plate tend to be linear. In this case, classical plate theories give acceptable results and EDN theories, give very good results. Otherwise, as the plate begins to be thicker, classical plate theories are strongly not recommended and ESL theories do not correctly model the discontinuities of displacement and stresses at layers interfaces and layerwise theories are needed to correctly represent them, whereas ESL are still capable to give a rough approximation of the macroscopic dynamical response of whole plate. This last statement falls down when thicker and very orthotropic plates, such as sandwiches, are considered. This is due to the huge differences between the mechanical properties of the core and that of the faces let their response to be difficultly described only by global variables, hence the adoption of LW theories becomes mandatory for all kind of analysis.

In *Problems* $I-VI$ the static response of various plates subjected at various loading conditions has been investigated. Plates considered have different lamination schemes, are made by different materials and in all problems a thin and a thick configuration have been adopted. All the analysis performed on thin plates had shown that ESL and LW theories, from medium to high order, are capable to get the precise displacements and stresses values and also the stresses distribution along the plate thickness. The analysis performed onto the thick plates had shown how difference between ESL and LW results grown as the orthotropicity of the plate layers becomes more marked, as for sandwich plates, or also the lamination scheme become antisymmetric. Moreover ESL theories are no longer able to get the correct stresses distribution in all thick cases, especially in the sandwich plate case.

In *Problems* $VII - IX$ the eigenvalue analysis of various plates with various boundary conditions and lamination schemes has been solved. The analysis had shown that a refined Ritz expansion is required if higher mode shall be well computed, especially in the case of clamped boundaries, which are characterized by local displacement gradients near the edge difficult to be well approximated by global polynomials of relatively low order. The frequencies resulting by models of both families of theories are all in good agreement for the thin plate, while the error of CPT increases rapidly when the plate becomes thicker. By comparing results of ESL and LW theories, the fundamental frequency is well estimated by both, hence without the need of a more computational demanding LW approach if the plate is not a sandwich. In this last case, results computed with ESL theories grossly overestimate the natural frequencies in comparison with LW models both for thin and moderately thick plates, due to the large stiffness ratio between the skins and the

core and led to a stiffer plate response. This discrepancy can be contrasted by the use of LW kinematic theories, which appears to be mandatory for sandwich plates with very soft core.

In *Problems* $XII - XIV$ the eigenvalue analysis of various plates loaded with various types of attached masses has been solved. The analysis had shown that the attached mass, punctual or distributed, affects negatively the convergence of the Ritz method, since the local effects generated by the presence of the mass are difficultly well approximated by global polynomials of relatively low order. The effect of the presence of an attached mass is seen in the general lowering of the natural frequencies of the plate, which is more visible for those frequencies associated with modal shapes with an antinode near the mass location.

In *Problem* XV the eigenvalue analysis of an isotropic plate loaded with a suspended mass with various combination of mass and relative stiffness has been solved. The presence of the suspended mass modifies the natural frequencies of the plate, while for some normal modes exists an effective decoupling of the spring-mass system from the plate. This happens when a nodal line of the plate oscillation contains the position of the attached system. In that case the mass does not disturb neither the mode nor the frequency of vibration. Moreover, when the relative rigidity of the spring is small, the first natural frequency practically coincides with the frequency of the one degree spring-mass system, with a negligible influence of the plate on it.

In *Problems* $XVI - XVIII$ the eigenvalue analysis of various plates loaded with various types of patches has been solved. The analysis had shown that the stiffening effect of the patch can be seen looking at the general increasing of the natural frequencies, which can be quite negligible for some frequencies, while becoming considerable for others. This is due to the relative modal shape associated at each natural frequency: if the mode shape deforms considerably the patch, its stiffness become more effective and then increase more that natural frequency than others.

In *Problems* $XIX - XX$ new results are achieved considering first an equipped composite laminate and then and equipped sandwich plate.

In *Problem* XIX the effects of the presence of patches and a suspended mass is investigated solving the eigenvalue problem and then evaluating the FRFs in various point of the laminate. Those analysis have been solved for different loading cases, from the not loaded plate to the fully equipped

system, with ESL theories of various order. The aim of the analysis was to shown how the stiffening effects of the patches influence the behaviour of the plate, increasing all natural frequencies and lowering the peak responses, and then recognize the effect of the suspended mass, with the presence of the natural frequency of the suspended mass before the first of the plate and then a further attenuation of all others peaks response.

In *Problem XX* the effects of the presence of various attached distributed masses is investigated solving the eigenvalue problem and then evaluating the transient responses and the FRFs in various point of the sandwich plate. Those analysis have been solved for different loading cases, from the not loaded plate to the fully equipped system, with ESL and LW theories of various order. As expected, ESL theories overestimate the stiffness of the sandwich leading to higher natural frequencies, a faster and with lower amplitude time response and FRFs with higher peak responses and lower quasi-static response. This indicates that, a priori, ESL theories should not be adopted to model sandwich plates in dynamical analysis, since they fail completely. The effect of the masses is seen as a slower and more irregular time response, since the natural frequencies are lowered and more modes are involved after they had been modified in theirs geometry by the presence of the masses. This difference can been then appreciated from the FRFs.

Suggestion for future improvement

This Thesis is the basis for a future comprehensive tool for the analysis of equipped plates. The first expected expansion is the formulation of a more refined kinematic for the equipments, defining them as boxes with definite dimensions, rotational inertia around x and y axes, translational inertia along z direction and a proper internal resonance frequency and elastically constrained at the plate, to be capable to model in a more refined way the interaction between the plate and the equipments.

An other development is the reformulation of the patch problem to solve the convergence problems which had led to the use of patches only for ESL theories. This adoption, needed to evaluate the patches stiffening effects in sandwich plate, should be seen as the starting point to a very useful improvement: the modelling of piezoelectric patches, which makes it possible to study active control strategies of piezoelectric plates through the use of electric external excitations.

Furthermore, the refined theories here adopted can be used not only for modelling composite rectangular and skew plates, but also improved at their bases to be capable of modelling laminated shells.

Bibliography

[1] C.H.Thai-L.V.Tran-D.T.Tran. Analysis of laminated composite plates using higher-order shear deformation plate theory and node-based smoothed discrete shear gap method. *Applied Mathematical Modelling 36:5657-5677*, 2012.

[2] C.T.Sun-J.M.Whitney. Theories for the dynamic response of laminated plates. *AIAA Journal, Vol. 11, No. 2:178-183*, 1973.

[3] D.V.Bambill-D.H.Felix-C.A.Rossit. Natural frequencies of thin, rectangular plates with holes or orthotropic "patches" carrying an elastically mounted mass. *International Journal of Solids and Structures 43:4116-4135*, 2006.

[4] D.Zhou-Y.K.Cheung-F.T.K.Au-S.H.Lo. Three-dimensional vibration analysis of thick rectangular plates using chebyshev polynomial and ritz method. *International Journal of Solids and Structures 39:6339-53*, 2002.

[5] E.Carrera. A class of two dimensional theories for multilayered plates analysis. *Atti Accademia delle Scienze di Torino. Memorie Scienze Fisiche 1920:49-87*, 1995.

[6] E.Carrera-A.Ciuffreda. A unified formulation to assess theories of multilayered plates for various bending problems. *Composite Structures 69:271-293*, 2005.

[7] G.Kirchhoff. Über das gleichgewicht und die bewegung einer elastischen scheibe. *Journal für die reine und angewandte Mathematik*, 1850.

[8] G.S.Aglietti-R.S.Langley-E.Rogers-S.B.Gabriel. An efficient model of an equipment loaded panel for active control design studies. *Journal Acoustical Society of America 108*, 2000.

[9] H.K.Cho-J.Rhee. Vibration in a satellite structure with a laminate composite hybrid sandwich panel. *Composite Structures 93:2566-2574*, 2011.

[10] J.N.Reddy. A simple higher-order theory for laminated composite plates. *Journal of applied Mechanics, 51(4):745-52*, 1984.

[11] J.N.Reddy. A generalization of two-dimensional theories of laminated composite plates. *Communications in Applied Numerical Methods, Vol. 3, No. 3:173-180*, 1987.

[12] J.N.Reddy. *Mechanics of laminated composite plates and shells*. 2004.

[13] J.N.Reddy-ND.Phan. Stability and vibration of isotropic, orthotropic and laminated plates according to a higher-order shear deformation theory. *Journal of Sound and Vibration, 98(2):157-70*, 1985.

[14] R.M. Jones. *Mechanics of Composite Materials*. 1975.

[15] J.R.Xiao-D.F.Gilhooley-R.C.Batra. Analysis of thick composite laminates using a higher-order shear and normal deformable plate theory (hosndpt) and a meshless method. *Composites: Part B 39:414-427*, 2008.

[16] K.Afaq-M.Karama-S.Mistou. A new refined model for laminated structures. *Comptes Rendus des JNC13:283-91*, 2003.

[17] K.Malekzadeh-A.Sayyidmousavi. Free vibration analysis of sandwich plates with a uniformly distributed attached mass, flexible core, and different boundary conditions. *Journal of Sandwich Structures and Materials, Vol. 12*, 2009.

[18] L.Demasi. Mixed plate theories based on the generalized unified formulation. part ii: Layerwise theories. *Composite Structures 87:12-22*, 2009.

[19] L.Demasi. Mixed plate theories based on the generalized unified formulation. part iv: Zig-zag theories. *Composite Structures 87:195-205*, 2009.

[20] L.Dozio. Exact vibration solutions for cross-ply laminated plates with two opposite edges simply supported using refined theories of variable order. *Journal of sound and vibration 333:2347-2359*, 2014.

[21] L.Dozio-E.Carrera. A variable kinematic ritz formulation for vibration study of quadrilateral plates with arbitrary thickness. *Journal of sound and vibration 330:4611-4632*, 2011.

[22] L.Dozio-E.Carrera. Ritz analysis of vibrating rectangular and skew multilayered plates based on advanced variable-kinematic models. *Composite Structures 94:2118-2128*, 2012.

[23] L.F.Qian-R.C.Batra-L.M.Chen. Free and forced vibrations of thick rectangular plates using higher-order shear and normal deformable plate theory and meshless petrov-galerkin (mlpg) method. *Computer Modeling in Engineering and Sciences, vol.4, no.5:519-534*, 2003.

[24] M.Cho-RR.Parmerter. Efficient higher order composite plate theory for general lamination configurations. *AIAA Journal:31(7):1299-306*, 1993.

[25] N.M.Newmark. A method of computation for structural dynamics. *Journal of Engineering Mechanics, ASCE, 85 (EM3) 67-94.*, 1959.

[26] R.R.Craig-A.J.Kurdila. *Fundamentals of Structural Dynamics.* 2006.

[27] W.O.Wong. The effects of distributed mass loading on plate vibration behavior. *Journal of sound and vibration 252:577*, 2002.